Majorana-Anderson Impurity Models

by

Sankaranarayanan Ganesh

A thesis submitted in partial fulfilment of the requirements for the degree of

Master of Science

Department of Physics

University of Alberta

Abstract

Majorana fermions emerge in topological superconductors as end zero modes in one dimension, and vortex-trapped zero modes or chiral edge modes in two dimensions. A question of much recent interest is the effect of electron-electron interactions on such Majorana fermions. We introduce[1] a class of interacting Majorana-Anderson impurity models which admit an exact solution at finite temperature for a wide range of parameters, including on-site interactions of arbitrary strength. A general model in this class is solved by mapping it via the $\mathbb{Z}_2$ slave-spin method to a non-interacting resonant level model for auxiliary Majorana fermions. The resulting gauge constraint is eliminated by exploiting the transformation properties of the Hamiltonian under a special local particle-hole transformation. To demonstrate our results, we study representative systems of a quantum dot coupled to (i) the end mode of a Kitaev chain, and (ii) the chiral edge modes of a Read-Green superconductor. In both cases, we obtain exact expressions for the dot spectral functions and host local density of states at any temperature. In case (i), we also study how the interaction strength and localisation length of the end mode affect physical properties of the dot, such as quasiparticle weight, double occupancy, and odd-frequency pairing correlations.

[1] Chapters 2 and 3 of this thesis are based on Ref. [1].

As with everything else, for my parents and my brother.

Acknowledgments

My foremost thanks goes to my advisor, Joseph Maciejko. His remarkable ideas, dedication to his students, great lectures, and vast breadth of knowledge, from differential geometry to scanning tunnelling microscopy, have been an inspiration. It is my privilege to learn this craft from him.

I also thank the condensed matter group (faculty, postdocs, and fellow graduate students) at the University of Alberta, especially Frank Marsiglio, Rufus Boyack, Chun Chen, Youssef Kora, Mason Protter, Joel Hutchinson, and Hennadii Yerzhakov for countless discussions on various topics in physics, including many aspects of the work presented in this thesis.

This work belongs to my parents and my brother as much as it does to me. It would never have been produced if not for all my family has given me. Some of the diagrams were produced by my brother.

I also thank Frank Marsiglio again, Alexander Penin, and Marie-Cécile Piro for agreeing to be part of my examining committee, and providing helpful comments on my work.

Contents

List of Figures

List of Acronyms

Wherever they occur, the following acronyms are defined.

BdG	Bogoliubov-de Gennes
GF	Green function
KMAI	Kitaev Majorana-Anderson impurity
LHS	Left-hand side
LDOS	Local density of states
MAI	Majorana-Anderson impurity
MZM	Majorana zero mode
QD	Quantum dot
RMAI	Read-Green Majorana-Anderson impurity
RHS	Right-hand side
SS	Slave-spin
STM	Scanning tunnelling microscopy
STS	Scanning tunnelling spectroscopy
TSC	Topological superconductor

Chapter 1

Overview

In 1937, Ettore Majorana introduced a representation of the Dirac equation that allowed real solutions [2]. These solutions correspond to fermions that are their own antiparticles, and which now bear his name. Majorana fermions were originally introduced as a candidate particle type for neutrinos, a proposition that survives even today. However, once exclusive to the realm of high-energy physics, Majorana fermions have recently entered the world of mainstream condensed matter physics through their experimental realisation in topological superconductors, with exciting prospects for quantum computation (see the reviews [3–7]).

At the intersection of topological physics and the study of strongly correlated systems, a promising new research direction has emerged that investigates the effect of interactions on such emergent Majorana fermions, with striking predictions ranging from emergent supersymmetry to exotic Kondo effects [8–12].

This thesis introduces a wide class of interacting quantum impurity models in Majorana fermion systems, analogous to the classic Anderson impurity model, that are exactly solvable at any temperature and for arbitrary interaction strengths.[1]

[1] Chapters 2 and 3 of this thesis are based on Ref. [1].

Models that fall in this class include an interacting quantum dot hybridising with a Majorana zero mode in a one-dimensional topological superconductor, a model of interest that has been experimentally realised recently [13]. An exact solution to such models presents a significant advance over existing approximate mean-field or numerical studies of similar models, and paves the way for future exact studies of the equilibrium and non-equilibrium properties of models of correlated Majorana fermions, including those of relevance to transport experiments in Majorana devices.

The *structure* of this thesis is as follows. Chapter 1 is an introduction to Majorana fermions in condensed matter. The concept is motivated from the perspective of error correction in quantum computation. Several toy models are constructed in which isolated Majorana fermions emerge, and these models are recognised as those of topological superconductors. Practical versions of these toy models, and a few experiments that have realised them, are then discussed briefly. It is then recognised that Majorana fermions present an opportunity to realise correlation physics in new degrees of freedom previously unavailable. A guide to the literature on the relatively new field of interacting Majorana fermions is then presented, with this avenue of research motivating the consideration of the models introduced in subsequent chapters. Chapter 2 introduces the general class of Majorana-Anderson impurity (MAI) models. The $\mathbb{Z}_2$ slave-spin representation is then reviewed in context, and used in conjunction with a Majorana representation of spin operators to map the general Hamiltonian of this class of models to a quadratic form. Noting that the slave-spin representation introduces a gauge structure, the fate of the associated constraint in calculations of correlation functions is then discussed. Some immediate extensions of the MAI class of models are then highlighted. Chapters 3 and 4 apply this method of exact solvability to study an interacting quantum dot coupled to emergent Majorana fermions in the toy models introduced in Chapter 1. Finally, we conclude with a brief summary of our key results, and discuss prospects for future work.

A good knowledge of the methods of many-body physics, particularly the Matsubara imaginary-time formalism, is assumed on the part of the reader. An acquaintance

with the basic aspects of the BCS theory of superconductivity is also assumed. These are the only overarching prerequisites. Isolated parts of the thesis make use of coherent state functional integrals, but these sections (or at least the computational details) can be safely skipped without loss of continuity. Throughout, we work in natural units $\hbar = c = 1$.

CHAPTER 2

Majorana fermions in condensed matter

2.1 Toy models of topological superconductors

In this chapter, we will construct toy models of condensed matter systems in which we may expect Majorana fermions as emergent excitations. One motivation to embark on such an endeavour comes from practical applications to quantum computation. A classical computer is a device that processes information stored in bits. A bit is classical system that can exist in one of two states (such as an on/off switch for a light bulb), which we denote as 0 and 1. A quantum computer operates on *qubits*, which are two-state quantum systems. A prototypical example is a spin-1/2 moment with states span$\{|0\rangle, |1\rangle\}$. The basis states are defined by $\sigma^z|0\rangle = -|0\rangle$ and $\sigma^z|1\rangle = |1\rangle$, where $\boldsymbol{\sigma} = (\sigma^x, \sigma^y, \sigma^z)$ is a Pauli spin-1/2 operator. Unlike a bit, a qubit may exist in a superposition of states such as $|\psi\rangle = \alpha|0\rangle + \beta|1\rangle$. In a multi-qubit system, this results in a far larger space of states than a classical counterpart constructed from bits, resulting in far more powerful computational ability [14].

However, using qubits to store information also leads to new kinds of error [5]. In classical computers, the only error that can occur is an erroneous discrete flip of a

bit from 0 to 1 (or vice versa). A classical computer corrects such errors by storing and comparing multiple copies of information. In addition to such *classical errors*, a quantum computer is also susceptible to *phase errors.* The exact source of such errors is not important in the present discussion, but may occur due to interactions with the environment or due to imprecise control in gate operations (processing of information). Let us understand what these errors are in more detail. Consider an n-qubit system, modelled by a chain of n spins and described by a general superposition state

$$\left|\psi\right\rangle = \sum_{\{\sigma\}} c_{\{\sigma\}} \left|\sigma_1\right\rangle \otimes \ldots \otimes \left|\sigma_n\right\rangle, \tag{2.1}$$

where $\{\sigma\}$ denotes a configuration of qubits (spins) and $c_{\{\sigma\}} = c_{\sigma_1 \ldots \sigma_n}$ are the expansion coefficients. The sum is over all such configurations. A classical error is represented by σ_j^x, which discretely flips the spin on the j-th site. A phase error is represented by σ_j^z, which generally introduces a relative phase difference between states in the superposition $\left|\psi\right\rangle$. As an example, for $n=3$ and $\left|\psi\right\rangle = a|110\rangle + b|100\rangle$, $\sigma_2^z \left|\psi\right\rangle = a|110\rangle - b|100\rangle$, which is physically distinct from $\left|\psi\right\rangle$.

Let us now try to construct a qubit that is protected from classical and phase errors, following Kitaev [15]. To this end, note that the qubit basis states $\{|0\rangle, |1\rangle\}$ can also be interpreted as the Fock (occupancy) states of a spin-polarised (spinless) electron on a lattice site. In a chain of such qubits, a single classical error is now forbidden, as this requires a single electron to disappear from the chain. This obviously cannot happen in a system that conserves electric charge, but also cannot happen in a system that spontaneously breaks this symmetry – a superconductor also conserves fermion parity (electric charge mod 2). However, an electron can presumably tunnel from one site to another, which would lead to two classical errors, but this may conceivably be avoided by simply placing the sites far apart.

Phase errors in such a chain of electrons are now mathematically represented by $(2c_j^\dagger c_j - 1)$. For example, a state $a|110\rangle + b|101\rangle \to a|110\rangle - b|101\rangle$ under the action of $(2c_2^\dagger c_2 - 1)$. For protection against phase errors, consider the following construction.

One can formally decompose the electron fields into real and imaginary parts as

$$c_j = \frac{1}{2}\left(\gamma_j + i\gamma_j'\right), \qquad c_j^\dagger = \frac{1}{2}\left(\gamma_j - i\gamma_j'\right), \tag{2.2}$$

which define *Majorana fermion operators* γ_j and γ_j' that are Hermitian, and satisfy the Clifford algebra

$$\{\gamma_i, \gamma_j\} = \{\gamma_i', \gamma_j'\} = 2\delta_{ij}, \qquad \{\gamma_i, \gamma_j'\} = 0. \tag{2.3}$$

'Complex fermions' such as electrons can be crudely regarded as bound pairs of Majorana fermions. The phase error operator $(2c_j^\dagger c_j - 1) = i\gamma_j\gamma_j'$ can be described as a pairing of the Majorana fermions γ_j and γ_j'. If we can engineer a system in which such pairing is unlikely, then such a system would be protected against phase errors. Roughly speaking, we must fractionalise the electrons into component Majorana fermions and then spatially separate the components. Since any physical fermionic Hamiltonian must conserve fermion parity[1], a single Majorana operator cannot appear as a standalone term; provided we can find Majorana fermions γ and γ' that are unpaired, then they must not appear in the Hamiltonian at all. Such Majorana fermions are termed *Majorana zero modes (MZMs)*, and qubits constructed from these are protected from classical and phase errors. The information stored in such qubits can be processed by gate operations that are physically implemented by *braiding*, that is controlled exchanges of MZMs, which generally satisfy non-Abelian exchange statistics [5, 16]. In the following sections, we will construct toy models that support such MZMs, and then look for experimentally realisable systems that may be described by these models.

2.1.1 *Kitaev chain*

To find a system that supports MZMs, note that an arbitrary quadratic Hamiltonian governing a chain of spinless electrons admits a Majorana representation. For

[1] This means the Hamiltonian must be constructed out of bosonic terms such as $c_i^\dagger c_j$ or $c_i c_j$, in order for it to be interpreted as an observable and for the existence of stationary states.

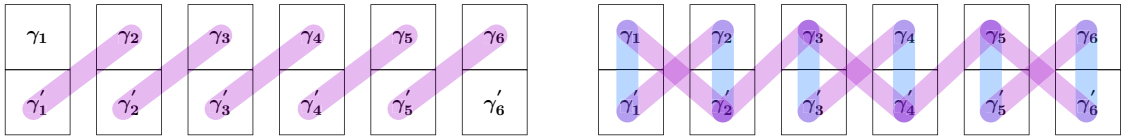

FIGURE 2.1 – (a) Construction of the Kitaev chain by pairing (purple bands) Majorana fermions between sites to obtain unpaired Majorana zero modes at the ends. (b) Pairing of Majorana fermions in a typical tight-binding chain. The blue bands indicate on-site pairing due to chemical potential terms and purple bands indicate nearest neighbour pairing due to hopping terms.

example, a N-site tight-binding chain is described by a Hamiltonian

$$\begin{aligned} H_T &= -t\sum_{j=1}^{N-1}(c_j^\dagger c_{j+1}+\text{h.c.}) - \mu\sum_{j=1}^{N} c_j^\dagger c_j, \\ &= -\frac{it}{2}\sum_{j=1}^{N-1}(\gamma_j\gamma'_{j+1} - \gamma'_j\gamma_{j+1}) - \frac{\mu}{2}\sum_{j=1}^{N}(1+i\gamma_j\gamma'_j), \end{aligned} \tag{2.4}$$

and can thus be thought of as the pairing of Majorana fermions on and between sites. There are two Majorana fermions, or equivalently one spinless electron, on every physical lattice site. In the tight-binding chain, it is easy to see that all available Majorana fermions are paired up in one way or another in the Hamiltonian (see Figure 2.1b). Beginning with an open chain of Majorana fermions, we can try to reverse engineer an electronic system that supports unpaired Majorana fermions. One simple scenario is shown in Figure 2.1a, and can be described by a Hamiltonian,

$$H_1 = it\sum_{j=1}^{N-1}\gamma'_j\gamma_{j+1}, \tag{2.5}$$

where Majorana fermions on neighbouring sites are paired. γ_1 and γ'_N are unpaired MZMs that do not appear in H_1, and are exactly localised at the ends of the chain. To see what electronic system H_1 corresponds to and attempt a possible realisation in real physical systems, we re-express H in terms of the electron fields $c_j^{(\dagger)} = \frac{1}{2}(\gamma_j \pm i\gamma'_j)$ to get

$$H_1 \quad = \quad -t\sum_{j=1}^{N}(c_j^\dagger c_{j+1} - c_j c_{j+1} + \text{h.c.}). \tag{2.6}$$

This is a mean-field BCS Hamiltonian of a one-dimensional superconducting chain with equal hopping integral and pairing potential.[2] To induce superconductivity in a system of spinless (spin-polarised) electrons requires odd-parity pairing, which in the case of a one-dimensional chain translates to a pairing potential $\Delta \propto \langle c_i c_{i+1} \rangle$. Such a system is described by a general Hamiltonian

$$\begin{aligned} H_K &= \sum_{j=1}^{N-1} \Big[-t(c_j^\dagger c_{j+1} + \text{h.c}) - \mu(c_j^\dagger c_j - 1/2) + \Delta(c_j c_{j+1} + \text{h.c}) \Big], \\ &= \frac{i}{2} \sum_{j=1}^{N-1} \Big[(\Delta + t)\gamma_j' \gamma_{j+1} + (\Delta - t)\gamma_j \gamma_{j+1}' - \mu \gamma_j \gamma_j' \Big]. \end{aligned} \tag{2.7}$$

where $\Delta > 0$ is the p-wave pairing potential that can be taken as real-valued without loss of generality.[3] This model is called the Kitaev chain. For $\Delta = t$ and $\mu = 0$, H_K reduces to H_1 and we recover unpaired MZMs γ_1 and γ_N'. These two modes form a highly non-local electronic state $f^{(\dagger)} = \frac{1}{2}(\gamma_1 \pm i\gamma_N')$, the occupancy of which describes a qubit. Note that the wavefunction of this electronic state is non-local, with support fractionalised between the ends of the chain.[4] We refer to the wavefunction piece localised at each end as a MZM wavefunction. Explicit expressions for the MZM wavefunctions are given in Appendix A of Ref. [17] and in Ref. [18]. The ground state of the Kitaev chain is thus two-fold degenerate, at least for $\Delta = t$ and $\mu = 0$, with respect to the occupancy of this non-local electronic state defined by $f^{(\dagger)}$. We denote these ground states by $\big|\psi\rangle$ and $f^\dagger \big|\psi\rangle$, which surprisingly differ in fermion parity. These degenerate ground states form basis states $|0\rangle$ and $|1\rangle$ for a qubit that is protected from both, classical and phase errors. The information stored in such

[2] In retrospect, that H_1 is a superconductor is not so surprising. The fact that γ_1 is an unpaired MZM in this system means symmetry transformations cannot mix it with other Majorana operators. A $U(1)$ transformation on the electron field c_1 implies $\gamma_1 \to \gamma_1 \cos\theta - \gamma_1' \sin\theta$, and so mixes γ_1 and γ_1'. If H_1 were to respect this symmetry, γ_1 must generally appear along with γ_1' in H_1. In a superconductor, this $U(1)$ symmetry is broken down to $\mathbb{Z}_2$. Since $\mathbb{Z}_2$ transformations do not mix different Majorana operators, unpaired Majorana fermions are possible in superconductors.

[3] A complex valued pair potential $\Delta = |\Delta| e^{i\theta}$ can be made real by a gauge transformation on the electron fields.

[4] The support of the wavefunction is the real-space domain where it is non-zero. This is where there is a non-zero probability of finding the particle. By fractionalised support for the f-electron wavefunction, we mean that it is piecewise defined with the two pieces localised at the ends of the chain. We refer to each piece as a MZM wavefunction.

a qubit can be processed by gate operations that are physically implemented by braiding the MZMs at the ends of the chain [5, 16]. However, braiding is well defined only in two-dimensional systems in which particles with non-Abelian statistics may occur. Nevertheless, one can construct wire networks from many Kitaev chains that remarkably permit non-Abelian statistics and therefore braiding of the MZMs in such networks [19].

In addition to supporting a zero-energy fermionic excitation, fractionalised between the ends of the chain, we expect the Kitaev chain to also have the usual Bogoliubov quasiparticle excitations in the bulk, which are separated from the ground state by an energy gap, characteristic of superconductors. To study the bulk properties, it is convenient to use periodic boundary conditions and pass to momentum space, in which H_K can be written in Bogoliubov-de Gennes (BdG) form as

$$H_K = \frac{1}{2}\sum_{k\in FBZ}\begin{pmatrix} c_k^\dagger & c_{-k}\end{pmatrix}\begin{pmatrix} -2t\cos k-\mu & 2i\Delta\sin k \\ -2i\Delta\sin k & 2t\cos k+\mu\end{pmatrix}\begin{pmatrix} c_k \\ c_{-k}^\dagger\end{pmatrix}, \tag{2.8}$$

where the sum is over momenta in the first Brillouin zone $(-\pi,\pi)$, and a lattice constant of unity has been assumed. The bulk energy spectrum is obtained from eigenvalues of the BdG matrix, which are $\pm E(k)$ where

$$E(k) = \sqrt{(2t\cos k+\mu)^2 + 4\Delta^2\sin^2 k}, \qquad k\in(-\pi,\pi). \tag{2.9}$$

Note that the BdG matrix doubles the number of physical degrees of freedom (electrons and holes considered separately), resulting in a redundancy in the number of energy levels which now occur in doubled $\pm E(k)$ pairs (see Figure 2.2). Only $E(k)\geq 0$ correspond to physically distinct energy levels. This can easily be seen by diagonalising the BdG matrix by a Bogoliubov-Valatin transformation on the electron fields; defining the quasiparticle fermion operators $a_k = u_k c_k + v_k c_{-k}^\dagger$ and choosing u_k, v_k to obtain the correct anti-commutation relations for $a_k, a_k^\dagger$ and to diagonalise the BdG matrix, one obtains

$$H_K = \frac{1}{2}\sum_{k\in FBZ}\begin{pmatrix} a_k^\dagger & a_k\end{pmatrix}\begin{bmatrix} E(k) & 0 \\ 0 & -E(k)\end{bmatrix}\begin{pmatrix} a_k \\ a_k^\dagger\end{pmatrix} = \sum_{k\in FBZ} E(k)\left(a_k^\dagger a_k - \frac{1}{2}\right). \tag{2.10}$$

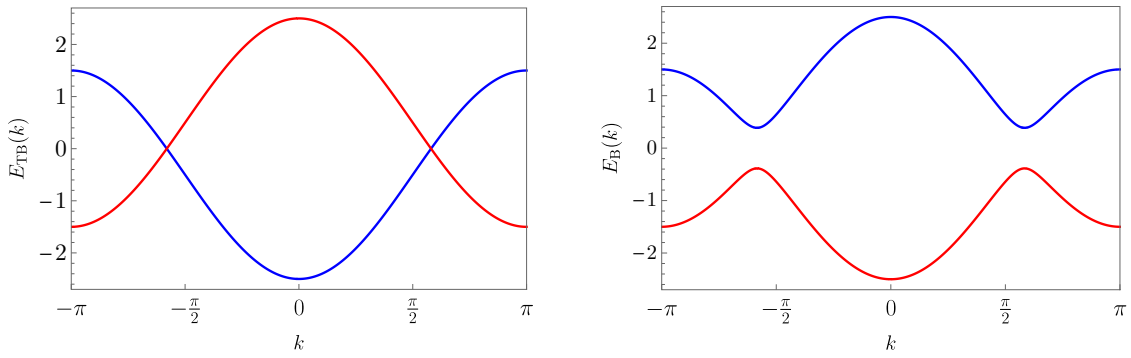

FIGURE 2.2 – (a) Doubled tight-binding dispersion for electrons (blue) and holes (red), for $\mu = 0.5t$. (b) Bulk dispersion of Bogoliubov quasiparticles (superposition of electrons and holes) in the Kitaev chain, for $\mu = 0.5t, \Delta = 0.2t$. Finite Δ opens a gap in the bulk excitation spectrum. As in (a), only the blue band with $E \geq 0$ is physical.

Before studying the bulk properties of the Kitaev chain in more detail, it is pertinent to ask if the MZMs it supports for $\Delta = t$ and $\mu = 0$ survive away from this special choice of parameters (henceforth called the *Kitaev point*). This is necessary for the sake of stability of our qubit, let alone the question of whether one is able to tune to these special parameters in an experiment. Consider small perturbations away from the Kitaev point. If the MZMs are destroyed, then the states $|\psi\rangle$ and $f^\dagger|\psi\rangle$ will split in energy, with one of them moving away from zero energy. Such a splitting is described by an effective Hamiltonian,

$$H_\delta = \delta f^\dagger f = \frac{\delta}{2}(1 + i\gamma_1 \gamma_N'), \tag{2.11}$$

and thus corresponds to pairing of the MZMs at the opposite ends of the chain. As stated earlier, the qubit is not immune to phase errors if such pairing is allowed in the Hamiltonian. There are two ways in which such pairing can effectively arise. (i) If the chain is closed (periodic boundary conditions), then the MZMs are paired just like other Majorana fermions in the bulk and the ground state is non-degenerate even at the Kitaev point. (ii) If the medium (bulk) separating the two MZMs is gapless, then we might intuitively expect the MZM wavefunctions to tunnel/delocalise into the bulk and overlap (pair). Case (i) can obviously be avoided. As regards protection against case (ii), a natural expectation is that a gapped bulk excitation spectrum,

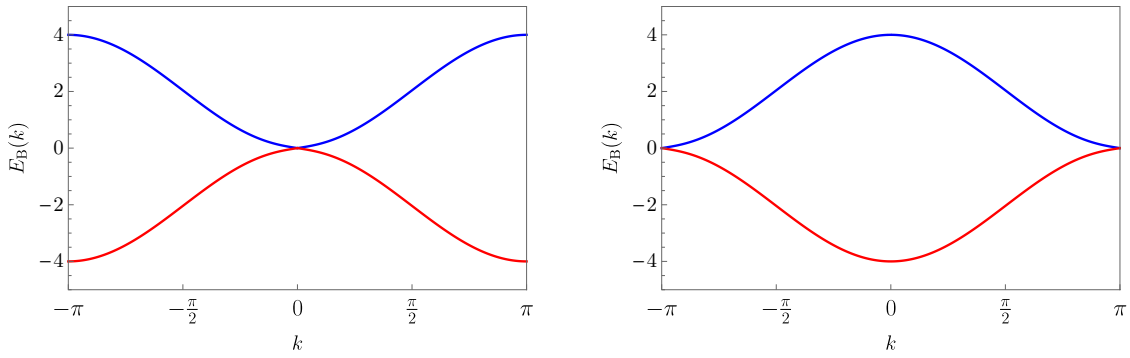

FIGURE 2.3 – Closures of the gap in the bulk excitation spectrum of the Kitaev chain. (a) For $\mu = -2t$, the bulk gap closes at $k = 0$, and (b) for $\mu = 2t$, the gap closes at $k = \pi$. In both plots, $\Delta = 0.2t$.

along with very large separation between the ends of the chain, will prevent overlap of the MZM wavefunctions. It may be helpful to think of the bulk as a potential barrier; the MZM wavefunction on one end will generally decay exponentially into the bulk and will not penetrate to the other end (beyond the barrier) and overlap with the other MZM wavefunction, if the barrier is effectively infinite in length [17, 18].

This intuition turns out to be correct, as we shall see shortly; the MZMs are protected as long as the bulk gap does not close. However, there clearly exist parameter values for which there are no MZMs. For example, $\Delta = t = 0$ and $\mu > 0$, the ground state of H_K is obtained by pairing Majorana fermions on-site to form the 'complex fermions' c_j with $c_j^\dagger c_j = 1$ for every j. This is the picture that also holds for $\mu/t \gg 1$, while $\forall j, c_j^\dagger c_j = 0$ characterises the ground state in the $\mu/t \ll 1$ limit. In both these (gapped) regimes, there seem to be no MZMs. However, as was just argued, the MZMs are protected by the bulk gap. Therefore, we expect the bulk gap to close as we vary μ from zero to $\pm\infty$, characteristic of a quantum phase transition. This is easily seen to be true from the bulk excitation spectrum given by Eq. (2.9), which closes at $k = 0, \pi$ for $\mu = \pm 2t$ respectively (see Figure 2.3). Since the Kitaev point is inside the region $|\mu| < 2t$, we may conjecture that the MZMs are protected inside the phase that this region defines. As $|\mu|$ is increased, the bulk gap closes at the lines $|\mu| = 2t$ of critical points, and is again finite for $|\mu| > 2t$. From anywhere in these regions with $|\mu| > 2t$, one can continuously tune to the trivial regime $\mu = \pm\infty$ without

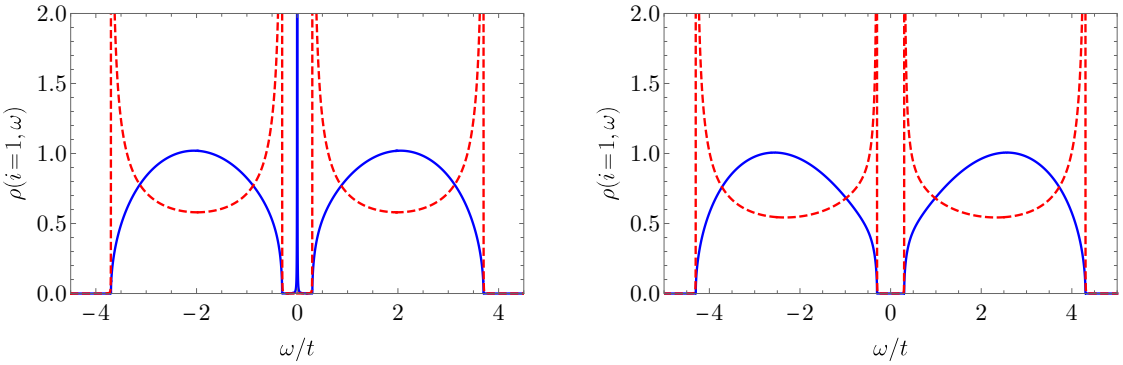

FIGURE 2.4 – Boundary LDOS (blue) of a semi-infinite Kitaev chain in (a) the topological phase with $\mu = 1.7t$, and (b) the trivial phase with $\mu = 2.3t$. In both plots, $\Delta = 0.5t$ and shown in dashed red is the bulk LDOS. Note in (a) the presence of a zero-energy subgap excitation at the boundary that is due to the MZM, which is missing in (b).

encountering a phase transition where the bulk gap closes. Since the MZMs are clearly absent in the trivial regime, we may conjecture that they are absent in the entire regions defined by $|\mu| > 2t$. These two distinct phases are called the *topological phase* ($|\mu| < 2t$) and the *trivial phase* ($|\mu| > 2t$) and are characterised respectively by the presence and absence of boundary MZMs.[5] Superconductors like the Kitaev chain that support protected gapless boundary modes in a certain phase are known as *topological superconductors* [4, 20–22]. We will shortly encounter the reason for this nomenclature. The local density of states (LDOS) at the ends of the Kitaev chain provides an explicit check of the verity of these statements. The boundary LDOS can be obtained from the boundary Green function of the Kitaev chain, which is explicitly calculated for a semi-infinite chain in Appendix A. The results for the topological and trivial phases are shown in Figures 2.4a-b. Figure 2.4a confirms our conjecture that a MZM (signified by the infinitely sharp peak at zero energy) is present even away from the Kitaev point, throughout the topological phase. Figure 2.4b, which shows the boundary LDOS in the trivial phase just beyond the critical line $\mu = 2t$, is characterised by the absence of a MZM and the associated subgap zero-energy excitation.

[5] Note that $\Delta = 0$ and $|\mu| < 2t$ is a line segment inside the topological region of the phase diagram that characterises a normal metal with a gapless excitation spectrum.

In Figures 2.4a-b, note that the bulk LDOS of both phases look qualitatively identical. The distinguishing feature between the two phases has thus far been the presence or absence of boundary localised MZMs, whose presence results in a two-fold degenerate ground state for an open, infinite chain. Even in the case of a closed chain, when there are no boundary MZMs present, the bulk gap closes at the lines of critical points $\mu = \pm 2t$. We then have no means (yet) of distinguishing between the different phases of the system, if at all they still exist. It is clear that we must study the bulk properties of both phases in more detail, hoping to find differences that can be used to construct something like an order parameter, in order to distinguish the two phases in the bulk itself. To this end, consider the bulk Hamiltonian of a closed Kitaev chain given by Eq. (2.8). Both regions, $\left|\mu\right| < 2t$ and $\left|\mu\right| > 2t$, are superconducting, so the usual local order parameter description (Landau-Ginzburg theory) is not sufficient to distinguish the two. There exists another picture of the BCS theory of superconductivity that exploits an analogy between the BdG Hamiltonian in (2.8) and that of a spin in a magnetic field, due to Anderson [23]. For details on the application of this formalism to s-wave superconductors, see Refs. [23, 24]. We apply this formalism to the Kitaev chain, following Refs. [3, 25]. The analogy with a magnet rests on the observation that the BdG matrix in (2.8) can be written as

$$h_K(k) = (-2t\cos k - \mu)\tau^z - (2\Delta \sin k)\tau^y \equiv \boldsymbol{d}_k \cdot \boldsymbol{\tau}, \tag{2.12}$$

where $\boldsymbol{d}_k = -(0, 2t\cos k + \mu, 2\Delta \sin k)$, and $\boldsymbol{\tau} = (\tau^x, \tau^y, \tau^z)$ is a Pauli spin-1/2 operator acting on the space of Nambu spinors, variously called the Nambu space, isospin space, or particle-hole space. Imagine a second-quantised isospin operator $\boldsymbol{\tau}_k = (c_k^\dagger \quad c_{-k})\boldsymbol{\tau}(c_k \quad c_{-k}^\dagger)^\intercal$ for every k in the first Brillouin zone. The $\boldsymbol{d}_k$ vector plays the role of a site (k) dependent magnetic field for a chain of isospins $\boldsymbol{\tau}_k$ in momentum space. If there are no pairing correlations ($\Delta = 0$), then $\boldsymbol{\tau}_k$ is magnetised aligned along $-\hat{z}$ (in isospin space) for $(-2t\cos k) < \mu$ i.e. for occupied electron states below the Fermi level, and along $\hat{z}$ for $(-2t\cos k) > \mu$ i.e. for empty electron states above the Fermi level. There is then a sharp domain wall in the isospin chain at the Fermi momentum,

where the $\boldsymbol{\tau}_k$ reverse their orientation. For non-zero pairing correlations Δ, $\boldsymbol{d}_k$ tilts the quantisation axis away from $\hat{z}$.

Let us see if we can use the perspective offered by this analogy with a magnet to distinguish between the topological and trivial phases of the Kitaev chain. Clearly, we must look at the profile of $\boldsymbol{d}_k$ as this dictates the form of the BdG matrix $h_K(k)$. To this end, we define the unit vector $\hat{\boldsymbol{d}}_k = \boldsymbol{d}_k/E(k)$ which is ill-defined at the transitions $\mu = \pm 2t$, and study its properties within the topological and trivial phases. Note that $\hat{\boldsymbol{d}}_k$ is restricted to the y-z plane, and so can be located anywhere on a unit circle (S^1) centred at the origin on this plane. The momentum k takes values in the first Brillouin zone $(-\pi, \pi)$, which is also a circle as the end points are identified due to being related by a reciprocal lattice vector 2π. Therefore, the function $\hat{\boldsymbol{d}}(k) = \hat{\boldsymbol{d}}_k$ is really a map $\hat{\boldsymbol{d}} : S^1 \to S^1$, which has an associated integer-valued winding number w captured by the homotopy group[6] $\pi_1(S^1) = \mathbb{Z}$ [26]. This expresses the fact that one can wrap a circle around a circle clockwise or anticlockwise, once, twice, thrice and so on. Maps that wrap with different winding numbers cannot be continuously deformed into one other; they are said to be *homotopically inequivalent*.

Consider first the trivial phase $|\mu| > 2t$. For $\mu < -2t$, the z-component $\hat{z} \cdot \boldsymbol{d}_k = -(2t\cos k + \mu)$ is strictly positive for all k. Therefore, as k sweeps through the (circular) Brillouin zone $(-\pi, \pi)$, the unit vector $\hat{\boldsymbol{d}}_k$ oscillates like a pendulum in the upper half plane, due to the $\sin k$ in the y-component. Similarly, for $\mu > 2t$, $\hat{z} \cdot \boldsymbol{d}_k$ is strictly negative for all k and so the unit vector $\hat{\boldsymbol{d}}_k$ oscillates in the lower half plane. In both cases, we note that $\hat{\boldsymbol{d}}_k$ does not wind around as k sweeps the Brillouin zone and so $w = 0$ (see Figure 2.5a).

Now, consider the topological phase $|\mu| < 2t$. This is the case when the Fermi level lies inside the conduction band $(-2t\cos k)$, and so the z-component $\hat{z} \cdot \boldsymbol{d}_k = -(2t\cos k + \mu)$

[6] Two maps are said to be homotopic if they can be 'continuously deformed' into one other. More formally, two maps $f_0, f_1 : X \to Y$ are homotopic if there exists, for $t \in [0,1]$, a t-parametrised family of continuous maps (called a homotopy) $f_t : X \to Y$ such that $f_{t=0} = f_0$ and $f_{t=1} = f_1$. This can be used to impose an equivalence relation on the space of maps from X to Y. $\pi_n(X)$ is defined to be the set of equivalence classes (under homotopy) of maps from the n-sphere S^n to the target space X. It can be shown that this set has a natural group structure, and so $\pi_n(X)$ is called the n-th *homotopy group* of X.

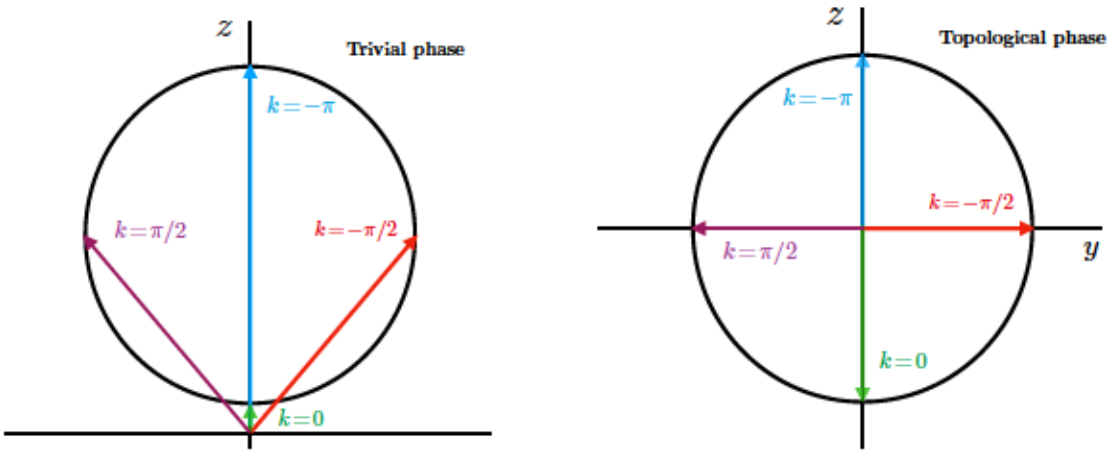

FIGURE 2.5 – Illustration of the winding of $\boldsymbol{d}_k$ as k sweeps the first Brillouin zone in (a) the trivial phase, and (b) the topological phase with $\Delta > 0$. Note that $\boldsymbol{d}_k$ winds clockwise once in (b), but does not wind in (a). For clarity, we have illustrated the winding of $\boldsymbol{d}_k$, instead of that of the unit vector $\hat{\boldsymbol{d}}_k$ as discussed in the text.

has two zeros where it changes sign. For $\Delta > 0$, it is easy to see by following the evolution of $\hat{\boldsymbol{d}}_k$ with k that it winds around once, clockwise and so $w = -1$ (see Figure 2.5b). Similarly, it can be seen that $\hat{\boldsymbol{d}}_k$ winds anti-clockwise once if $\Delta < 0$ and so $w = 1$. If the isospins are visualised as a chain of spins in momentum space with length equal to the first Brillouin zone, these two cases with a non-zero winding number result in topologically non-trivial textures on this chain that cannot be deformed into one another or to a trivial texture (with all isospins pointed up for example) by means of purely local deformations. Note that for $\Delta = 0$ (the gapless metal inside the topological region), there is again no winding. We thus arrive at the conclusion that the topological and trivial phases are distinguished by the winding number w (called a topological invariant) of the map $\hat{\boldsymbol{d}} : k \to \hat{\boldsymbol{d}}_k$. Although the local bulk properties of both phases remain the same, they are topologically inequivalent as the maps $\boldsymbol{d}_{\mathrm{TR}}$ and $\boldsymbol{d}_{\mathrm{TP}}$ that define the BdG Hamiltonians in the trivial and topological phases are not homotopic. This allows us to distinguish the different phases in the bulk itself, without looking at the boundaries.

Note that even though the winding number w is integer-valued, only the phases with $w = \pm 1$ are accessible to the Kitaev chain. That w is integer-valued is due to

the fact that the $\hat{x} \cdot \hat{\boldsymbol{d}}_k = 0$, which restricts $\hat{\boldsymbol{d}}_k$ to the unit circle in the y-z plane. No other model specific properties are invoked; it can be seen that taking multiple copies of the Kitaev chain Hamiltonian will also result in a similar $\hat{\boldsymbol{d}}_k$ vector with the x-component equal to zero. To access phases with winding numbers $|w| > 1$, multiple such copies are required.[7] An equivalent statement to the above is that the BdG matrix $h_K(k)$ of the Kitaev chain satisfies a chiral symmetry that places it in the BDI symmetry class in the classification table of non-interacting topological insulators and superconductors [27–29]. The BDI class has a $\mathbb{Z}$ topological invariant. If we consider perturbations to the Kitaev chain Hamiltonian that result in $\hat{x} \cdot \hat{\boldsymbol{d}}_k \neq 0$, then this moves the Hamiltonian to class D, which admits only a $\mathbb{Z}_2$ topological invariant and thus only two topologically distinct phases, of which one will be a trivial phase with no end modes in an open chain. Finally, we remark that in the presence of interactions, the winding number does not correctly classify the different phases of Majorana chains. Fidkowski and Kitaev [30, 31] have shown that the $\mathbb{Z}$ classification is broken down to $\mathbb{Z}_8$ in the presence of interactions for a Majorana chain in class BDI. Even in the absence of interactions, a homotopy classification based on winding numbers is insufficient to classify all topological superconductors, but generally works for two-band Hamiltonians like those of the Kitaev chain in the BdG formulation of Eq. (2.8)[27].

With this, we pause the discussion of the Kitaev chain to pursue other toy models that might support emergent, unpaired Majorana fermions. A discussion of experimental realisations of the Kitaev chain is relegated to a future section.

2.1.2 *Read-Green superconductor*

Let us now try to construct a two-dimensional version of the Kitaev chain. Since the Kitaev chain is a one-dimensional spinless p-wave superconductor, it is natural to also look for unpaired Majorana fermions in a two-dimensional, spinless p-wave

[7] This will also result in multiple MZMs at the ends of the chain. In absence of the protecting symmetries that define the BDI class, multiple MZMs at one end of the chain will generally pair up and move away from zero energy.

superconductor. To construct a specific model Hamiltonian, we begin by stacking (along $\hat{y}$) N Kitaev chains that have N fermionic sites each. In addition to intra-chain hopping and pairing, there can now also be inter-chain hopping and pairing of electrons. We know how to generalise the tight-binding dispersion in the Kitaev chain to a square lattice; $-2t\cos k \to -2t(\cos k_x + \cos k_y)$. In the limit $N \to \infty$ and with periodic boundary conditions, a natural guess for the bulk Hamiltonian can be obtained from generalising that of the Kitaev chain in Eq. (2.8) to

$$H_R = \frac{1}{2}\sum_{\mathbf{k}\in FBZ}\begin{pmatrix} c_{\mathbf{k}}^\dagger & c_{-\mathbf{k}}\end{pmatrix}\begin{bmatrix} -2t(\cos k_x+\cos k_y)-\mu & 2i\Delta\sin k_x + f(\mathbf{k}) \\ -2i\Delta\sin k_x + f^*(\mathbf{k}) & 2t(\cos k_x+\cos k_y)+\mu\end{bmatrix}\begin{pmatrix} c_{\mathbf{k}} \\ c_{-\mathbf{k}}^\dagger\end{pmatrix}, \quad (2.13)$$

where $\mathbf{k} = (k_x, k_y)$ is now a momentum vector in the first Brillouin zone $(-\pi,\pi)\times(-\pi,\pi)$ and $f(\mathbf{k})$ is a contribution to the p-wave pairing potential that must be determined according to our preferences; we would like the bulk excitation spectrum to look as close to the Kitaev chain as possible, in the hope that the two-dimensional model will also support unpaired Majorana fermions. The eigenvalues of the BdG matrix are $\pm E(\mathbf{k})$, where the bulk excitation spectrum is

$$E(\mathbf{k}) = \sqrt{(2t\cos k_x + 2t\cos k_y + \mu)^2 + 4\Delta^2\sin^2 k_x + |f|^2 + 2i\Delta\sin k_x(f - f^*)}. \quad (2.14)$$

Two intuitive choices are $f = \pm 2\Delta\sin k_y$, which sets the last term inside the square root to zero.[8] For the choice $f = -2\Delta\sin k_y$, the BdG Hamiltonian in Eq (2.13) becomes

$$H_R = \frac{1}{2}\sum_{\mathbf{k}\in FBZ}\begin{pmatrix} c_{\mathbf{k}}^\dagger & c_{-\mathbf{k}}\end{pmatrix}\begin{bmatrix} -2t(\cos k_x+\cos k_y)-\mu & 2i\Delta(\sin k_x + i\sin k_y) \\ -2i\Delta(\sin k_x - i\sin k_y) & 2t(\cos k_x+\cos k_y)+\mu\end{bmatrix}\begin{pmatrix} c_{\mathbf{k}} \\ c_{-\mathbf{k}}^\dagger\end{pmatrix}, \quad (2.15)$$

which has a bulk excitation spectrum given by

$$E(\mathbf{k}) = \sqrt{(2t\cos k_x + 2t\cos k_y + \mu)^2 + 4\Delta^2(\sin^2 k_x + \sin^2 k_y)}. \quad (2.16)$$

This model of a spinless $k_x + ik_y$ superconductor will henceforth be called the Read-Green superconductor, after Read and Green [32] who studied the continuum version

[8] This choice can also be motivated from the need to avoid gapless nodal points or lines in the Brillouin zone, for generic values of μ and Δ. except perhaps at isolated critical points.

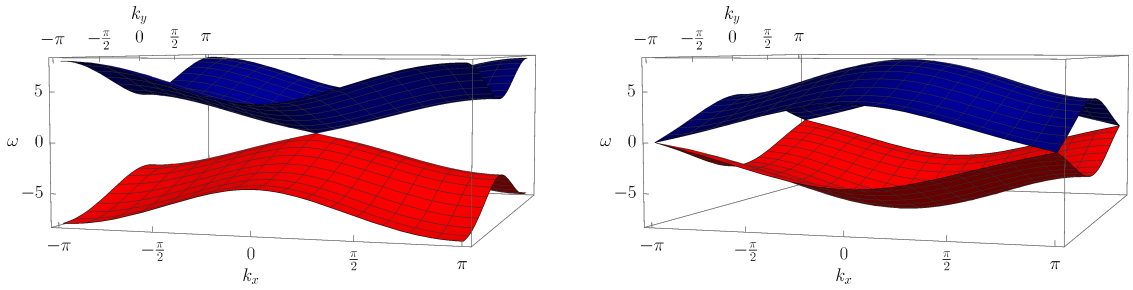

FIGURE 2.6 – Closures of the gap in the bulk excitation spectrum $\omega(\mathbf{k})$ of the Read-Green superconductor. (a) For $\mu = -4t$, the gap closes at $\mathbf{k} = 0$, and (b) for $\mu = 4t$, the gap closes at $\mathbf{k} = (\pi, \pi)$. In both plots, $\Delta = 0.7t$. Recall that only one band (blue) with energies $\omega \geq 0$ contains physically distinct states.

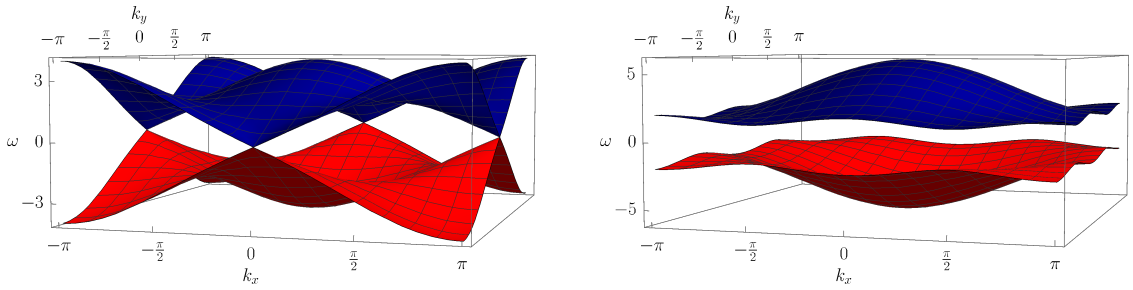

FIGURE 2.7 – (a) Closure of the bulk gap at $\mathbf{k} = (0, \pi)$ and $\mathbf{k} = (\pi, 0)$ for $\mu = 0$. (b) Bulk excitation spectrum away from critical points for $\mu = 2t$. In both plots $\Delta = 0.7t$.

of the lattice model above. Note that the bulk excitation spectrum becomes gapless at the points $\mathbf{k} \in \{(0, \pi), (\pi, 0)\}$ for $\mu = 0$, at $\mathbf{k} = (\pi, \pi)$ for $\mu = 4t$, and at $\mathbf{k} = 0$ for $\mu = -4t$ (see Figures 2.6a-b and Figure 2.7a). Away from these critical values of μ, the bulk remains fully gapped throughout the Brillouin zone (see Figure 2.7b). The line of critical points at $\mu = \pm 4t$ might have been anticipated as a straightforward generalisation of the critical lines at $\mu = \pm 2t$ in the Kitaev chain. In analogy, one may guess that the regions $|\mu| > 4t$ are topologically trivial with no edge states (in particular, the unpaired Majorana fermions we are looking for). The difference between the regions $-4t < \mu < 0$ and $0 < \mu < 4t$, separated by a line of gapless critical points, remains to be seen. The presence or absence of edge states will manifest in the edge spectral function of the Read-Green superconductor. An inverse Fourier transform of Eq. 2.15 gives the real space lattice Hamiltonian, which for a semi-infinite plane geometry

with a single edge reads as

$$H_R = \sum_{x=-\infty}^{\infty}\sum_{y=1}^{\infty}\Big[-t\left(c^\dagger_{x+1,y}c_{x,y} + c^\dagger_{x,y+1}c_{x,y} + \text{h.c.}\right) + \left(\Delta c^\dagger_{x+1,y}c^\dagger_{x,y} + i\Delta c^\dagger_{x,y+1}c^\dagger_{x,y} + \text{h.c.}\right) - \mu c^\dagger_{x,y}c_{x,y}\Big]. \quad (2.17)$$

Since translation invariance is broken only along $\hat{y}$, one may work in a mixed (k_x, y) representation and calculate the edge spectral function $A_E(k_x, \omega)$. This has been done in Appendix A, and results for the three distinct phases discovered above are shown in Figures 2.8a-c. As expected, the regions $|\mu| > 4t$ form a trivial phase with an edge spectral function not very different to that of the bulk, fully gapped with only the usual Bogoliubov quasiparticle excitations. However, the regions $-4t < \mu < 0$ and $0 < \mu < 4t$ are distinct topological phases that host linearly dispersing, chiral edge excitations that lie within the bulk energy gap. The two phases, $-4t < \mu < 0$ and $0 < \mu < 4t$, are distinguished by the opposite chiralities of their edge modes, as evident from the opposite signs of the group velocities $(\partial\omega/\partial k_x)$ of the subgap excitations in Figures 2.8a-b. For example, the edge modes of the $-4t < \mu < 0$ phase are all right-moving on the single boundary of the semi-infinite plane.

In order to distinguish between these phases without regard to the edge modes, one can try to construct a topological invariant as done for the Kitaev chain earlier. To this end, we cast the BdG matrix in Eq. (2.15) as an isospin Hamiltonian,

$$h_R(\mathbf{k}) = -\Big[2t(\cos k_x + \cos k_y) + \mu\Big]\tau^z - (2\Delta \sin k_x)\tau^y - (2\Delta \sin k_y)\tau^x \equiv \hat{\boldsymbol{d}}(\mathbf{k}) \cdot \boldsymbol{\tau}. \quad (2.18)$$

Unlike the Kitaev chain, all three components of $\boldsymbol{d}(\mathbf{k})$ are non-zero, which implies the unit vector $\hat{\boldsymbol{d}}(\mathbf{k})$ can generally point anywhere on the unit sphere S^2. This indirectly also implies that the Read-Green superconductor falls under symmetry class D in the periodic table of topological superconductors [27–29]. Also in two-dimensions, the Brillouin zone $(-\pi, \pi)\times(-\pi, \pi)$ is a Cartesian product of two circles S^1, and is therefore a torus T^2, which means we must now consider homotopy classes of maps $\hat{\boldsymbol{d}} : T^2 \to S^2$ and can therefore no longer rely on the exhaustive table of

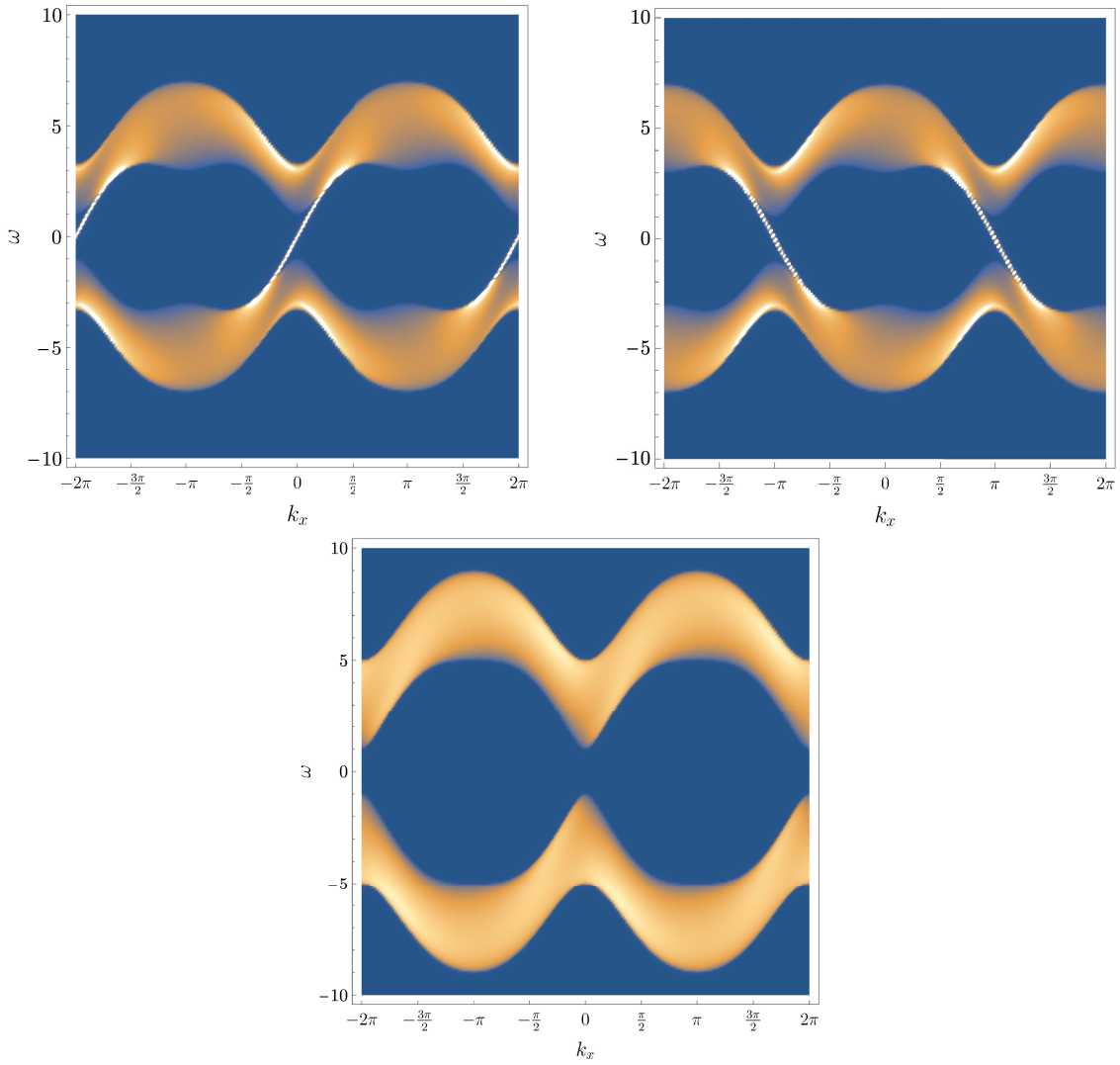

FIGURE 2.8 – (Clockwise from top left) Intensity plot of the edge spectral function $A_E(k_x, \omega)$ of a semi-infinite planar Read-Green superconductor in (a) topological phase with $\mu = -3t$, (b) topological phase with $\mu = 3t$, and (c) trivial phase with $\mu = -5t$. In all plots, $\Delta = 1.5t$, ω is in units of t, and k is really ka where a is a lattice constant we have set to unity. The two distinct topological phases [(a) and (b)] host chiral edge modes of opposing chiralities, featuring as linearly dispersing subgap states. Recall that only excitations with energies $\omega > 0$ are physical. The two-band structure is an artifact of the BdG formalism, which doubles the number of physical degrees of freedom.

homotopy groups $\pi_n(S^m)$.[9] Classifying maps between general topological manifolds up to homotopy is an extremely difficult problem. However, in the present case of interest, that is maps from T^2 to S^2, we find our salvation in the Hopf theorem [33] in differential topology; two continuous maps from a compact, oriented, n-dimensional manifold to the n-sphere S^n are homotopic if and only if they have the same *Brouwer degree*. The Brouwer degree of a continuous map is (informally) the number of times it wraps the domain manifold around S^n, and is therefore integer-valued.[10] An immediate result of the Hopf theorem is that homotopy classes of maps $\hat{\boldsymbol{d}} : T^2 \to S^2$ are indexed by an integer. Therefore, we arrive at the result that there exists a $\mathbb{Z}$ topological invariant for the Read-Green superconductor, in accordance with the result in Refs. [27–29] for class D superconductors in two dimensions. The topological invariant in this case (which we simply state without proof) is the first Chern number

$$C_1 = \frac{1}{4\pi}\int_{\mathrm{FBZ}} \mathrm{d}^2k \frac{\boldsymbol{d}(\mathbf{k})}{|\boldsymbol{d}(\mathbf{k})|^3}\cdot\left(\frac{\partial \boldsymbol{d}}{\partial k_x}\times\frac{\partial \boldsymbol{d}}{\partial k_y}\right). \tag{2.19}$$

Similar to the Kitaev chain, only the phases with Chern numbers 0 (trivial) and ±1 (topological with opposite chiralities) are accessible to the Read-Green lattice Hamiltonian as presented above.

From an explicit calculation of the edge spectral function of a Read-Green superconductor in a semi-infinite plane geometry, we have seen the existence of gapless, linearly dispersing, chiral edge modes. We will now show that these are *chiral Majorana fermions*, following Refs. [3, 32, 34]. To this end, it is convenient to work with a continuum model, instead of the lattice version discussed above. To obtain such a model, note that the phase transition at $\mu = -4t$ is accompanied by a closing of the bulk energy gap at $\mathbf{k} = 0$. Linearising Eq. (2.15) near this point, and defining $\tilde{\mu} = \mu + 4t$,

[9] Each choice of parameters μ, Δ in the Hamiltonian defines a map $\hat{\boldsymbol{d}}$, and so there is an entire family of them. The problem is that of classifying these maps up to homotopy.

[10] As the domain manifold and S^n are both oriented, there is a notion of orientation for the wrapping, which is why the degree can be positive or negative. This is just a generalisation of the concept of winding numbers of maps between circles, discussed in the previous section on the Kitaev chain.

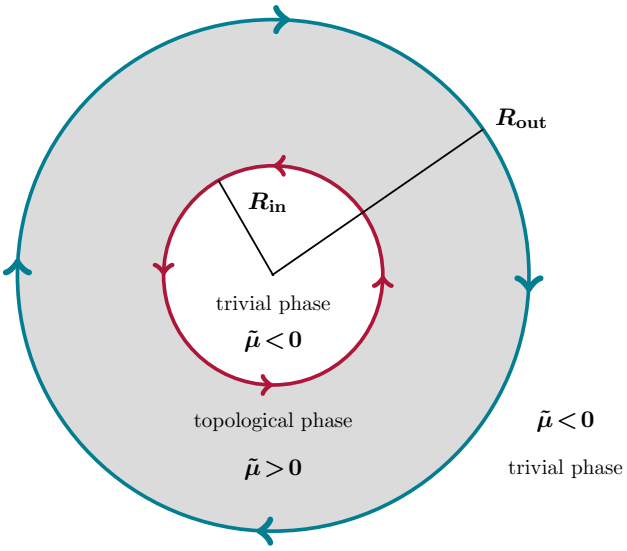

FIGURE 2.9 – Read-Green superconductor on an annulus. The inner and outer edges host chiral Majorana fermions with opposing chiralities.

we obtain[11]

$$\begin{aligned} H_R &= \frac{1}{2}\int \mathrm{d}^2\mathbf{k} \begin{pmatrix} c_{\mathbf{k}}^\dagger & c_{-\mathbf{k}} \end{pmatrix} \begin{bmatrix} -\tilde{\mu} & 2i\Delta(k_x+ik_y) \\ -2i\Delta(k_x-ik_y) & \tilde{\mu} \end{bmatrix} \begin{pmatrix} c_{\mathbf{k}} \\ c_{-\mathbf{k}}^\dagger \end{pmatrix}, \\ &= \frac{1}{2}\int \mathrm{d}(x,y)\,\mathrm{d}(x',y')\,\delta(x-x')\delta(y-y') \\ &\qquad \times \begin{pmatrix} c_{x',y'}^\dagger & c_{x',y'} \end{pmatrix} \begin{bmatrix} -\tilde{\mu} & 2\Delta(\partial_x+i\partial_y) \\ -2\Delta(\partial_x-i\partial_y) & \tilde{\mu} \end{bmatrix} \begin{pmatrix} c_{x,y} \\ c_{x,y}^\dagger \end{pmatrix}, \end{aligned} \tag{2.20}$$

where we have Fourier transformed back to real space in the second line, and $\mathrm{d}(x,y) = \mathrm{d}x\,\mathrm{d}y$. This model then captures the transition from the topological ($\tilde{\mu}>0$) to trivial phase ($\tilde{\mu}<0$) at $\tilde{\mu}=0$. Instead of a rectangular geometry, we consider this model in its topological phase on an annulus of inner (outer) radius R_{in} (R_{out}), with a trivial phase (or vacuum) forming outside (see Figure 2.9) [3]. Using polar coordinates $\mathbf{r}=(r,\theta)$, a

[11] The continuum and lattice models only agree near $\mathbf{k}=0$. This means that the momentum integral should be regulated in the Hamiltonian. We could also just consider the continuum version as a model of its own right, severing ties with the lattice model. Such subtleties are not our concern here.

Hamiltonian describing such a setup can be written as

$$H_R = \frac{1}{2}\int \mathrm{d}(r,\theta)\,\mathrm{d}(r',\theta')\begin{pmatrix} c^\dagger_{r',\theta'} & c_{r',\theta'}\end{pmatrix}\delta(r-r')\delta(\theta-\theta')h_R(r,\theta)\begin{pmatrix} c_{r,\theta} \\ c^\dagger_{r,\theta}\end{pmatrix}, \tag{2.21}$$

where $\mathrm{d}(r,\theta) = r\,\mathrm{d}r\,\mathrm{d}\theta$ and the BdG Hamiltonian $h_R(r,\theta)$ is defined as

$$h_R(r,\theta) \equiv \begin{bmatrix} -\tilde{\mu}(r) & 2\Delta e^{i\theta}(\partial_r + ir^{-1}\partial_\theta) \\ -2\Delta e^{-i\theta}(\partial_r - ir^{-1}\partial_\theta) & \tilde{\mu}(r)\end{bmatrix}, \tag{2.22}$$

where $\tilde{\mu}(r) > 0$ inside the annulus, and $\tilde{\mu} < 0$ outside. Instead of a discontinuous step function, we assume a smooth, slowly varying profile for $\tilde{\mu}(r)$ [one example is $\tanh(r)$ near R_{in} and $\tanh(-r)$ near R_{out} with some smooth interpolation in between]. The factor $e^{i\theta}$ disappears upon rewriting H_R in terms of new fermion fields $\psi^\dagger_{r,\theta} = e^{i\theta/2}c^\dagger_{r,\theta}$ and $\psi_{r,\theta} = e^{-i\theta/2}c_{r,\theta}$.[12] Note, however, that $\psi^{(\dagger)}_{r,\theta}$ obey *anti-periodic* boundary conditions $\psi^{(\dagger)}_{r,\theta+2m\pi} = (-1)^m\psi^{(\dagger)}_{r,\theta}$.

Say the BdG Hamiltonian has eigenvectors $\chi_m(r,\theta) = [u_m(r,\theta) \quad v_m(r,\theta)]^\intercal$ with eigenvalues E_m defined by $h_R\chi_m = E_m\chi_m$. Since h_R is self-adjoint, it admits a spectral decomposition of the form

$$\delta(r-r')\delta(\theta-\theta')h_R(r,\theta) = \sum_m E_m\chi_m(r,\theta)\chi^\dagger_m(r',\theta'). \tag{2.23}$$

Using this in Eq. (2.21), we find

$$H_R = \sum_m \frac{E_m}{2}\left\{\int \mathrm{d}(r',\theta')\left[u_m(r',\theta')\psi^\dagger_{r',\theta'} + v_m(r',\theta')\psi_{r',\theta'}\right] \right. \\ \left. \times \int \mathrm{d}(r,\theta)\left[u^*_m(r,\theta)\psi_{r,\theta} + v^*_m(r,\theta)\psi^\dagger_{r,\theta}\right]\right\}, \tag{2.24}$$

which is diagonal in the Bogoliubov quasiparticle operators

$$\gamma_m = \int \mathrm{d}(r,\theta)\,(u^*_m\psi_{r,\theta} + v^*_m\psi^\dagger_{r,\theta}), \quad \gamma^\dagger_m = \int \mathrm{d}(r,\theta)\,(u_m\psi^\dagger_{r,\theta} + v_m\psi_{r,\theta}). \tag{2.25}$$

The requirement of non-zero γ_m imposes anti-periodic boundary conditions (4π periodicity) on $u_m(r,\theta)$ and $v_n(r,\theta)$, so that the integrands in Eq. (2.25) are not odd in $\theta \in (0, 2\pi)$.

[12] Note that the pairing term actually transforms as $e^{i\theta}c^\dagger_{r,\theta}(\partial_r + ir^{-1}\partial_\theta)c^\dagger_{r,\theta} = \psi^\dagger_{r,\theta}(\partial_r + ir^{-1}\partial_\theta + 1/2r)\psi^\dagger_{r,\theta}$. The extra $1/2r$ factor disappears as $(\psi^\dagger_{r,\theta})^2 = 0$. Similarly for the pairing term involving $\psi_{r,\theta}$.

Let us now solve for the eigenvectors χ_m, whose component functions u_m and v_m are solutions to the following system of coupled first-order differential equations:

$$-\tilde{\mu}(r)u(r,\theta) + 2\Delta(\partial_r + ir^{-1}\partial_\theta)v(r,\theta) = Eu(r,\theta), \tag{2.26}$$

$$\tilde{\mu}(r)v(r,\theta) - 2\Delta(\partial_r - ir^{-1}\partial_\theta)u(r,\theta) = Ev(r,\theta). \tag{2.27}$$

We are primarily interested in the nature of the chiral edge states we found in a brute force calculation of the edge spectral function in the lattice model. To this end, we may approximate r^{-1} in Eqs. (2.26)-(2.27) by $R^{-1} \in \{R_{\text{out}}^{-1}, R_{\text{in}}^{-1}\}$, which form the two boundaries of the annulus under consideration. Solving Eqs. (2.26)-(2.27) is equivalent to solving a single second-order partial differential equation for one of $u(r,\theta)$ or $v(r,\theta)$. The former satisfies

$$\frac{2\Delta}{\tilde{\mu}(r)^2 - E^2}\left[\partial_r^2 u(r,\theta) + R^{-2}\partial_\theta^2 u(r,\theta)\right] - \frac{1}{2\Delta}u(r,\theta) \\ - \frac{2}{1-[E/\tilde{\mu}(r)]^2}\cdot\frac{\partial_r\tilde{\mu}(r)/\tilde{\mu}(r)}{\tilde{\mu}(r)/\Delta}\left[\partial_r u(r,\theta) - iR^{-1}\partial_\theta u(r,\theta)\right] \approx 0. \tag{2.28}$$

Let us assume that $\partial_r\tilde{\mu}(r)/\tilde{\mu}(r) \ll \tilde{\mu}(r)/\Delta \sim \xi^{-1}$, where ξ is the coherence length of the superconductor; the last term in Eq. (2.28) can thus be dropped. This is similar to a WKB approximation; one considers r 'slightly away' from the edge of the annulus (where $\tilde{\mu}(r)$ changes sign) so that the spatial variation of $\tilde{\mu}(r)$ is slow, but close enough to the edge that the approximation $r^{-1} \approx R^{-1}$ made above still holds. Using a separation of variables, by substituting in $u(r,\theta) = f(r)g(\theta)$ and then dividing throughout by $f(r)g(\theta)$, we obtain

$$\frac{1}{f(r)}\partial_r^2 f + \left[\frac{E^2 - \tilde{\mu}(r)^2}{4\Delta^2}\right] = -\frac{1}{R^2 g(\theta)}\partial_\theta^2 g \equiv \lambda^2, \tag{2.29}$$

where λ^2 is a constant, since θ and r are independent variables. A specific solution to the angular equation is $g(\theta) = \exp(iR\lambda\theta)$. Using the anti-periodic boundary condition $g(\theta + 2\pi) = -g(\theta)$ determines $\lambda = m/2R$, where $m \in 2\mathbb{Z}+1$ is an odd integer. Therefore, the angular part of $u_m(r,\theta)$ is then

$$g_m(\theta) = \exp\left(\frac{im\theta}{2}\right), \qquad m \in 2\mathbb{Z} + 1. \tag{2.30}$$

The radial equation is then

$$\partial_r^2 f + \left[\frac{E^2}{4\Delta^2} - \frac{m^2}{4R^2} - \frac{\tilde{\mu}(r)^2}{4\Delta^2}\right] f(r) = 0. \tag{2.31}$$

Now, *assume* $E_m = \pm m\Delta/R$. Then given $R \in \{R_{\text{in}}, R_{\text{out}}\}$, the two solutions (to the radial equation) are

$$f_{\text{in}}(r) \approx \exp\left[-\frac{1}{2\Delta}\int_{R_{\text{in}}}^{r} \mathrm{d}r'\,\tilde{\mu}(r')\right], \qquad f_{\text{out}}(r) \approx \exp\left[-\frac{1}{2\Delta}\int_{r}^{R_{\text{out}}} \mathrm{d}r'\,\tilde{\mu}(r')\right]. \tag{2.32}$$

These solutions are valid in the respective approximations $r \sim R_{\text{in}}$ and $r \sim R_{\text{out}}$; since $\tilde{\mu} > 0$ inside the domain of integration in the exponents of f_{in} and f_{out}, these solutions are exponentially suppressed away from the inner and outer boundaries (respectively) of the annulus.[13] It remains to be seen which of $E_m = \pm m\Delta/R$ correspond to E_m^{in} and E_m^{out}.

The eigenfunctions $v_m^{\text{in/out}}(r,\theta)$ can be obtained from $u_m^{\text{in/out}}(r,\theta)$ using Eq. (2.27). For $v_m^{\text{in}}(r,\theta)$,

$$\begin{aligned} v_m^{\text{in}}(r,\theta) &= -\left[\frac{2\Delta}{E_{\text{in}} - \tilde{\mu}(r)}\right](\partial_r - iR_{\text{in}}^{-1}\partial_\theta)u_m^{\text{in}}(r,\theta), \\ &= u_m^{\text{in}}(r,\theta)\left[\frac{\tilde{\mu}(r) - m\Delta/R_{\text{in}}}{E_m^{\text{in}} - \tilde{\mu}(r)}\right], \end{aligned} \tag{2.33}$$

where the Leibniz integral rule has been used to calculate $\partial_r f_{\text{in}}$. For $E_m^{\text{in}} = m\Delta/R_{\text{in}}$, we then have the result $v_m^{\text{in}}(r,\theta) = -u_m^{\text{in}}(r,\theta)$. Similarly,

$$v_m^{\text{out}}(r,\theta) = -u_m^{\text{out}}(r,\theta)\left[\frac{\tilde{\mu}(r) + m\Delta/R_{\text{out}}}{E_m^{\text{out}} - \tilde{\mu}(r)}\right],$$

and for $E_m^{\text{out}} = -m\Delta/R_{\text{out}}$, we get $v_m^{\text{out}}(r,\theta) = u_m^{\text{out}}(r,\theta)$. The eigenvectors $\chi_m^{\text{in/out}} = (u_m^{\text{in/out}} \quad v_m^{\text{in/out}})^{\intercal}$ and respective eigenvalues $E_m^{\text{in/out}}$ of the BdG Hamiltonian $h_R(r,\theta)$,

[13] That these are solutions to the radial equation can be verified by direct substitution into the radial equation, and calculating the derivatives $\partial_r f$ and $\partial_r^2 f$ using the Leibniz integral rule. In calculating $\partial_r^2 f$, one actually obtains a term proportional to $\partial_r \tilde{\mu}$. Such terms can be ignored under the assumption $\partial_r \tilde{\mu}(r)/\tilde{\mu}(r) \ll \tilde{\mu}(r)/\Delta$ made earlier.

with a suitable choice of normalisation constant $\mathcal{N}^{-1/2}$, read

$$\chi_m^{\text{in}}(r,\theta) = \frac{1}{\sqrt{\mathcal{N}}} e^{im\theta/2} f_{\text{in}}(r) \begin{pmatrix} i \\ -i \end{pmatrix}, \quad E_m^{\text{in}} = \frac{m\Delta}{R_{\text{in}}}, \quad m \in 2\mathbb{Z}+1 \tag{2.34}$$

$$\chi_n^{\text{out}}(r,\theta) = \frac{1}{\sqrt{\mathcal{N}}} e^{in\theta/2} f_{\text{out}}(r) \begin{pmatrix} 1 \\ 1 \end{pmatrix}, \quad E_n^{\text{out}} = -\frac{n\Delta}{R_{\text{out}}}, \quad n \in 2\mathbb{Z}+1 \tag{2.35}$$

where $f_{\text{in/out}}(r)$ are specified by Eq. (2.32). Note that the excitations with wavefunctions given by $\chi_m^{\text{in/out}}$ are exponentially localised at the inner and outer edges of the annulus. In the thermodynamic limit $R_{\text{in/out}} \to \infty$, these excitations become gapless.

To show that the edge excitations are *chiral Majorana fermions*, note that H_R in Eq. (2.24) can be roughly separated into two parts as $H_R = H_{\text{bulk}} + H_{\text{edge}}$, where H_{bulk} describes the gapped quasiparticle excitations in the bulk (irrespective of the topology of the system) and H_{edge} describes the edge excitations just described. Using Eqs. (2.34)-(2.35) in Eq. (2.25), the quasiparticle operators *(edge modes)* that diagonalise H_{edge} are given by

$$\gamma_m^{\text{in}} = \int \frac{\mathrm{d}(r,\theta)}{\sqrt{\mathcal{N}}} e^{im\theta/2} f_{\text{in}}(r) \frac{1}{i} (\psi_{r,\theta} - \psi_{r,\theta}^\dagger), \tag{2.36}$$

$$\gamma_m^{\text{out}} = \int \frac{\mathrm{d}(r,\theta)}{\sqrt{\mathcal{N}}} e^{im\theta/2} f_{\text{out}}(r) (\psi_{r,\theta} + \psi_{r,\theta}^\dagger). \tag{2.37}$$

Crucially, note that $(\gamma_m^{\text{in/out}})^\dagger = \gamma_{-m}$, and the operators $\gamma_m^{\text{in/out}}$ satisfy the Clifford algebra $\{\gamma_m^{\text{in}}, \gamma_{-n}^{\text{in}}\} = \{\gamma_m^{\text{out}}, \gamma_{-n}^{\text{out}}\} = 2\delta_{mn}$ and $\{\gamma_m^{\text{in}}, \gamma_n^{\text{out}}\} = 0$. This identifies the modes on each edge as Majorana fermions. To see this more explicitly and the fact that they are chiral, note that the effective Hamiltonian describing excitations on both edges, using Eq. (2.24), is

$$\begin{aligned} H_{\text{edge}} &= \frac{1}{2} \sum_m \frac{m\Delta}{R_{\text{in}}} \gamma_{-m}^{\text{in}} \gamma_m^{\text{in}} - \frac{1}{2} \sum_n \frac{n\Delta}{R_{\text{out}}} \gamma_{-n}^{\text{out}} \gamma_n^{\text{out}}, \qquad m,n \in \{\dots,-3,-1,1,3,\dots\}, \\ &= \sum_p \frac{p\Delta}{R_{\text{in}}} \gamma_{-p}^{\text{in}} \gamma_p^{\text{in}} - \sum_q \frac{q\Delta}{R_{\text{out}}} \gamma_q^{\text{out}} \gamma_{-q}^{\text{out}}, \quad p \in \{1,3,5,\dots\},\ q \in \{-1,-3,-5,\dots\}, \end{aligned}$$

where we have used the property $(\gamma_m^{\text{in/out}})^\dagger = \gamma_{-m}$ to restrict the angular momentum quantum numbers $p\,(q)$ to the positive (negative) odd integers. These are the only

physical excitations; to see why, recall that the BdG Hamiltonian [for example, in Eq. (2.21)] doubles the number of physical degrees of freedom, so that energy eigenvalues appear in doubled $\pm E$ pairs. This implies that only states with $E_m^{\text{in/out}} \geq 0$ are physically distinct from each other. Therefore, the inner and outer edge modes have positive and negative angular momentum respectively, and are thus *chiral*, with the inner (outer) edge excitations moving anti-clockwise (clockwise), as shown in Figure 2.9. To show that the inner and outer edge modes are separately Majorana fermions, let us consider H_{edge} above in the thermodynamic limit $R_{\text{in/out}} \to \infty$, so that the inner and outer modes both have a gapless dispersion k. Constructing the operators

$$f_k = \frac{1}{2}(\gamma_k^{\text{in}} + i\gamma_k^{\text{out}}), \qquad f_k^\dagger = \frac{1}{2}(\gamma_{-k}^{\text{in}} + i\gamma_{-k}^{\text{out}}), \tag{2.38}$$

it is easily seen that $\{f_k, f_k^\dagger\} = 1$ and $\{f_k, f_k\} = 0$, using the fact that $\gamma_k^{\text{in/out}}$ satisfy the Clifford algebra. The operators $f_k, f_k^\dagger$ therefore destroy and create complex fermions, albeit highly non-local fractionalised ones, with weight equally distributed between the two well-separated edges of the annulus. Now, a chiral Hamiltonian for the f-fermions can be written as [14]

$$\begin{aligned}
H &= \sum_k 2k f_k^\dagger f_k, \\
&= \sum_{k\geq 0} 2k \left(f_k^\dagger f_k - f_{-k}^\dagger f_{-k} \right), \\
&= \sum_{k\geq 0} \frac{k}{2} \left[(\gamma_{-k}^{\text{in}} - i\gamma_{-k}^{\text{out}})(\gamma_k^{\text{in}} + i\gamma_k^{\text{out}}) - (\gamma_k^{\text{in}} - i\gamma_k^{\text{out}})(\gamma_{-k}^{\text{in}} + i\gamma_{-k}^{\text{out}}) \right], \\
&= \sum_{k\geq 0} k\gamma_{-k}^{\text{in}}\gamma_k^{\text{in}} - \sum_{k\leq 0} k\gamma_k^{\text{out}}\gamma_{-k}^{\text{out}}, \\
&= H_{\text{edge}}.
\end{aligned} \tag{2.39}$$

Therefore, a chiral complex fermion is constructed from two chiral Majorana fermions. If instead of the annulus, we consider the Read-Green superconductor on a geometry with a single edge, such as a disk or a semi-infinite plane, then only a single species of

[14] The sums should strictly be replaced by integrals, but we ignore such issues of rigour here.

chiral Majorana modes with a gapless dispersion will be seen. This is the case in Figures 2.8a-b, which show the edge spectral function of a Read-Green superconductor on a semi-infinite plane. The subgap states with a linear (in momentum) dispersion are precisely the chiral Majorana fermions we discovered above.

These edge states are quite different to the on-site localised, unpaired, zero-energy Majorana modes (MZMs) that appeared as end modes in the Kitaev chain. The ground state in that case was twofold degenerate, and these states could form a qubit protected by an energy gap from the bulk excitations of the system. In the Read-Green superconductor, the discussion above seems to imply that zero-energy modes only appear in the thermodynamic limit when the chiral edge modes become gapless. This also means that zero energy states, when they occur, are not protected by an energy gap from other excitations of the system. It is pertinent to ask if we can realise protected MZMs in the Read-Green superconductor, as it is one dimension closer to the real world than the Kitaev chain. In the annulus geometry considered above, recall that the inner edge states have quantised energies $E_m^{\text{in}} = m\Delta/R_{\text{in}}$, where m is a positive odd integer. Recall that the condition of odd m has its origins in the anti-periodic boundary conditions on the fermion fields $\psi_{r,\theta}$ in Eq. (2.24), which follow from the $\exp(i\theta)$ factors in the BdG Hamiltonian in polar coordinates [see Eq. (2.22) and the discussion below there]. If we could somehow remove the $\exp(i\theta)$ factor in the pairing terms in Eq. (2.22), then the fields $\psi_{r,\theta}$ would satisfy the usual periodic boundary conditions, which would presumably lead to even angular momentum quantum numbers m and thus to the desired zero-energy mode. This is easy to do; imagine that the core trivial region of the annulus in 2.9 is a vortex in the order parameter field [35]. The precise mechanism of the formation of such a vortex is unimportant for the discussion here. This implies that the phase $\phi(r,\theta)$ of the order parameter field Δ winds by 2π around the vortex (if it is threaded by one flux quantum $hc/2e$). One choice of the phase field that satisfies this is $\phi(r,\theta) = -\theta$. One can then replace $\Delta \to \Delta\exp(-i\theta)$ in Eq. (2.22), which gets rid of all $\exp(i\theta)$

factors there.[15] Now solving for the eigenfunctions of the BdG Hamiltonian with *periodic* boundary conditions, one finds edge states with energies $E_m^{\text{in}} = m\Delta/R_{\text{in}}$ and $E_m^{\text{out}} = -m\Delta/R_{\text{out}}$ where $m \in \{0, 2, 4, \dots\}$. The energy spectrum thus includes two MZMs, with one localised on each edge of the annulus. If the core trivial region is a vortex formed by an external magnetic field, then we expect R_{in} i.e. the size of the vortex to be on the order of the coherence length of the superconductor, which would result in the next excited vortex-bound state to be separated by an energy gap from the MZM. Several such vortices, each harbouring a trapped MZM, can thus be used to construct a system of qubits that are protected from errors, provided the vortices are spatially well separated to prevent tunnelling of MZMs between vortices [36–38]. Braiding of the vortex-trapped MZMs, which are actually non-Abelian anyons, can be used to process information stored in the qubits they construct [5, 16].

2.2 PRACTICAL REALISATIONS

The Kitaev chain, constructed in section 2.1.1 as a toy model with MZMs, is a one-dimensional p-wave superconductor made of spinless fermions. At first sight, it seems an impossible endeavour to experimentally realise such a system, as:

1. The model involves spinless (spin-polarised) fermions, but we only have spinful electrons at our disposal in solid-state systems.
2. Off-diagonal long-range order, defining of a superconducting state, cannot spontaneously form in one-dimensional systems by virtue of the Mermin-Wagner theorem [39–41]. Even in the case of quasi-long-range order at zero temperature, the importance of fluctuations in the order parameter makes the BCS mean-field formalism used in the model suspect.
3. The model involves spin-triplet superconducting pairing, as must be the case for spin-polarised fermions. Nearly all superconductors in nature involve spin-singlet s-wave pairing.

[15] Strictly, $\Delta \to \Delta(r)\exp(-i\theta)$ as $\Delta(r)$ must be zero inside the vortex. This can be done by assuming the same profile for $\Delta(r)$ and $\tilde{\mu}(r)$, and does not change our conclusions.

We briefly sketch how these issues can be addressed by modifying the Hamiltonian of the Kitaev chain, while trying to preserve its topological phase with MZMs, following Ref. [42]. One can add a spin index to all the fermion fields in the Hamiltonian [Eq. 2.7] to obtain a model of spin-1/2 electrons. This generates two decoupled copies of the Kitaev chain, which implies there are now two MZMs at each end. In the absence of protecting symmetries (time-reversal), the MZMs will generally pair up and form a local complex fermion with non-zero energy. However, we can add a Zeeman term $-h(c^\dagger_{j\uparrow}c_{j\uparrow}-c^\dagger_{j\downarrow}c_{j\downarrow})$ to the Hamiltonian, and tune h relative to the chemical potential μ so that the spin-up electrons are in the topological phase $|\mu|<2t$ while the spin-down electrons are in the trivial phase $|\mu|>2t$. This would then result in a single MZM at each end of the chain.

Since the chain of electrons cannot spontaneously order (long range), it is clear that superconductivity would have to be induced by proximity to a bulk superconductor. This would then justify the BCS form used for the Hamiltonian of the Kitaev chain, as fluctuations in the order parameter are governed by the bulk superconductor. Nearly all superconductors are s-wave spin-singlet in nature, and we must somehow induce p-wave spin-triplet superconductivity in the chain while proximitising it with an s-wave superconductor. Simply changing the pairing in the spinful Kitaev chain to s-wave destroys the topological features of the model. However, in conjunction with s-wave pairing, if one adds Rashba spin-orbit coupling [43, 44] of the form $k\sigma^y_j=-ik(c^\dagger_{j\uparrow}c_{j\downarrow}-c^\dagger_{j\downarrow}c_{j\uparrow})$, where k is the momentum and σ^y is the y-component of the electrons' spin, it can be shown that one effectively obtains p-wave pairing terms for small momenta in the Hamiltonian [3].

Given a one-dimensional electronic system, the three key ingredients required to overcome the issues (1)-(3) above and engineer a Kitaev chain are then (i) a magnetic field to 'spin-split' electron bands, (ii) an s-wave superconductor to proximity-induce superconductivity, and (iii) spin-orbit coupling along an axis perpendicular to the Zeeman field to render the induced superconductivity p-wave. There are several different designs that use these ingredients to create specific realisations of the Kitaev

chain. The semiconductor nanowire proposal of Refs.[45, 46], building on earlier work in Refs. [47, 48], involves proximitising a Rashba spin-orbit coupled semiconductor nanowire (such as InSb) with an s-wave superconductor in the presence of a transverse magnetic field. For a moderately large magnetic field, the nanowire enters a topological phase with predicted boundary MZMs. Another proposal [49, 50] involves gapping the edge modes of a quantum spin Hall insulator (2d topological insulator) [21, 22, 51, 52]. The quantum spin Hall insulator supports two counter-propagating chiral edge fermions with opposite spins and a linear Dirac dispersion, which thus form a spin-orbit coupled one-dimensional electronic system. To render the system spinless, one applies a Zeeman field to open a gap in the Dirac spectrum and locates the chemical potential inside the gap. Proximity effects from an s-wave superconductor can then induce inter-band p-wave superconductivity. Yet another proposal [25, 53] utilises a ferromagnetic chain deposited on a superconducting lead substrate that also provides spin-orbit coupling.

The Read-Green (spinless, p_x+ip_y) superconductor can be engineered in a similar fashion. In fact, all the proposals referred to above began with the seminal work [49] of Fu and Kane, who showed that proximitising the surface of a three-dimensional topological insulator with a bulk s-wave superconductor induces a time-reversal symmetric relative of the Read-Green superconductor on the interface. To localise unpaired Majorana fermions, however, requires time-reversal symmetry breaking. To realise chiral Majorana fermions, one requires a one-dimensional boundary for the 2d p_x+ip_y superconductor. In the Fu-Kane proposal, since the latter state itself is formed on the boundary of the 3d topological insulator, it cannot have a boundary of its own. However, such a boundary can be created by forming a domain wall between the p_x+ip_y state on the surface, and a ferromagnetic insulator that breaks time-reversal symmetry. Chiral Majorana fermions will then flow on this domain wall. One can also lift time-reversal symmetry by creating a vortex in the surface state using an applied magnetic field. Such a vortex will then trap a localised and unpaired MZM, precisely like the Read-Green superconductor as discussed in section 2.1.2.

Unlike the Kitaev chain, which must be specifically engineered using heterostructures of ordinary materials, we mention that there do exist materials that might intrinsically realise spin-triplet p-wave superconductivity in two dimensions. Sr_2RuO_4 is a leading candidate as a spinful p_x+ip_y superconductor [54], and more recently the surface states of certain iron-based superconductors [55–57] have also attracted attention. Such superconductors admit half-quantum $hc/4e$ vortices that trap MZMs, in addition to $hc/2e$ vortices that do not. The fractional quantum Hall state at filling fraction $\nu = 5/2$ is also predicted to realise a *spinless* p_x+ip_y superconductor (albeit of composite fermions), and is in fact the original context in which such a phase was proposed by Read and Green [32]. However, predictions of Majorana edge states in the A phase of superfluid Helium-3 under confinement precede the advent of topological superconductors, and its status as a topological p_x+ip_y superfluid is reviewed in Ref. [58].

2.3 EXPERIMENTAL SIGNATURES

Now that practical realisations of the Kitaev chain and Read-Green superconductor have been discussed, the question of how to detect Majorana fermions in these systems remains. We very briefly outline the most basic measurement protocol aimed at detecting the *presence* of a MZM and associated key experiments, referring the reader to Refs. [6, 59] for extensive reviews of the current experimental status of the field.

For the Kitaev chain, the simplest means of detecting the presence of a MZM is through tunnelling spectroscopy; a tunnel junction is created between the Kitaev chain in its topological phase and a normal metallic probe. An applied bias voltage causes electrons to flow from the metallic probe into the superconductor. The measured tunnelling conductance, as a function of bias voltage, then probes the local density of states of the Kitaev chain at the junction. Due to the presence of a zero-energy MZM at the end of the chain, there can be a non-zero ($2e^2/h$) conductance even at zero bias voltage [60, 61]. Such measurements were first made by Mourik *et al.*

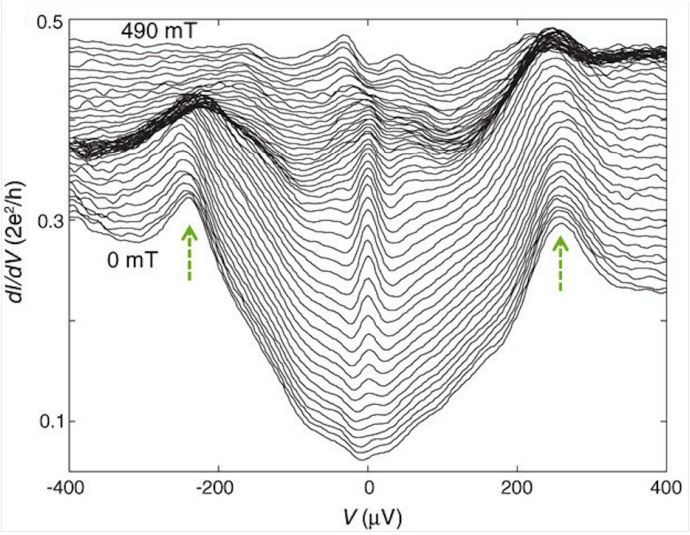

FIGURE 2.10 – Tunnelling conductance as a function of applied bias voltage in the Mourik *et al.* experiment [62], shown for various magnetic fields (0 to 490 mT in 10 mT steps). The proximity-induced superconducting gap in the nanowire is between the green arrows. Note the zero bias peak for a range of magnetic fields from approximately 100-400 mT.

[62], on a device constructed after the semiconductor nanowire proposals of Lutchyn, Oreg *et al.* [45, 46]. Their pioneering measurements (subsequently reproduced by other groups), shown in Figure 2.10, clearly display a zero-bias peak that develops for a range of magnetic fields, consistent with the presence of a MZM at the end of the nanowire. However, not all features of the data align with predictions based on the Lutchyn-Oreg realisation of the Kitaev chain. For example, the onset of the zero-bias peak is predicted to be accompanied by a phase transition, signalled by the closing and re-opening of the superconducting gap. No such transition is seen in the data. The zero bias conductance is also much smaller than the predicted $2e^2/h$. Also, it turns out that the finite length of the nanowire used in this experiment is not negligible, and should result in some visible splitting of the zero-bias peak due to a residual coupling between the two MZMs of the nanowire. The lack of such a splitting in the data is yet another discrepancy with theoretical predictions. An extensive debate regarding the conclusions of the experiment followed, and it was realised [63] that the presence of disorder could also result in zero bias peaks that

could mimic the signature of a MZM (even in the trivial phase). In all subsequent experiments, the key issue has become that of distinguishing zero bias peaks due to non-topological, subgap Andreev bound states (resulting from disorder), from the zero bias peak contributed by a topologically protected MZM [64]. A conclusive demonstration of the existence of MZMs in such semiconductor devices would thus have to incorporate signatures other than the zero bias peak. One must show that (i) there is a state pinned to zero energy; (ii) this zero-energy state exists in a limited parameter range of chemical potential and applied magnetic field; (iii) the onset of a zero bias peak that indicates the existence of such a zero energy state must be accompanied by a closing and re-opening of the bulk gap; (iv) the zero bias peak must be observed at both ends of the nanowire. While these requirements have been individually satisfied in various experiments, no one experiment has conclusively demonstrated all these properties in a single device, to the best of our knowledge.

More recently, the Yazdani group at Princeton has experimentally realised [65] the Kitaev chain in ferromagnetic iron (Fe) atomic chains deposited on a superconducting lead (Pb) substrate, which also provides the necessary spin-orbit coupling, following an earlier theoretical proposal [53]. Their approach, using scanning tunnelling spectroscopy (STS), permits measurements of the LDOS across the entire Fe chain. Their results, partially reproduced in Figure 2.11, clearly show zero bias peaks in the STS spectra on each end of the chain that are resolved from the other subgap Yu-Shiba-Rusinov states [66–68]. Spatial and energy resolved maps of the LDOS clearly show strongly localised zero-energy excitations at the ends of the chain. Subsequent experiments [69–72] from the same and other groups have since reproduced and improved upon these results, including measurements of the localisation length of an MZM that agree remarkably well with expectations from theory. There is now a consensus that the results of all these experiments, taken together, indicate that MZMs have indeed been observed, although no one explanation seems to fit all aspects of the data in any experiment.

The vortex-bound MZMs present in $p_x + ip_y$ superconductors can also be de-

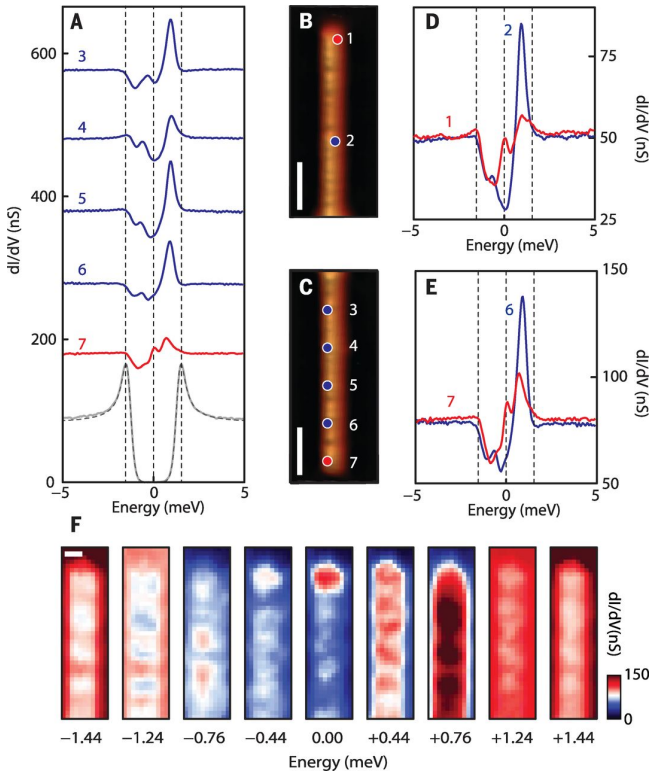

FIGURE 2.11 – STS measurements by Nadj-Perge *et al.* [65] of the spatially resolved LDOS across an Fe chain deposited on a superconducting Pb substrate. (B) and (C) show the topography respectively of the upper and lower ends of the Fe chain. (A, D, E) show STM spectra measured at the various locations on the Fe chain marked in (B) and (C). There are zero bias peaks (in red in A, D, E) at the ends (locations 1 and 7) of the Fe chain, that are well resolved from the other subgap Yu-Shiba-Rusinov states. (F) Spatial and energy resolved conductance maps near the end of another Fe chain. Note the increased conductance at zero energy at the end of the chain, which supports the existence of a localised MZM there.

tected by spectroscopy measurements. Experiments on Fu-Kane heterostructures are extensively reviewed in Ref. [74]. We choose to highlight here the results of two experiments that potentially bear relevance to the models discussed later in this thesis. The first is a recent experiment by Machida *et al.* [73], which presents spectroscopy data on hundreds of vortex cores in an Abrikosov vortex lattice in the iron-based superconductor Fe(Se,Te), previously established (in both theory and experiment) to host a topological p_x+ip_y state with $hc/4e$ vortex-trapped MZMs on its surface [55–57, 75, 76]. Their results, partially reproduced in Figure 2.12, show a large fraction of zero bias peaks in the STS spectra of the vortex lattice that is heavily

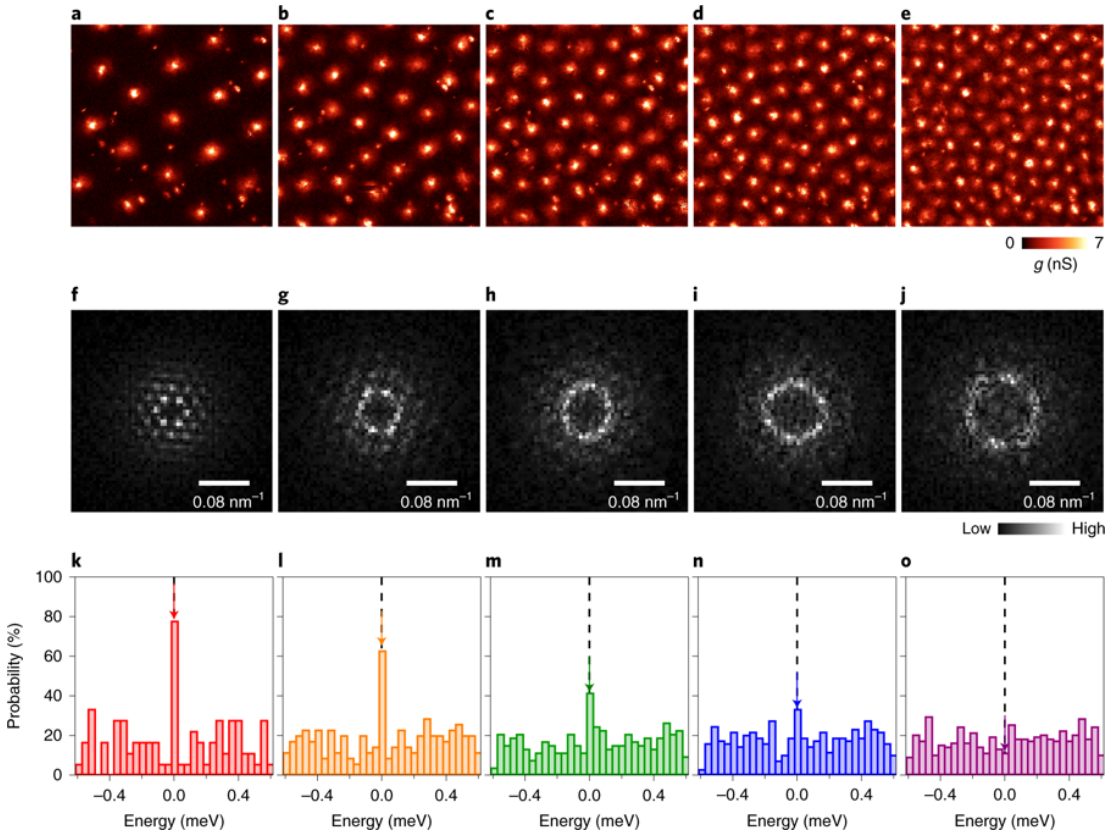

FIGURE 2.12 – (a-e) STM images of vortices by mapping the zero-energy conductance on the surface p_x+ip_y state of the iron-based superconductor Fe(Se,Te) [73]. Images are of the same field of view, for increasing magnetic fields of (a) 1 T, (b) 2 T, (c) 3 T, (d) 4 T, and (e) 6 T. (f-j): Fourier transformed images of (a-e). (k-o): Probabilities of observing peaks at given energies in the STS spectra of all the vortices, in correspondence with (a-e). Note that the fraction of observed zero bias peaks decreases with increasing magnetic field.

suppressed with increasing magnetic field, which results in a denser vortex lattice. A preliminary analysis of the data [77] indicates that this is explained by hybridisation (tunnelling) of MZMs between vortices, in addition to disordered vortex distributions. The importance of the experiment is in the fact that it is a step towards realising a system of *interacting* Majorana fermions, where the interactions result from the overlap of MZM wavefunctions from (at least) four vortex cores [78].

Experiments aimed at detecting chiral Majorana edge modes of p_x+ip_y superconductors have been relatively scarce, partly due to the difficulty in engineering the heterostructures required to observe such a phenomenon, though concrete proposals

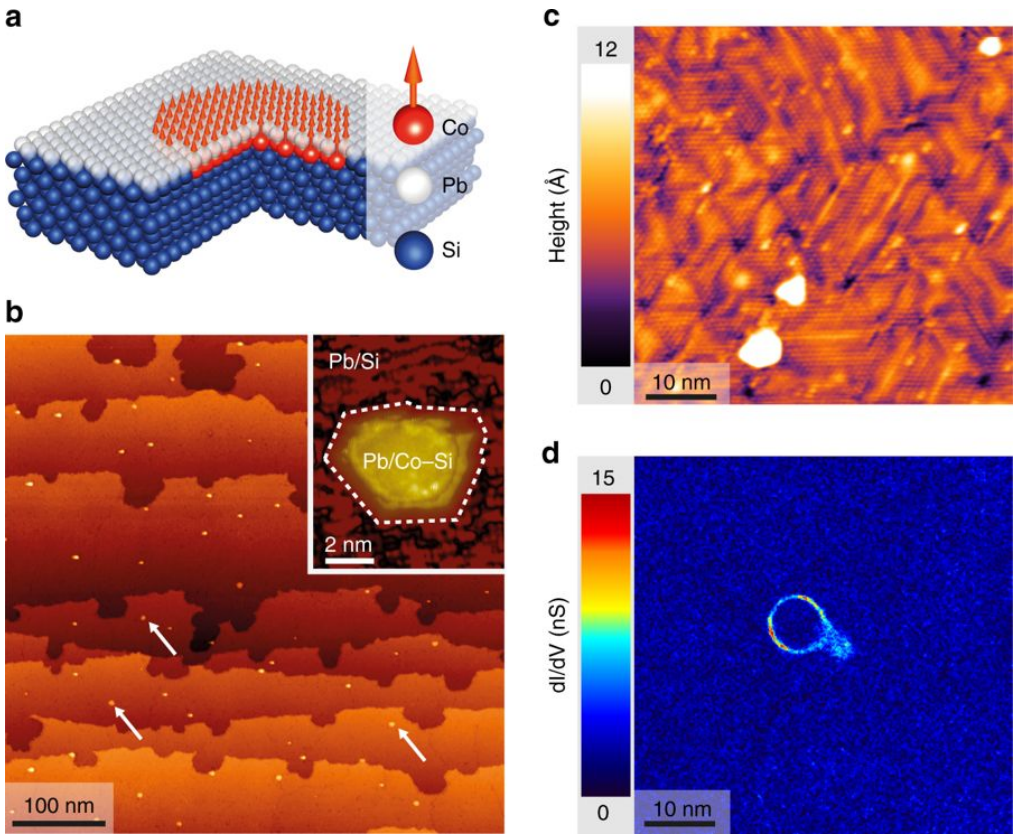

FIGURE 2.13 – STM experiment by Menard *et al.* [79] on a (a) Si(111)/Pb/Co heterostruture (schematic shown), which realises a p_x+ip_y superconductor with magnetic islands. (b-c) Topography of the sample, showing in-grown magnetic clusters of Co-Si on the lead surface. (d) Conductance map at a subgap energy on the area shown in (c), showing gapless states localised at the boundary between the Co-Si disk and the superconductor. Everywhere else, a superconducting gap persists (dark blue regions) with no low energy excitations.

for such experiments have existed for a while [50, 80–82]. However, we mention a recent STM experiment by Menard *et al.* [79] that shows promising results. A heterostructure, combining the three essential ingredients required for spinless p_x+ip_y superconductivity, is fabricated by growing a monolayer of superconducting lead on top of the semiconductor Si(111), after which magnetic islands of Co-Si are grown on the surface (see Figure 2.13a). As mentioned in the previous section, gapless and chiral Majorana modes are expected to localise on the one-dimensional boundary between these magnetic islands and the superconducting state. A conductance map of the heterostructure at a subgap energy reveals gapless excitations localised at the

boundary between a magnetic disk and the surrounding superconductor (see Figure 2.13d).

2.4 INTERACTIONS IN MAJORANA SYSTEMS

The experiment by Machida *et al.*, discussed in the previous section, presents an interesting avenue of research. Vortex-bound MZMs, when brought together, will generally hybridise and form Majorana bands. If the vortex lattice is dense enough to allow nearest neighbour MZM wavefunctions to overlap, the low energy physics at energy scales below the superconducting gap is expected to be entirely dominated by these Majorana degrees of freedom [78, 83]. The richness of strongly correlated electron systems is motivation enough to realise and study interaction effects in correlated Majorana systems. The vortex lattices of topological superconductors present a natural setting to realise such interacting Majorana fermions. To describe such systems, Majorana-Hubbard [84–89] and Majorana-Falicov-Kimball [90–92] models on various lattice geometries have been proposed, with interaction effects in some cases leading to rich phase diagrams and exotic effects such as emergent supersymmetry at critical points. This work has been reviewed recently in Ref. [83]. We mention in particular the Majorana-Falicov-Kimball model of Ref. [92], which models an itinerant band of Majorana fermions interacting with a species of localised fermions, and admits an exact solution at finite temperature by means of the $\mathbb{Z}_2$ slave-spin technique [93]. The methods of Ref. [92] provide the motivation for the exact solution of the Majorana-Anderson impurity models presented in the following chapters of this thesis.

We also mention a few other settings in which correlations between Majorana fermions become important, and lead to new physical effects. One is the avenue of research motivated by transport experiments on superconducting Rashba nanowires, exploring interacting Anderson-type impurity models involving small numbers of MZMs on mesoscopic islands coupled to dissipative baths, some of which are predicted to exhibit exotic Kondo effects [9–12]. Another is motivated by the search for

so-called Fibonacci anyons, whose braiding structure is richer and more suitable for quantum computation than MZMs [5]. For example, Ref. [94] shows that Fibonacci anyons emerge in a constructed model with interactions between *chiral* Majorana fermions.

CHAPTER 3

Majorana-Anderson impurity models

3.1 General structure of models

Motivated by studies of interaction effects in Majorana fermion systems, we consider Majorana-Anderson impurity (MAI) models described by a lattice Hamiltonian of the form

$$H = H_C + H_A + H_{\text{hyb}}, \tag{3.1}$$

where H_C describes an arbitrary host material or leads that couple to the quantum dot. We assume that H_C is bilinear in fermion operators $\{c_j, c_j^\dagger\}$, where j denotes the set of all quantum numbers required for a description of the host. For example, $c_{i\alpha}$ with $\alpha \in \{L, R\}$ and lattice-site index i could describe left (L) and right (R) leads that couple to the quantum dot. The dot is modelled as an Anderson impurity[1] with Hamiltonian

$$H_A = U\left(2n_{d\uparrow} - 1\right)\left(2n_{d\downarrow} - 1\right) + \frac{\epsilon}{2}\left(n_{d\uparrow} + n_{d\downarrow} - 1\right) - \frac{h}{2}\left(n_{d\uparrow} - n_{d\downarrow}\right), \tag{3.2}$$

[1] The terms 'quantum dot' and 'impurity' are used interchangeably in this thesis, and are synonymous within the current scope of discussion.

where $n_{d\sigma} = d_\sigma^\dagger d_\sigma$ is the number operator for impurity fermions of spin $\sigma \in \{\uparrow, \downarrow\}$. U describes on-site Coulomb repulsion, h is a Zeeman field, and ϵ is a shift in the chemical potentials of the impurity fermions. The hybridisation between the host and impurity is described by

$$H_{\text{hyb}} = -i \sum_j V_j \left(c_j + c_j^\dagger\right)\left(d_\uparrow + d_\uparrow^\dagger\right) \tag{3.3}$$

which allows for the possibility of spatially extended hybridisation (strength V_j). This form of Majorana hybridisation arises naturally if the host material supports localised Majorana zero modes (MZMs) in proximity to the quantum dot. As MZMs arise in effectively spin-polarised superconductors, it is reasonable to expect that only one impurity spin species will hybridise [95–98]. In Ref. [96], Hoffmann *et al.* consider a quantum dot hybridising with a superconducting Rashba nanowire (Kitaev chain) and prove the existence of a fully spin-polarised tunnelling regime such as that considered here by tuning the distance between the dot and an end MZM hosted by the nanowire.

Note also that the number $n_{d\downarrow}$ of spin-down fermions commutes with the Hamiltonian and is thus conserved. The problem studied here can therefore be thought of as a Majorana version of the X-ray edge problem [99, 100]. By contrast with the classic Nozières-De Dominicis solution of the original problem [100], which is restricted to asymptotically low frequencies, here we find an exact solution for the impurity spectral functions at all frequencies. As $n_{d\downarrow}$ is conserved, the Hilbert space of many-body eigenstates of H breaks into two sectors labelled by the eigenvalues $n_{d\downarrow} = \pm 1$, within which H is bilinear and so can be exactly diagonalised. However, this is a weak notion of exact solvabilty. To calculate zero temperature properties, one must know which of the two sectors contains the ground state, and this requires numerics and becomes rapidly tedious as the number of impurities increases. Also, at any finite temperature, the system is specified by a mixed state (density matrix) operator that involves states from both sectors. Calculation of the temperature dependent weights assigned to individual states in each sector is a very difficult problem which

again requires numerics. By contrast, we obtain an exact solution to the MAI class of models for arbitrary temperatures.

3.2 $\mathbb{Z}_2$ SLAVE-SPIN REPRESENTATION

The key ingredient in constructing an exact solution of the MAI models introduced in section 3.1 is a slave-spin technique [93, 101, 102] in the minimal $\mathbb{Z}_2$ formulation of Rüegg *et al.* [93, 102]. We review this method here in the context of our impurity models, following Ref. [93]. The idea behind any slave-particle method is to represent local degrees of freedom by auxiliary ones in an enlarged Hilbert space. The auxiliary degrees of freedom are then subjected (enslaved) to constraints in order to account for this enlargement of the Hilbert space and obtain a faithful representation of the original problem. The $\mathbb{Z}_2$ slave-spin method rests on the observation that an interaction of the form

$$U\Big(2n_{d\uparrow}-1\Big)\Big(2n_{d\downarrow}-1\Big), \tag{3.4}$$

has two distinct eigenvalues $\pm U$ determined by the local fermion occupancy modulo 2 (or equivalently the local magnetic moment), which can be viewed as the two states of a spin-1/2 degree of freedom. Building on this observation, let us introduce a spin-1/2 (Pauli) operator $\boldsymbol{\mu} = (\mu^x, \mu^y, \mu^z)$ such that

$$\mu^z|\pm\rangle = \pm|\pm\rangle. \tag{3.5}$$

Now, the interaction on the quantum dot has as its eigenstates the four d-fermion Fock states and so the physical impurity Hilbert space is

$$\mathcal{H}_d = \mathrm{span}\left(\{|0\rangle_d, |\uparrow\rangle_d, |\downarrow\rangle_d, |\uparrow\downarrow\rangle_d\}\right). \tag{3.6}$$

We wish to associate the states $|0\rangle_d, |\uparrow\downarrow\rangle_d$ with no local moment and $|\uparrow\rangle_d, |\downarrow\rangle_d$ with a moment to the eigenstates of μ^z, say $|+\rangle$ and $|-\rangle$ respectively. But to ensure that the anti-commutation properties of fermions are preserved, we need to introduce auxiliary fermions f_σ and construct a tensor product space $\mathcal{H}_{SS}$ from the two μ^z

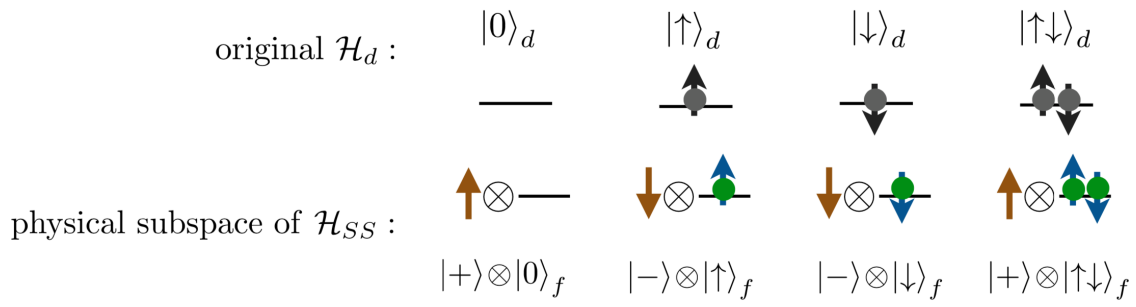

FIGURE 3.1 – Illustration of $\mathbb{Z}_2$ slave-spin representation. Figure adapted from [93].

eigenstates $|\pm\rangle$ and the f-fermion Fock states $\{|0\rangle_f, |\uparrow\rangle_f, |\downarrow\rangle_f, |\uparrow\downarrow\rangle_f\}$, that is define a 'slave-spin Hilbert space'

$$\mathcal{H}_{SS} \equiv \text{span}\Big(\{|+\rangle, |-\rangle\} \otimes \Big\{|0\rangle_f, |\uparrow\rangle_f, |\downarrow\rangle_f, |\uparrow\downarrow\rangle_f\Big\}\Big).$$

Note that $\dim \mathcal{H}_{SS} = 8$, twice as large as the physical Hilbert space $\mathcal{H}_d$. This means $\mathcal{H}_{SS}$ is endowed with a gauge structure – there are redundant or unphysical states in $\mathcal{H}_{SS}$. We will shortly see how to deal with this problem. The physical fermion operators (d_σ) that act on $\mathcal{H}_d$ are then represented on $\mathcal{H}_{SS}$ as

$$d_\sigma^{(\dagger)} \to \mu^x f_\sigma^{(\dagger)}. \tag{3.7}$$

We note that the anti-commutation relations of $d_\sigma^{(\dagger)}$ are preserved in this definition. It is also consistent with our requirement that μ^z describe the local moment; the left and right hand sides (LHS and RHS) of this definition both change the local moment when acting on $\mathcal{H}_d$ and $\mathcal{H}_{SS}$ respectively. It also provides a natural formulation of the constraint required to eliminate the extra unphysical states in $\mathcal{H}_{SS}$. The fact that $n_{d\sigma} \to n_{f\sigma}$ and our requirement that μ^z describe the local d-fermion moment as $\big(2n_{d\uparrow} - 1\big)\big(2n_{d\downarrow} - 1\big) \to \mu^z$ also constrains the f-fermion moment as

$$\big(2n_{f\uparrow} - 1\big)\big(2n_{f\downarrow} - 1\big) = \mu^z, \tag{3.8}$$

allowing the identification of the physical subspace of $\mathcal{H}_{SS}$ (see Figure 3.1). States in $\mathcal{H}_{SS}$ such as $|+\rangle\otimes|\uparrow\rangle_f$ are therefore unphysical and one should ensure that these

do not contribute to any physically observable quantities by enforcing the constraint above.

In the literature, the relation $d_\sigma \to \mu^x f_\sigma$ in the slave-spin representation is written as an equality. Strictly speaking, this is not well defined – the operators on either side of the relation act on different vector spaces that are *not* isomorphic (the dimension of the slave-spin Hilbert space is larger than that of the physical space). What is typically meant by the equality is the following – the slave-spin Hilbert space contains a physical subspace that is isomorphic to the physical space of states (Figure 3.1). The equality between d_σ and $\mu^x f_\sigma$ holds *only* when the domain of the latter is restricted to this subspace, that is when the gauge constraint is strictly imposed.

The constraint equation also allows a simplified rewriting of the interaction term in MAI models in terms of a single spin-1/2 operator. With a view towards the exact solution to be presented later, we also rewrite the impurity chemical potential and Zeeman terms in Eq. (3.2) [103]. To this end, note that the idempotency of the number operators $n_{f\sigma}$ implies

$$\begin{aligned}\mu^z\left(2n_{f\downarrow}-1\right) &= \left(4n_{f\uparrow}n_{f\downarrow}-2n_{f\uparrow}-2n_{f\downarrow}+1\right)\left(2n_{f\downarrow}-1\right)\\ &= n_{f\uparrow}-\frac{1}{2}.\end{aligned} \tag{3.9}$$

Therefore, using the results in Eqs. (3.7)-(3.9), we arrive at the slave-spin (SS) representation of the MAI class of models [Eqs. (3.1)-(3.3)], specified by the Hamiltonian

$$H_{SS} = H_C - \sum_j iV_j\left(c_j + c_j^\dagger\right)\left(f_\uparrow + f_\uparrow^\dagger\right)\mu^x + U\mu^z + \frac{1}{2}\left[\epsilon + h + (\epsilon - h)\mu^z\right]\left(n_{f\downarrow} - \frac{1}{2}\right). \tag{3.10}$$

3.3 MAJORANA REPRESENTATION OF SPIN

The next step towards an exact solution of the MAI class of models is to rewrite the SS Hamiltonian entirely in terms of fermion operators. To this end, we define the operators

$$\Gamma_\uparrow^\alpha = \mu^\alpha\left(f_\uparrow + f_\uparrow^\dagger\right), \qquad \alpha \in \{x, y, z\}. \tag{3.11}$$

It is easily seen that the operators $\Gamma_{\uparrow}^{\alpha}$ satisfy the Clifford algebra

$$\left\{\Gamma_{\uparrow}^{\alpha}, \Gamma_{\uparrow}^{\beta}\right\} = 2\delta^{\alpha\beta}, \tag{3.12}$$

and are thus Majorana fermion operators. Using the Pauli matrix identity,

$$\mu^{\alpha}\mu^{\beta} = \delta^{\alpha\beta} + i\epsilon^{\alpha\beta\gamma}\mu^{\gamma}, \tag{3.13}$$

the spin operators μ^{α} may be expressed as Majorana fermion bilinears in terms of $\Gamma_{\uparrow}^{\alpha}$ as

$$\mu^{x} = -i\Gamma_{\uparrow}^{y}\Gamma_{\uparrow}^{z}, \qquad \mu^{y} = -i\Gamma_{\uparrow}^{z}\Gamma_{\uparrow}^{x}, \qquad \mu^{z} = -i\Gamma_{\uparrow}^{x}\Gamma_{\uparrow}^{y}. \tag{3.14}$$

Since a pair of Majorana operators form a complex fermion that has a Hilbert space dimension of 2, one may formally assign a Hilbert space dimension of $\sqrt{2}$ to each Majorana fermion [104]. The tensor product of the $\boldsymbol{\mu}$ spin space and $(f_{\uparrow} + f_{\uparrow}^{\dagger})$ Majorana Hilbert space thus has a dimension of $2\sqrt{2} = (\sqrt{2})^3$, which is also the dimension of the Hilbert space spanned by the three $\Gamma_{\uparrow}^{\alpha}$, which attests to the consistency of the definition in Eq. (3.11).

Using Eqs. (3.11) and (3.14), one may rewrite the SS Hamiltonian (H_{SS}) entirely in terms of fermions as

$$H_{SS} = H_C - \sum_j iV_j\left(c_j + c_j^{\dagger}\right)\Gamma_{\uparrow}^{x} - iU\Gamma_{\uparrow}^{x}\Gamma_{\uparrow}^{y} + \frac{1}{2}\left[\epsilon + h - i(\epsilon - h)\Gamma_{\uparrow}^{x}\Gamma_{\uparrow}^{y}\right]\left(n_{f\downarrow} - \frac{1}{2}\right). \tag{3.15}$$

For $\epsilon = h$, H_{SS} is bilinear in fermion operators and is thus exactly solvable. The chemical potential ϵ of the physical impurity fermions can be tuned via applied gate potentials on the quantum dot, and h can be controlled using an applied magnetic field. We thus expect this exactly solvable limit to be realisable in an experimental situation. Henceforth, this exactly solvable limit will be assumed unless specified otherwise.

3.4 FATE OF THE GAUGE CONSTRAINT

Although we have arrived at an exactly solvable representation of the original physical model, the redundant states in the enlarged Hilbert space $\mathcal{H}_{SS}$ introduced by the SS

representation necessitates the application of a gauge constraint in calculating all physical quantities, in order to ensure that unphysical states do not contribute. In practice, this is done by including in all expectation values a projector that projects out these unphysical states. To construct such a projector, note that the gauge constraint in Eq. (3.8) can be rewritten as

$$\mu^z = 2\left(n_{f\uparrow} + n_{f\downarrow} - 1\right)^2 - 1 = (-1)^{n_f} \tag{3.16}$$

where we have used the fact that $n_{f\sigma}^2 = n_{f\sigma}$ in arriving at the first equality, and $n_f = n_{f\uparrow} + n_{f\downarrow}$ is the total f-fermion number. Multiplying both sides of the equation by μ^z and re-arranging terms, we obtain a natural definition for the projector,

$$\mathbb{P} = \frac{1}{2}[1 + (-1)^{n_f}\mu^z]. \tag{3.17}$$

As required, $\mathbb{P} = 1$ when acting on physical states that satisfy the gauge constraint and $\mathbb{P} = 0$ on unphysical states. The physical partition function is therefore expressed in the SS representation as

$$Z = \mathrm{tr}\, e^{-\beta H} = \mathrm{tr}\, e^{-\beta H_{SS}}\mathbb{P}. \tag{3.18}$$

We now show that the partition function for MAI models can actually be computed directly in the SS representation without the necessity of the projector, even away from the exactly solvable point $\epsilon = h$. The proof is similar to those constructed for other such constraint-free models studied using the $\mathbb{Z}_2$ slave-spin method [92, 103, 105, 106]. Defining a local particle-hole transformation $\mathcal{D}_\uparrow$ that acts only on $d_\uparrow$-fermions as

$$\mathcal{D}_\uparrow d_\uparrow \mathcal{D}_\uparrow^{-1} = d_\uparrow^\dagger, \tag{3.19}$$

let us consider the transformation of the physical Hamiltonian in Eqs. (3.1)-(3.3) under $\mathcal{D}_\uparrow$. Clearly, the host Hamiltonian H_C and the hybridisation H_{hyb} are invariant. However,

$$\begin{aligned}\mathcal{D}_\uparrow H_A(U,\epsilon,h)\mathcal{D}_\uparrow^{-1} &= -4U\left(n_{d\uparrow} - \frac{1}{2}\right)\left(n_{d\downarrow} - \frac{1}{2}\right) - \frac{\epsilon}{2}\left(n_{d\uparrow} - n_{d\downarrow}\right) + \frac{h}{2}\left(n_{d\uparrow} + n_{d\uparrow} - 1\right) \\ &= H_A(-U,h,\epsilon),\end{aligned} \tag{3.20}$$

where we have used the relation $\mathcal{D}_\uparrow n_{d\uparrow}\mathcal{D}_\uparrow^{-1} = 1 - n_{d\uparrow}$ to obtain the first equality. However, since the physical partition function is invariant under similarity transformations of the Hamiltonian, we have

$$Z(U,\epsilon,h) = Z(-U,h,\epsilon), \tag{3.21}$$

where the dependence on other parameters (such as the hybridisation V) has been suppressed as they are unaffected by $\mathcal{D}_\uparrow$.

Now, the action of $\mathcal{D}_\uparrow$ in the SS representation (on H_{SS}) is represented by μ^x, and so

$$\mu^x H_{SS}(U,\epsilon,h)\mu^x = H_{SS}(-U,h,\epsilon), \tag{3.22}$$

as is obvious from Eq. (3.10). Exploiting this property in the calculation of the partition function, we obtain

$$\begin{aligned} Z(-U,\epsilon,h) &= \operatorname{tr} \mu^x e^{-\beta H_{SS}(U,h,\epsilon)} \mu^x \mathbb{P}, \\ &= \operatorname{tr} e^{-\beta H_{SS}} \mu^x \mathbb{P} \mu^x, \end{aligned} \tag{3.23}$$

where the cyclicity of the trace has been used in the second step. To simplify further, we observe from (3.17) that $\mu^x \mathbb{P} \mu^x = 1 - \mathbb{P}$, and thus

$$\begin{aligned} Z(-U,h,\epsilon) &= \operatorname{tr} e^{-\beta H_{SS}(U,\epsilon,h)} (1 - \mathbb{P}) \\ &= \operatorname{tr} e^{-\beta H_{SS}(U,\epsilon,h)} - Z(U,\epsilon,h). \end{aligned} \tag{3.24}$$

Now using Eq. (3.21), we obtain

$$Z(U,\epsilon,h) = \frac{1}{2} \operatorname{tr} e^{-\beta H_{SS}(U,\epsilon,h)} = \frac{1}{2} Z_{SS}(U,\epsilon,h), \tag{3.25}$$

with no projector in sight, thus proving that the physical partition function can be computed directly in the SS representation (with H_{SS}) without applying the gauge constraint.

It is natural to ask now if the projector can also be disposed of in calculating correlation functions. Let G be a correlation function of M operators $O_1, \ldots, O_M$

constructed out of the physical fermion operators $\{c_j^{(\dagger)}, d_\sigma^{(\dagger)}\}$. Considering a given imaginary-time ordering of the operators $\{O_i\}$, we have

$$G = \langle O(\tau_1)...O(\tau_M)\rangle = \frac{1}{Z}\,\mathrm{tr}\, e^{-\beta H}\prod_{i=1}^{M} e^{\tau_i H} O_i e^{-\tau_i H}. \tag{3.26}$$

Inserting two identity operators inside the trace as $\mathcal{D}_\uparrow\mathcal{D}_\uparrow^{-1}$ and then using the cyclicity of the trace,

$$\begin{aligned} G(U,\epsilon,h) &= \frac{1}{Z(U,\epsilon,h)}\,\mathrm{tr}\,{\mathcal{D}_\uparrow}^{-1}\mathcal{D}_\uparrow e^{-\beta H(U,\epsilon,h)}{\mathcal{D}_\uparrow}^{-1}\mathcal{D}_\uparrow \prod_{i=1}^{M} e^{\tau_i H(U,\epsilon,h)} O_i e^{-\tau_i H(U,\epsilon,h)} \\ &= \frac{1}{Z(-U,h,\epsilon)}\,\mathrm{tr}\, e^{-\beta H(-U,h,\epsilon)}\mathcal{D}_\uparrow\left[\prod_{i=1}^{M} e^{\tau_i H(U,\epsilon,h)} O_i e^{-\tau_i H(U,\epsilon,h)}\right]\mathcal{D}_\uparrow^{-1}, \end{aligned} \tag{3.27}$$

where in the last step, the results $\mathcal{D}_\uparrow H(U,\epsilon,h)\mathcal{D}_\uparrow^{-1} = H(-U,h,\epsilon)$ and $Z(U,\epsilon,h) = Z(-U,h,\epsilon)$ have been used. Again inserting multiple identities $\mathcal{D}_\uparrow{\mathcal{D}_\uparrow}^{-1}$ inside the product,

$$G(U,\epsilon,h) = \frac{1}{Z(-U,h,\epsilon)}\,\mathrm{tr}\, e^{-\beta H(-U,h,\epsilon)}\left[\prod_{i=1}^{M} e^{\tau_i H(-U,h,\epsilon)}\mathcal{D}_\uparrow O_i \mathcal{D}_\uparrow^{-1} e^{-\tau_i H(-U,h,\epsilon)}\right]. \tag{3.28}$$

If we now make the assumption that $\forall i$, $\left[O_i, \mathcal{D}_\uparrow\right] = 0$, then it follows that $G(U,\epsilon,h) = G(-U,h,\epsilon)$. In the SS representation, the same correlation function G is expressed as

$$G = \left(\frac{2}{Z_{SS}}\right)\mathrm{tr}\, e^{-\beta H_{SS}}\left[\prod_{i=1}^{M} e^{\tau_i H_{SS}} O_i^{(SS)} e^{-\tau_i H_{SS}}\right]\mathbb{P}. \tag{3.29}$$

Since the action of $\mathcal{D}_\uparrow$ is implemented by μ^x in the SS representation, inserting the identity $\mu^x\mu^x$ and repeating the steps in Eqs. (3.27)-(3.28), making use of the results $G(U,\epsilon,h) = G(-U,h,\epsilon)$ and $\mu^x\mathbb{P}\mu^x = 1-\mathbb{P}$, yields

$$G(U,\epsilon,h) = \frac{2}{Z_{SS}}\,\mathrm{tr}\, e^{-\beta H_{SS}(U,\epsilon,h)}\left[\prod_{i=1}^{M} e^{\tau_i H_{SS}(U,\epsilon,h)}\mu^x O_i^{(SS)}\mu^x e^{-\tau_i H_{SS}(U,\epsilon,h)}\right](1-\mathbb{P}). \tag{3.30}$$

The operators $\{O_i^{(SS)}\}$ are the SS representations of $\{O_i\}$, and so are constructed from c_j, slave-fermions d_σ, and slave-spin μ^x operators. This implies that $\mu^x O_i^{(SS)}\mu^x = O_i^{(SS)}$ for all i, from which it immediately follows that

$$G = \frac{1}{Z_{SS}}\,\mathrm{tr}\, e^{-\beta H_{SS}}\left[\prod_{i=1}^{M} e^{\tau_i H_{SS}} O_i^{(SS)} e^{-\tau_i H_{SS}}\right]. \tag{3.31}$$

Therefore, correlation functions of operators O_i that are invariant under the particle-hole transformation $\mathcal{D}_\uparrow$ can be calculated in the SS representation without constraint. For example, this includes any operator function of $d_\downarrow$ and c_j. Correlation functions involving $d_\uparrow$ cannot typically be calculated without constraint.

However, it turns out to be possible to exactly implement the constraint in *any* correlation function in the MAI class of models. This rests on the observation that the projector $\mathbb{P}$ in Eq. (3.17), expressed equivalently as

$$\mathbb{P} = \frac{1}{2}\Big[1 + \Big(2n_{f\uparrow} - 1\Big)\Big(2n_{f\downarrow} - 1\Big)\mu^z\Big], \tag{3.32}$$

admits a representation entirely in terms of fermions. Using the Majorana operators $\Gamma^z_\uparrow = \mu^z(f_\uparrow + f_\uparrow^\dagger)$ and $\gamma'_{f\uparrow} = -i(f_\uparrow - f_\uparrow^\dagger)$ to write $2n_{f\uparrow} - 1 = i\mu^z\Gamma^z\gamma'_{f\uparrow}$, we obtain

$$\mathbb{P} = \frac{1}{2}\Big[1 + i\Gamma^z\gamma'_{f\uparrow}(2f_\downarrow^\dagger f_\downarrow - 1)\Big], \tag{3.33}$$

which only involves fermion operators in terms of which the SS Hamiltonian is quadratic. As seen above, a (time-ordered) correlation function G' of a physical operator O that does not commute with $\mathcal{D}_\uparrow$ must be calculated in the SS representation *with* the projector,

$$\begin{aligned} G' &= 2\langle T_\tau O_{SS}(\tau_1) O_{SS}(\tau_2)\mathbb{P}\rangle_{SS} \\ &= \Big\langle T_\tau O_{SS}(\tau_1) O_{SS}(\tau_2)\Big[1 + i\Gamma^z(0)\gamma'_{f\uparrow}(0)\Big\{2f_\downarrow^\dagger(0)f_\downarrow(0) - 1\Big\}\Big]\Big\rangle_{SS} \end{aligned} \tag{3.34}$$

As the expectation value on the RHS is taken with respect to the quadratic H_{SS} (at the exactly solvable point $\epsilon = h$), the RHS can be Wick contracted into a product of one-particle Green functions of free fermions that can be evaluated exactly. Since the gauge constraint can be explicitly implemented in this way, *all* correlation functions can be calculated exactly for the MAI class of models.

3.5 EXTENSIONS OF THE MAI CLASS OF MODELS

In this section, we briefly comment on two immediate extensions of the MAI class of models that are possible while retaining exact solvability. The first is a generalisation

of the hybridisation term in Eq. 3.3. While applications to spin-polarised topological superconductors naturally justify a spin-selective choice of hybridisation [95–98], it is possible to generalise the latter in MAI models such that impurity fermions of both spins hybridise equally with the host fermions and retain exact solvability. To this end, consider a general hybridisation of the form

$$H'_{\text{hyb}} = -i \sum_{j\sigma} \frac{V_j}{\sqrt{2}} (c_j + c_j^\dagger)(d_\sigma + d_\sigma^\dagger), \tag{3.35}$$

where the index j denotes a complete set of quantum numbers required to describe the host fermions. Now, the operator $(d_\uparrow + d_\uparrow^\dagger + d_\downarrow + d_\downarrow^\dagger)/\sqrt{2}$ is Hermitian, squares to one, and so can be thought of as a Majorana operator. In the SS representation,

$$H'_{\text{hyb}} \to -i \sum_{j\sigma} \frac{V_j}{\sqrt{2}} (c_j + c_j^\dagger)(f_\sigma + f_\sigma^\dagger)\mu^x.$$

If we now carry out similar transformations as done in sections 3.2 and 3.3, with $\Gamma_\uparrow^\alpha$ replaced by new Majorana operators $\chi^\alpha = \sum_\sigma \mu^\alpha (d_\sigma + d_\sigma^\dagger)/\sqrt{2}$, where $\alpha \in \{x, y, z\}$ as before, and $\chi^4 = (d_\uparrow + d_\uparrow^\dagger - d_\downarrow - d_\downarrow^\dagger)/\sqrt{2}$, we find that the resulting slave-spin Hamiltonian is bilinear in fermions for $\epsilon = h = 0$. The definition of the χ^4 fermion is again required in order for the slave-spin Hilbert space to be of dimension equal to eight and thus be a faithful representation of the original problem. Therefore, generalising the hybridisation in the MAI class of models comes at the cost of setting the impurity chemical potential and Zeeman terms to zero.

Another extension is to consider periodic Majorana-Anderson models, which can be thought of as a Majorana version of the periodic Anderson model [107]. This model describes a lattice of Anderson impurities hybridising with the itinerant fermions of some host Hamiltonian, and is obtained simply by adding a site index to all the impurity fermion operators in the MAI Hamiltonian –

$$\begin{aligned} H_{PMA} = H_C - i \sum_j V_j (c_j + c_j^\dagger)(d_{j\uparrow} + d_{j\uparrow}^\dagger) \\ + \sum_j U_j \left(2n_{j\uparrow}^{(d)} - 1\right)\left(2n_{j\downarrow}^{(d)} - 1\right) + \frac{\epsilon_j}{2}\left(n_{j\uparrow}^{(d)} + n_{j\downarrow}^{(d)} - 1\right) - \frac{h_j}{2}\left(n_{j\uparrow}^{(d)} - n_{j\downarrow}^{(d)}\right), \end{aligned} \tag{3.36}$$

where $n^{(d)}_{j\sigma} = d^\dagger_{j\sigma} d_{j\sigma}$. The exact solution of this model for $\epsilon_j = h_j$ is obtained following the same methods as for the MAI model in sections 3.2 and 3.3. The bilinear SS representation of H_{PMA} is simply that of the MAI model in Eq. (3.15) with lattice indices for all the slave-fermions.

In the case of periodic Majorana-Anderson models, since the impurity Hilbert space is enlarged on every site, there is correspondingly a local gauge constraint to implement on every site. A proof that this constraint can be disposed of in calculations of the partition and most correlation functions in the SS representation follows along the same vein as the one given for MAI models in section 3.4. We briefly sketch the proof for the partition function, for the sake of completeness. Considering an on-site partial particle-hole transformation $\mathcal{D}_{j\uparrow}$ that acts only on $d_{j\uparrow}$ as $\mathcal{D}_{j\uparrow} d_{j\uparrow} \mathcal{D}^{-1}_{j\uparrow} = d^\dagger_{j\uparrow}$, we find $\mathcal{D}_{j\uparrow} H_{PMA}(U_j, \epsilon_j, h_j) \mathcal{D}^{-1}_{j\uparrow} = H_{PMA}(-U_j, h_j, \epsilon_j)$ and so $Z_{PMA}(U_j, \epsilon_j, h_j) = Z_{PMA}(-U_j, h_j, \epsilon_j)$. In the SS representation, $\mathcal{D}_{j\uparrow}$ is implemented by μ^x_j and so

$$\begin{aligned} Z_{PMA}(U_1, \epsilon_1, h_1, U_2, ...) &= \mathrm{tr}\, \mu^x_1 e^{-\beta H^{(SS)}_{PMA}(U_1, \epsilon_1, h_1, U_2, ...)} \mu^x_1 \mathbb{P}_1 \prod_{j>1} \mathbb{P}_j, \\ &= \mathrm{tr}\, e^{-\beta H^{(SS)}_{PMA}(U_1, \epsilon_1, h_1, U_2, ...)} (1 - \mathbb{P}_1) \prod_{j>1} \mathbb{P}_j, \\ &= \frac{1}{2} \mathrm{tr}\, e^{-\beta H^{(SS)}_{PMA}(U_1, \epsilon_1, h_1, U_2, ...)} \prod_{j>1} \mathbb{P}_j, \end{aligned} \tag{3.37}$$

where the projector $\mathbb{P}_j$ is the same as that for the MAI model [Eq. (3.17)], but with site indices for all slave-spin and slave-fermion operators. Repeating this for every site $j \in \{1, ..., N\}$ immediately gives $Z_{PMA} = Z^{(SS)}_{PMA} / 2^N$, which implies that the physical partition function can be calculated in the SS representation without constraint. A similar proof holds for correlation functions of operators that commute with $\mathcal{D}_{j\uparrow}$ for every j. However, there is one important difference in this regard between the periodic Majorana-Anderson and MAI class of models. In the latter, since the projector $\mathbb{P}$ could be explicitly implemented (see section 3.4), *all* correlation functions could be exactly calculated. In the case of periodic Majorana-Anderson models, correlation functions in the SS representation will involve an infinite string of projectors as in Eq. (3.37), also similar to the Majorana-Falicov-Kimball model [92]. Although $\mathbb{P}_j$ admits

a representation in terms of the slave-fermions that appear in the bilinear $H^{(SS)}_{PMA}$, Wick contraction of the infinite string of projectors inside correlation functions will result in an infinite product of slave-fermion Green functions which likely cannot be computed practically. Therefore, at least in the thermodynamic limit, one is restricted to computation of correlation functions of operators that commute with all the $\mathcal{D}_{j\uparrow}$.

CHAPTER 4

Kitaev Majorana-Anderson impurity model

As a first application and concrete demonstration of our results in chapter 3, we consider the case of a quantum dot hybridising with the end mode of a semi-infinite Kitaev chain, motivated by a recent experiment on such a hybrid system [13]. The geometry of the setup is shown schematically in Figure 4.1. The Hamiltonian,

$$H_K = \sum_{i=1}^{\infty}\left[-tc_i^\dagger c_{i+1} + \Delta c_i c_{i+1} + \text{h.c.}\right] - \mu\sum_{i=1}^{\infty} c_i^\dagger c_i, \tag{4.1}$$

describes a semi-infinite Kitaev chain with hopping integral t, p-wave pairing potential Δ, and chemical potential μ. As discussed in section 2.1.1 the Kitaev chain supports two phases - a topologically trivial phase for $|\mu| > 2t$ characterised by strong pairing of on-site Majorana modes $\gamma_i = c_i + c_i^\dagger$ and $\gamma_i' = -i(c_i - c_i^\dagger)$, and a topological phase for $|\mu| < 2t$ that is characterised by strong pairing of nearest neighbour modes γ_i' and γ_{i+1}. The latter phase supports Majorana zero modes (MZMs) γ_1 and γ_N' ($N \to \infty$ in a semi-infinite chain) that are exponentially localised at the left and right ends.

The quantum dot is modelled as an Anderson impurity, coupled to the Majorana

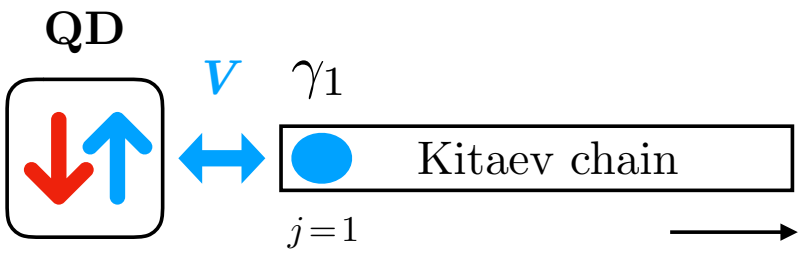

FIGURE 4.1 – Geometry of the setup described by the KMAI model.

end mode γ_1 of the Kitaev chain. The resulting system is described by a Hamiltonian,

$$H = H_K - iV\gamma_1 d_\uparrow + iV d_\uparrow^\dagger \gamma_1 + H_A, \tag{4.2}$$

where H_A is the Hamiltonian describing the Anderson impurity, given by Eq. (3.2). This model is hereafter referred to as the KMAI (Kitaev-Majorana-Anderson impurity) model. The SS representation of the KMAI model is obtained by simply substituting $H_C = H_K$ and $V_j = V\delta_{j1}$ in Eq. (3.15) to get

$$H_{SS} = H_K - iV(c_1 + c_1^\dagger)\Gamma_\uparrow^x - iU\Gamma_\uparrow^x\Gamma_\uparrow^y + \epsilon(n_{f\downarrow} - 1/2), \tag{4.3}$$

where we have specialised to the exactly solvable limit $\epsilon = h$.

4.1 CALCULATIONS OF CORRELATION FUNCTIONS

4.1.1 *Slave-fermion Green functions*

All physical GFs can be expressed in terms of the GFs of slave-fermion operators $\{\Gamma_\uparrow^x, \Gamma_\uparrow^y, \Gamma_\uparrow^z, f_\downarrow, \gamma'_{f\uparrow} = -i(f_\uparrow - f_\uparrow^\dagger)\}$, which we denote by

$$\mathcal{G}_\uparrow^{\alpha\beta}(\tau_1 - \tau_2) = -\left\langle T_\tau \Gamma_\uparrow^\alpha(\tau_1)\Gamma_\uparrow^\beta(\tau_2)\right\rangle, \qquad \alpha \in \{x, y, z\} \tag{4.4}$$

$$\mathcal{G}_{\gamma'_{f\uparrow}}(\tau_1 - \tau_2) = -\left\langle T_\tau \gamma'_{f\uparrow}(\tau_1)\gamma'_{f\uparrow}(\tau_2)\right\rangle, \tag{4.5}$$

$$\mathcal{G}_{f\downarrow}(\tau_1 - \tau_2) = -\left\langle T_\tau f_\downarrow(\tau_1) f_\downarrow^\dagger(\tau_2)\right\rangle. \tag{4.6}$$

The calculation of these slave-fermion GFs is the subject of this subsection. The one-particle GFs of $\Gamma^z_\uparrow$, $\gamma'_{f\uparrow}$, and $f_\downarrow$ are trivial to calculate using the equation of motion method [108] - the $f_\downarrow$ are decoupled from the other fermions and have an energy ϵ, and $\Gamma^z_\uparrow$, $\gamma'_{f\uparrow}$ are zero energy Majorana modes that do not appear in H_{SS} [see Eq. (4.3)]. For example,

$$\begin{aligned}\mathcal{G}^{zz}_\uparrow(\tau) &= -\left\langle T_\tau \Gamma^z_\uparrow(\tau)\Gamma^z_\uparrow(0)\right\rangle, \\ &= -\theta(\tau)\left\langle \Gamma^\alpha_\uparrow(\tau)\Gamma^\beta_\uparrow(0)\right\rangle + \theta(-\tau)\left\langle \Gamma^z_\uparrow(0)\Gamma^z_\uparrow(-\tau)\right\rangle,\end{aligned} \tag{4.7}$$

where $\theta(\tau)$ is the Heaviside step function. Taking derivatives with respect to τ, and using $\Gamma^z_\uparrow(\tau) = \exp(\tau H_{SS})\Gamma^z_\uparrow \exp(-\tau H_{SS})$, we obtain

$$-\partial_\tau \mathcal{G}^{zz}_\uparrow(\tau) = \delta(\tau)\left\{\Gamma^z_\uparrow, \Gamma^z_\uparrow\right\} + \left\langle T_\tau\left[H_{SS}, \Gamma^z_\uparrow(\tau)\right]\Gamma^z_\uparrow(0)\right\rangle. \tag{4.8}$$

Since $\Gamma^z_\uparrow$ does not appear in the Hamiltonian, the two operators commute. Using the fact that $\{\Gamma^\alpha_\uparrow, \Gamma^\beta_\uparrow\} = 2\delta^{\alpha\beta}$, and Fourier transforming to the Matsubara frequency representation, we obtain

$$\mathcal{G}^{zz}_\uparrow(ik_n) = \frac{2}{ik_n}, \tag{4.9}$$

where ik_n are fermionic Matsubara frequencies. The Matsubara GFs of $\gamma'_{f\uparrow}$ and $f_\downarrow$ can be similarly calculated, with the results

$$\mathcal{G}_{\gamma'_{f\uparrow}}(ik_n) = \frac{2}{ik_n}, \tag{4.10}$$

$$\mathcal{G}_{f\downarrow}(ik_n) = \frac{1}{ik_n - \epsilon}, \tag{4.11}$$

The calculations of the GFs of $\Gamma^x_\uparrow$ and $\Gamma^y_\uparrow$ are nontrivial and necessitate the use of boundary Green function methods [109, 110], to which we turn next. For this purpose, it turns out to be convenient to express H_{SS} entirely in terms of complex fermions. Defining new complex fermion operators,

$$\eta = \frac{1}{2}(\Gamma^y_\uparrow + i\Gamma^x_\uparrow), \qquad \eta^\dagger = \frac{1}{2}(\Gamma^y_\uparrow - i\Gamma^x_\uparrow), \tag{4.12}$$

H_{SS} in Eq. (4.3) can be expressed, apart from trivial additive constants which do not affect correlation functions, as

$$H_{SS} = H_K - V(c_1^\dagger \eta + c_1 \eta + \text{h.c.}) + U(2\eta^\dagger\eta - 1) + \epsilon(n_{f\downarrow} - 1/2). \tag{4.13}$$

Later, we will show that the GFs of the Majorana fermions $\{\Gamma^x_\uparrow, \Gamma^y_\uparrow\}$ can be calculated from the Nambu GF of the spinor $(\eta \quad \eta^\dagger)^\intercal$. Eq. (4.13) can be rewritten in Bogoliubov-de-Gennes (BdG) form with Nambu spinor

$$\Psi = (f_\downarrow \quad f_\downarrow^\dagger \quad \eta \quad \eta^\dagger \quad c_1 \quad c_1^\dagger \quad c_2 \quad c_2^\dagger \quad ...)^\intercal$$

and semi-infinite BdG matrix h_{SS} as

$$H_{SS} = \frac{1}{2}\Psi^\dagger h_{SS}\Psi, \qquad h_{SS} = \left(\begin{array}{cccc|cccc} \epsilon_0 & 0 & 0 & 0 & 0 & 0 & 0 & ... \\ 0 & -\epsilon_0 & 0 & 0 & 0 & 0 & 0 & ... \\ 0 & 0 & 2U & 0 & -V & -V & 0 & ... \\ 0 & 0 & 0 & -2U & V & V & 0 & ... \\ \hline 0 & 0 & -V & V & -\mu & 0 & -t & -\Delta \\ 0 & 0 & -V & V & 0 & \mu & \Delta & t \\ 0 & 0 & 0 & 0 & -t & \Delta & -\mu & 0 \\ \vdots & \vdots & \vdots & \vdots & -\Delta & t & 0 & \ddots \end{array}\right). \tag{4.14}$$

Defining the matrices

$$T = \begin{pmatrix} -t & -\Delta \\ \Delta & t \end{pmatrix}, \quad C = \begin{pmatrix} -V & -V \\ V & V \end{pmatrix}, \tag{4.15}$$

the BdG matrix can be written in block tridiagonal form as

$$h_{SS} = \left(\begin{array}{cc|c|cc|c} \epsilon_0\sigma^z & 0 & 0 & 0 & 0 & \dots \\ 0 & 2U\sigma^z & C & 0 & 0 & \dots \\ \hline 0 & C^\dagger & -\mu\sigma^z & T & 0 & \dots \\ \hline 0 & 0 & T^\dagger & -\mu\sigma^z & T & 0 \\ 0 & 0 & 0 & T^\dagger & -\mu\sigma^z & T \\ \vdots & \vdots & \vdots & 0 & T^\dagger & \ddots \end{array}\right) \equiv \left(\begin{array}{c|c|c} H_A & J & 0 \\ \hline J^\dagger & H_S & T_{SB} \\ \hline 0 & T_{SB}^\dagger & H_B \end{array}\right), \tag{4.16}$$

where the new symbols defined in the matrix on the far right are to be identified with the corresponding partitions of the matrix in the middle, and $\{\sigma^x, \sigma^y, \sigma^z\}$ are Pauli matrices in Nambu space. Physically, H_A describes the impurity, H_S the boundary site of the Kitaev chain, H_B the bulk of the Kitaev chain, J the coupling between

the boundary and impurity, and T_{SB} the coupling between the boundary and bulk. Partitioning the resolvent matrix $\mathbf{G} = (z - h_{SS})^{-1}$ in correspondence with the partitions of h_{SS}, we write[1]

$$\mathbf{G} = \begin{pmatrix} \mathbf{G}_A & \mathbf{G}_{AS} & \mathbf{G}_{AB} \\ \mathbf{G}_{SA} & \mathbf{G}_S & \mathbf{G}_{SB} \\ \mathbf{G}_{BA} & \mathbf{G}_{BS} & \mathbf{G}_B \end{pmatrix}. \tag{4.17}$$

The identity $(z - h_{SS})\mathbf{G} = 1$ leads to a set of nine simultaneous equations for the submatrices of $\mathbf{G}$ that include

$$\begin{aligned} (z - H_A)\,\mathbf{G}_A - J\mathbf{G}_{SA} &= 1, \\ -T_{SB}^\dagger \mathbf{G}_{SA} + (z - H_B)\mathbf{G}_{BA} &= 0, \\ -J^\dagger \mathbf{G}_A + (z - H_S)\mathbf{G}_{SA} - T_{SB}\mathbf{G}_{BA} &= 0, \end{aligned} \tag{4.18}$$

from which we obtain for the impurity part of the resolvent,

$$\begin{aligned} \mathbf{G}_A^{-1} &= z - H_A - J\left[z - H_S - T_{SB}(z - H_B)^{-1} T_{SB}^\dagger\right]^{-1} J^\dagger \\ &\equiv z - H_A - J\mathbf{g}_S(z)J^\dagger. \end{aligned} \tag{4.19}$$

Since H_S describes the boundary site of the Kitaev chain, an interpretation of $T_{SB}(z - H_B)^{-1}T_{SB}^\dagger$ as the self-energy due to coupling the boundary site to the bulk leads to the identification of the term in square brackets in the first line as the left boundary (Nambu) GF of the Kitaev chain (*without* an impurity), which we denote as $\mathbf{g}_S(z)$ in the second line.[2] The expression for $\mathbf{G}_A^{-1}$ itself can be interpreted similarly, with the third term being the self-energy due to coupling (J) the impurity (H_A) to the boundary of the Kitaev chain. An explicit expression for $\mathbf{g}_S(z)$ can be calculated following the method outlined in Ref. [112]. The strategy is as follows - we first calculate the bulk GF of an infinite Kitaev chain and then obtain the boundary GF

[1] $z \in \mathbb{C}$ is a general complex-valued frequency. Evaluation of the resolvent $\mathbf{G}(z)$ on the imaginary axis $z = ik_n$ yields the frequency representation of the corresponding Matsubara GF whereas the substitutions $z = \omega \pm i\eta$, with $\omega \in \mathbb{R}$ and η a positive infinitesimal, yield the (real) frequency representation of the retarded and advanced GFs respectively [111].

[2] In other words, $\mathbf{g}_S$ is the real-space Nambu GF of the spinor $(c_1 \quad c_1^\dagger)^\intercal$, where $c_1^{(\dagger)}$ annihilates (creates) a fermion at the boundary site $j = 1$.

from the Dyson equation that results when the chain is effectively cut in half by an infinite local potential. Since the calculation is somewhat tedious and lies outside the current line of development, it has been relegated to Appendix A. Substitution of H_A and J from Eq. (4.16) into Eq. (4.19) yields

$$\mathbf{G}_A^{-1} = \begin{pmatrix} z - \epsilon_0 \sigma^z & 0 \\ 0 & z - 2U\sigma^z - V^2\left[\sum_{\mu,\nu=1}^{2} \mathbf{g}_S^{\mu\nu}(z)\right](1-\sigma^x) \end{pmatrix}. \tag{4.20}$$

The sum of all matrix elements of the Nambu GF $\mathbf{g}_S(z)$ is simply the frequency representation of the boundary Majorana GF $g_{\gamma_1}(\tau) = -\langle T_\tau \gamma_1(\tau)\gamma_1(0)\rangle$, where $\gamma_1 = c_1 + c_1^\dagger$. The inverse of the first diagonal block of $\mathbf{G}_A$ is clearly the Nambu GF of $(f_\downarrow \quad f_\downarrow^\dagger)^\intercal$ and is consistent with Eq. (4.9), while the inverse of the second block is that of $(\eta \quad \eta^\dagger)^\intercal$ which we denote as $\mathbf{G}_\eta$ and is given by

$$\mathbf{G}_\eta(z) = \frac{1}{z^2 - 4U^2 - 2V^2 z g_{\gamma_1}(z)} \begin{pmatrix} z + 2U - V^2 g_{\gamma_1}(z) & -V^2 g_{\gamma_1}(z) \\ -V^2 g_{\gamma_1}(z) & z - 2U - V^2 g_{\gamma_1}(z) \end{pmatrix}. \tag{4.21}$$

The GFs of the Majorana fermions $\Gamma_\uparrow^x$ and $\Gamma_\uparrow^y$ can be computed from $\mathbf{G}_\eta$, as $\eta^{(\dagger)} = (\Gamma_\uparrow^y \pm i\Gamma_\uparrow^x)/2$. For example, the Matsubara GF of $\Gamma_\uparrow^y = \eta + \eta^\dagger$ is

$$\begin{aligned} \mathcal{G}_\uparrow^{yy}(\tau) &= -\left\langle T_\tau[\eta(\tau) + \eta^\dagger(\tau)][\eta(0) + \eta^\dagger(0)]\right\rangle = \sum_{\mu,\nu=1}^{2} \mathbf{G}_\eta^{\mu\nu}(\tau), \\ \implies \mathcal{G}_\uparrow^{yy}(z) &= \frac{2z - 4V^2 g_{\gamma_1}(z)}{z^2 - 4U^2 - 2V^2 z g_{\gamma_1}(z)}. \end{aligned} \tag{4.22}$$

Similarly,

$$\begin{aligned} \mathcal{G}_\uparrow^{xx}(\tau) &= -(-i)^2\left\langle T_\tau[\eta(\tau) - \eta^\dagger(\tau)][\eta(0) - \eta^\dagger(0)]\right\rangle = \sum_{\mu,\nu=1}^{2} (-1)^{\mu+\nu} \mathbf{G}_\eta^{\mu\nu}(\tau) \\ \implies \mathcal{G}_\uparrow^{xx}(z) &= \frac{2z}{z^2 - 4U^2 - 2V^2 z g_{\gamma_1}(z)}. \end{aligned} \tag{4.23}$$

Mixed GFs such as $\mathcal{G}_\uparrow^{xy}(z)$ can also be calculated from appropriate linear combinations of the matrix elements $\mathbf{G}_\eta^{\mu\nu}(z)$ in Eq. (4.21).

4.1.2 *Impurity Green functions*

Recall from section 3.4 that correlation functions of physical operators that commute with the local particle-hole transformation $\mathcal{D}_\uparrow$ can be calculated in the SS representation without constraint. The one-particle Green function (GF) of the impurity $d_\downarrow$-fermion is an example. The corresponding Matsubara function is expressed in the SS representation using Eqs. (3.7) and (3.31) as

$$\begin{aligned}\mathcal{G}_{d\downarrow} &= -\left\langle T_\tau \mu^x(\tau) f_\downarrow(\tau) \mu^x(0) f_\downarrow^\dagger(0)\right\rangle_{SS}, \\ &= -\left\langle T_\tau \Gamma_\uparrow^y(\tau)\Gamma_\uparrow^y(0)\Gamma_\uparrow^z(\tau)\Gamma_\uparrow^z(0) f_\downarrow(\tau) f_\downarrow^\dagger(0)\right\rangle_{SS}, \end{aligned} \tag{4.24}$$

where the Pauli matrices μ^x, μ^y have been expressed in terms of Majorana fermions (Γ) using Eq. (3.14). Since the expectation value on the RHS is with respect to the thermal ensemble defined by the quadratic H_{SS}, one may Wick contract the RHS into

$$\begin{aligned}\mathcal{G}_{d\downarrow}(\tau) &= -\left\langle T_\tau \Gamma_\uparrow^y(\tau)\Gamma_\uparrow^y(0)\right\rangle_{SS}\left\langle T_\tau \Gamma_\uparrow^z(\tau)\Gamma_\uparrow^z(0)\right\rangle_{SS}\left\langle T_\tau f_\downarrow(\tau) f_\downarrow^\dagger(0)\right\rangle_{SS}, \\ &= \mathcal{G}_\uparrow^{yy}(\tau)\mathcal{G}_\uparrow^{zz}(\tau)\mathcal{G}_{f\downarrow}(\tau). \end{aligned} \tag{4.25}$$

The GFs on the RHS are those of slave-fermions and therefore strictly defined only with respect to the slave-spin Hamiltonian H_{SS}, whereas the LHS is a physical GF defined with respect to H. It is to be understood from context whether a GF is physical or defined only in the SS representation. Working in the Matsubara frequency representation, we obtain

$$\mathcal{G}_{d\downarrow}(ik_n) = \frac{1}{\beta^2}\sum_{ip_n}\sum_{iq_n}\mathcal{G}_\uparrow^{yy}(ip_n)\mathcal{G}_\uparrow^{zz}(iq_n)\mathcal{G}_{f\downarrow}(ik_n - ip_n - iq_n), \tag{4.26}$$

which is diagrammatically represented in Figure 4.2. $\beta = T^{-1}$ is the inverse temperature and ip_n, iq_n, ik_n are fermionic Matsubara frequencies. Therefore, the $d_\downarrow$-fermion in the SS representation corresponds to $f_\downarrow$ dressed by a two-particle bubble of the spin-up Majorana fermions $\Gamma_\uparrow^y$ and $\Gamma_\uparrow^z$, similar to the localised fermions in the Majorana-Falicov-Kimball model [92]. However, in contrast to usual diagrammatic perturbation theory, the bubble diagram in Figure 4.2 gives the exact, fully resummed

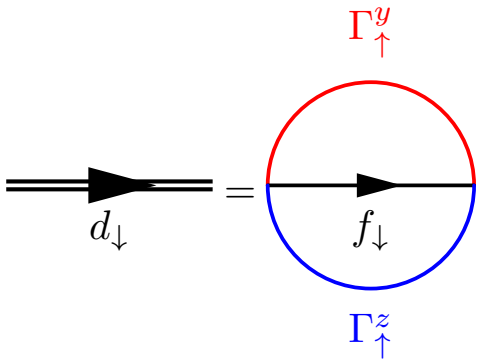

FIGURE 4.2 – Diagrammatic representation of the physical $d_\downarrow$ impurity propagator in terms of slave-fermion propagators. Matsubara frequencies are omitted for simplicity.

propagator of the physical $d_\downarrow$-fermion. The fact that the physical impurity GF is a convolution product of free slave-fermion GFs gives rise to temperature dependence in the physical spectral function, as will be seen below. This emphasises that the physical impurity degrees of freedom are interacting, even though the slave-fermions are not. The slave-fermion GFs appearing in the RHS of Eq. (4.26) were calculated explicitly in section 4.1.1. Substituting the results for $\mathcal{G}^{zz}_\uparrow$ and $\mathcal{G}_{f\downarrow}$,

$$\begin{aligned}\mathcal{G}_{d\downarrow}(ik_n) &= \frac{1}{\beta^2}\sum_{ip_n}\sum_{iq_n}\mathcal{G}^{yy}_\uparrow(ip_n)\frac{2}{iq_n}\frac{1}{ik_n - ip_n - iq_n - \epsilon},\\ &= \frac{1}{\beta}\sum_{ip_n}\mathcal{G}^{yy}_\uparrow(ip_n)\frac{2n_F(\epsilon)-1}{ik_n - ip_n - \epsilon},\end{aligned} \tag{4.27}$$

where the Matsubara sum over iq_n has been performed in the second line and $n_F(x) = [\exp(x/T)+1]^{-1}$ is the Fermi function at a temperature T. Note that if $\epsilon = 0$ (when the physical Hamiltonian H enjoys full particle-hole symmetry), the sum over iq_n gives $\beta\delta_{k_n,p_n}/2$ and so $\mathcal{G}^{ph}_{d\downarrow}(ik_n) = \mathcal{G}^{yy}_\uparrow(ik_n)/2$, where the superscript ph denotes the GF in the particle-hole symmetric limit. Denoting the corresponding spectral function as $A^{ph}_{d\downarrow}(\omega) = -2\,\mathrm{Im}\left\{\mathcal{G}^{ph}_{d\downarrow}(ik_n \to \omega + i\eta)\right\}$ and introducing the spectral representation of

this GF, we obtain

$$\begin{aligned}\mathcal{G}_{d\downarrow}(ik_n) &= \int_{-\infty}^{\infty}\frac{\mathrm{d}\omega'}{2\pi}A^{ph}_{d\downarrow}(\omega')\frac{2}{\beta}\sum_{ip_n}\frac{1}{ip_n-\omega'}\frac{2n_F(\epsilon)-1}{ik_n-ip_n-\epsilon},\\ &= \int_{-\infty}^{\infty}\frac{\mathrm{d}\omega'}{2\pi}\frac{A^{ph}_{d\downarrow}(\omega')}{ik_n-\epsilon-\omega'}\cdot 2\left[2n_F(\omega')-n_B(\epsilon)-1\right]\left[2n_F(\epsilon)-1\right], \end{aligned} \tag{4.28}$$

where $n_B(x)=[\exp(x/T)-1]^{-1}$ is the Bose function at a temperature T. Although the integral cannot be computed in closed form, the spectral function can be obtained upon analytic continuation $ik_n\to\omega+i\eta$ to real frequencies using the distribution identity $(x-x_0+i\eta)^{-1}=\mathcal{P}(1/x-x_0)-i\pi\delta(x-x_0)$,where $\mathcal{P}$ denotes the Cauchy principal value, with the result

$$A_{d\downarrow}(\omega,T)=2\left[1-2n_F(\epsilon)\right]\{n_B(\epsilon)n_F(\omega-\epsilon)+\left[n_B(\epsilon)+1\right]\left[1-n_F(\omega-\epsilon)\right]\}A^{ph}_{d\downarrow}(\omega-\epsilon), \tag{4.29}$$

where

$$A^{ph}_{d\downarrow}(\omega)=-\operatorname{Im}\mathcal{G}^{yy}_{\uparrow}(\omega)=-2\operatorname{Im}\frac{\omega+i\eta-2V^2g_{\gamma_1}(\omega)}{(\omega+i\eta)^2-4U^2-2V^2(\omega+i\eta)g_{\gamma_1}(\omega)}, \tag{4.30}$$

is the temperature independent spectral function in the particle-hole symmetric limit $\epsilon=0$. A discussion of the various features of $A_{d\downarrow}$ is relegated to section 4.2.

Recall from section 3.4 that the one-particle GF for the hybridising $d_\uparrow$ impurity fermion must be calculated in the SS representation with constraint,

$$\begin{aligned}\mathcal{G}_{d\uparrow}(\tau_1-\tau_2) &= -\left\langle T_\tau d_\uparrow(\tau_1)d^\dagger_\uparrow(\tau_2)\right\rangle,\\ &= -\left\langle T_\tau \mu^x(\tau_1)f_\uparrow(\tau_1)\mu^x(\tau_2)f^\dagger_\uparrow(\tau_2)\mathbb{P}\right\rangle_{SS}. \end{aligned} \tag{4.31}$$

To express the operators inside the expectation value in terms of the slave-fermions that define H_{SS}, we may use $\mu^x=-i\Gamma^y_\uparrow\Gamma^z_\uparrow$ [see Eq. (3.14)], the fermion representation of $\mathbb{P}$ in Eq. (3.33), and

$$\begin{aligned}f^{(\dagger)}_\uparrow &= \frac{1}{2}\left[(f_\uparrow+f^\dagger_\uparrow)\pm(f_\uparrow-f^\dagger_\uparrow)\right],\\ &= \frac{1}{2}\left(\mu^z\Gamma^z_\uparrow\pm i\gamma'_{f\uparrow}\right),\\ &= \frac{i}{2}\left(-\Gamma^x_\uparrow\Gamma^y_\uparrow\Gamma^z_\uparrow\pm\gamma'_{f\uparrow}\right). \end{aligned} \tag{4.32}$$

Substituting these into Eq. (4.31), some tedious but straightforward algebraic simplification and Wick contraction gives

$$\begin{aligned}\mathcal{G}_{d\uparrow}(\tau_1-\tau_2) = \frac{1}{4}[&\mathcal{G}^{xx}_{\uparrow}(\tau_1-\tau_2) + \mathcal{G}^{yy}_{\uparrow}(\tau_1-\tau_2)\mathcal{G}^{zz}_{\uparrow}(\tau_1-\tau_2)\mathcal{G}_{\gamma'_{f\uparrow}}(\tau_1-\tau_2)\\ &+ 2i\mathcal{G}_{f\downarrow}(0)\mathcal{G}^{xy}_{\uparrow}(\tau_1-\tau_2)\mathcal{G}^{zz}_{\uparrow}(\tau_2)\mathcal{G}_{\gamma'_{f\uparrow}}(\tau_2)\\ &+ 2i\mathcal{G}_{f\downarrow}(0)\mathcal{G}^{xy}_{\uparrow}(\tau_1-\tau_2)\mathcal{G}^{zz}_{\uparrow}(\tau_1)\mathcal{G}_{\gamma'_{f\uparrow}}(\tau_1)\\ &- i\mathcal{G}^{xy}_{\uparrow}(\tau_1-\tau_2)\mathcal{G}^{zz}_{\uparrow}(\tau_2)\mathcal{G}_{\gamma'_{f\uparrow}}(\tau_2)\\ &- i\mathcal{G}^{xy}_{\uparrow}(\tau_1-\tau_2)\mathcal{G}^{zz}_{\uparrow}(\tau_1)\mathcal{G}_{\gamma'_{f\uparrow}}(\tau_1)].\end{aligned} \tag{4.33}$$

Note that the exact $d_\uparrow$-fermion GF is not represented by a single two-bubble diagram of slave-fermion propagators, but is a finite series of diagrams. This is unlike the $d_\downarrow$-fermion GF shown in Figure 4.2. A laborious Fourier transform to the Matsubara frequency representation, substitution of the relevant slave-fermion GFs from section 4.1.1, and tortuous algebra including Matsubara sums yields the simple result

$$\mathcal{G}_{d\uparrow}(ik_n) = \frac{ik_n - V^2 g_{\gamma_1}(ik_n) + 2U\,[2n_F(\epsilon)-1]}{(ik_n)^2 - 4U^2 - 2ik_n V^2 g_{\gamma_1}(ik_n)}. \tag{4.34}$$

4.1.3 *Local Green functions of the host material*

The host c_j-fermion operators that appear in the slave-spin Hamiltonian H_{SS} are the same as the physical c_j-fermions, as only the impurity fermion Hilbert space is enlarged in the slave-spin method. The local GFs of the c_j-fermions can be calculated in the same boundary GF framework presented in section 4.1.1, by repartitioning and considering appropriate blocks of the BdG and resolvent matrices in Eqs. (4.16) and (4.17). Let us first calculate the boundary Nambu GF, that is of $(c_1 \quad c_1^\dagger)^\intercal$, in the KMAI model. This corresponds to the $\mathbf{G}_S$ block in the resolvent matrix in Eq. (4.17). The identity $(z - h_{SS})\mathbf{G} = 1$ yields the following simultaneous equations for $\mathbf{G}_S$,

$$\begin{aligned}(z-H_A)\mathbf{G}_{AS}-JG_S&=0,\\ -J^\dagger\mathbf{G}_{AS}+(z-H_S)\mathbf{G}_S-T_{SB}\mathbf{G}_{BS}&=1,\\ -T_{SB}^\dagger\mathbf{G}_S+(z-H_B)\mathbf{G}_{BS}&=0,\end{aligned}\tag{4.35}$$

from which we obtain

$$\begin{aligned}\mathbf{G}_S^{-1}&=z-H_S-T_{SB}(z-H_B)^{-1}T_{SB}^\dagger-J^\dagger(z-H_A)^{-1}J,\\ &=\mathbf{g}_S^{-1}(z)-J^\dagger(z-H_A)^{-1}J,\\ &=\mathbf{g}_S^{-1}(z)-\frac{2V^2z}{z^2-4U^2}(1+\sigma^x),\end{aligned}\tag{4.36}$$

where $\mathbf{g}_S(z)$ is the left boundary Nambu GF of the Kitaev chain in the *absence* of an impurity, as defined earlier in Eq. (4.19) and calculated in Appendix A. The second term in the second and third lines of Eq. (4.36) is thus the self-energy due to hybridisation with an interacting Anderson impurity. For convenience, we relabel $\mathbf{G}_S(z)\to\mathbf{G}_c(j=1;z)$, where j is a lattice site index and the subscript c denotes that it is a c-fermion GF. The interior, local GFs for $j>1$ can be calculated using the Dyson equation,

$$\mathbf{G}_c^{-1}(j>1;z)=\mathbf{g}_S^{-1}(z)-T^\dagger\rho_{j-1}(i=j-1;z)T,\tag{4.37}$$

where T is a coupling matrix defined earlier in Eqs. (4.15)-(4.16) and $\rho_{j-1}(i=j-1;z)$ is the *right boundary* Nambu GF of a *finite* $(j-1)$-site (subscript) Kitaev chain coupled to an Anderson impurity at the left boundary ($i=j-1$). This is a finite KMAI system with a finite slave-spin BdG Hamiltonian $h_{SS}^{(j-1)}$ that is obtained simply by truncating h_{SS} in Eq. (4.16) appropriately, at the $(j-1)$-th $\mu\sigma^z$ block. $\rho_{j-1}(i=j-1;z)$ itself can be calculated from the Dyson equation,

$$\begin{aligned}\rho_{j-1}(i=j-1;z)&=\left[z+\mu\sigma^z-T^\dagger\rho_{j-2}(i=j-2;z)T\right]^{-1},\\ &=T^{-1}\left[(z+\mu\sigma^z)T^{-1}-T^\dagger\rho_{j-2}(i=j-2;z)\right]^{-1}.\end{aligned}\tag{4.38}$$

The RHS of this equation is a matrix Möbius transformation [109] of $\rho_{j-2}(i=j-2;z)$. Given a $2M\times 2M$ matrix $\Lambda=\left(\begin{smallmatrix}\mathbf{a}&\mathbf{b}\\ \mathbf{c}&\mathbf{d}\end{smallmatrix}\right)$, where $\mathbf{a},\mathbf{b},\mathbf{c},\mathbf{d}$ are $M\times M$ matrices, the matrix

Möbius transformation of another $M\times M$ matrix $\mathbf{x}$ *by* Λ is defined as $\Lambda\bullet\mathbf{x}=(\mathbf{a}\mathbf{x}+\mathbf{b})(\mathbf{c}\mathbf{x}+\mathbf{d})^{-1}$. Therefore, we have

$$\begin{aligned}\rho_{j-1}(i=j-1;z)&=\begin{pmatrix}0 & T^{-1}\\ -T^{\dagger} & (z+\mu\sigma^z)\,T^{-1}\end{pmatrix}\bullet\rho_{j-2}(i=j-2;z),\\ &=\begin{pmatrix}0 & T^{-1}\\ -T^{\dagger} & (z+\mu\sigma^z)\,T^{-1}\end{pmatrix}^{j-2}\bullet\rho_1(z),\end{aligned}\tag{4.39}$$

where $\rho_1(z)$ is the GF of a single site coupled to an Anderson impurity, and so given by

$$\begin{aligned}\rho_1(z)&=\left[z+\mu\sigma^z-J^{\dagger}(z-H_A)^{-1}J\right]^{-1},\\ &=\left[z+\mu\sigma^z-\frac{2V^2z}{z^2-4U^2}\,(1+\sigma^x)\right]^{-1}.\end{aligned}\tag{4.40}$$

The local density of states (LDOS) on a general site j can be calculated from the corresponding local GF as $-\mathrm{Im}\,\mathrm{tr}\,\mathbf{G}_c(j;z)$.

4.2 IMPURITY SPECTRAL FUNCTIONS

We now turn to a discussion of the various features of the impurity spectral functions $A_{d\sigma}(\omega,T)$ in the KMAI model, beginning with a study of their temperature dependence. We reproduce from section 4.1.1 the relevant results - the $d_\downarrow$-fermion spectral function is

$$A_{d\downarrow}(\omega,T)=2\left[1-2n_F(\epsilon)\right]\{n_B(\epsilon)n_F(\omega-\epsilon)+\left[n_B(\epsilon)+1\right]\left[1-n_F(\omega-\epsilon)\right]\}A^{ph}_{d\downarrow}(\omega-\epsilon),\tag{4.41}$$

where the temperature independent spectral function at the particle-hole symmetric point $\epsilon=0$ is

$$A^{ph}_{d\downarrow}(\omega)=-2\,\mathrm{Im}\,\frac{\omega+i\eta-2V^2g_{\gamma_1}(\omega)}{(\omega+i\eta)^2-4U^2-2V^2(\omega+i\eta)g_{\gamma_1}(\omega)}.\tag{4.42}$$

The first term in Eq. (4.41) corresponds to the absorption of a spin-up bosonic two-particle fluctuation of energy ϵ by a spin-down fermion of energy $\omega-\epsilon$, while the

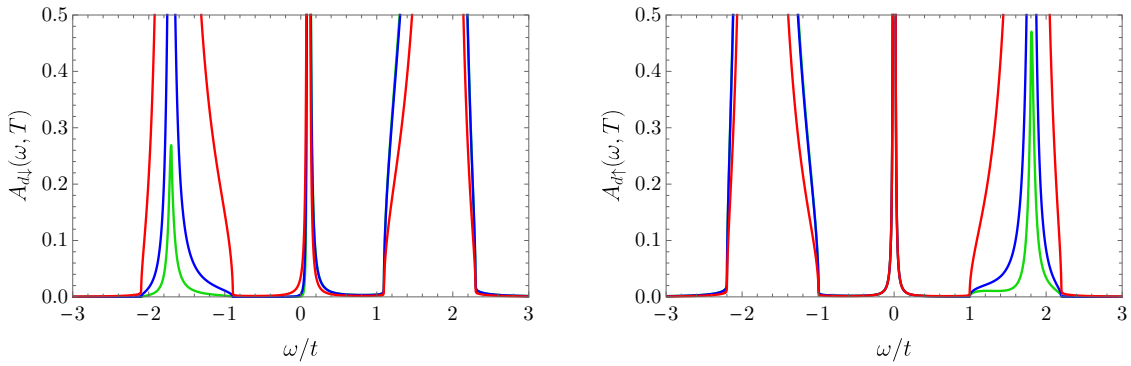

FIGURE 4.3 – Spectral functions of (a) localised $d_\downarrow$ and (b) hybridising $d_\uparrow$-fermions for various temperatures T, shown in the topological phase. In all plots, $\mu = 0.2t$, $\Delta = 0.5t$, $V = 0.4t$, $U = 0.8t$, $\epsilon = 0.1t$ are fixed. $T = 0.02t$ (green), $T = 0.03t$ (blue), $T = 0.5t$ (red) .

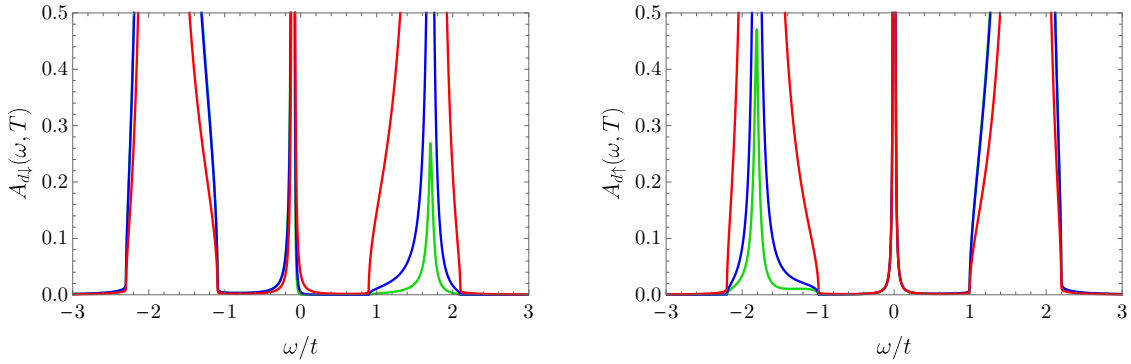

FIGURE 4.4 – Spectral functions of (a) localised $d_\downarrow$ and (b) hybridising $d_\uparrow$-fermions for various temperatures T, shown in the topological phase. In all plots, $\mu = 0.2t$, $\Delta = 0.5t$, $V = 0.4t$, $U = 0.8t$, $\epsilon = -0.1t$ are fixed. $T = 0.02t$ (green), $T = 0.03t$ (blue), $T = 0.5t$ (red). Note that $\epsilon < 0$ and the spectral asymmetry is reversed here in comparison to the plots in Figure 4.3.

second term describes the emission, stimulated or spontaneous, of such a two-particle fluctuation by a fermion of energy ω. Turning now to the hybridising $d_\uparrow$-fermion, its spectral function is given by

$$A_{d\uparrow}(\omega, T) = -2\,\mathrm{Im}\,\frac{\omega + i\eta - V^2 g_{\gamma_1}(\omega) + 2U\,[2n_F(\epsilon) - 1]}{(\omega + i\eta)^2 - 4U^2 - 2(\omega + i\eta)V^2 g_{\gamma_1}(\omega)}. \tag{4.43}$$

It is easy to see that the deviation ϵ from particle-hole symmetry sets the scale for the interaction-induced temperature dependence of both spectral functions. Low temperature and $\epsilon > 0$ accentuate the spectral asymmetry in $A_{d\downarrow}$ (or $A_{d\uparrow}$) about

$\omega = \epsilon$ (or $\omega = 0$), shifting spectral weight towards excitations with energy $\omega > \epsilon$ (or $\omega < 0$). It can be seen from Eq. (4.41) that, in the limit $T \gg \epsilon$, the temperature-dependent prefactors of $A^{ph}_{d\downarrow}(\omega)$ tend to unity, and particle-hole symmetry is restored (see Figure 4.3a). Similarly, the temperature-dependent factor $2U[2n_F(\epsilon) - 1]$ in Eq. (4.43) tends to zero for $T \gg \epsilon$ and particle-hole symmetry is also restored to $A_{d\uparrow}$ in this limit (see Figure 4.3b). This behaviour with respect to temperature can be intuitively understood in the atomic limit ($V = 0$) of an isolated impurity. In this limit, the GFs of the impurity fermions can be calculated exactly, as the exact eigenstates and eigenvalues of H_A in Eq. (3.2) are known - these are the Fock states $\{|0\rangle_d, |\uparrow\rangle_d, |\downarrow\rangle_d, |\uparrow\downarrow\rangle_d\}$ [see Eq. (3.6)] with respective eigenvalues $\{U - \epsilon/2, -U - \epsilon/2, -U + \epsilon/2, U + \epsilon/2\}$ in the exactly solvable limit $\epsilon = h$. Using the Lehmann representation of the spectral function[3], it is easy to show that the spectral functions in the atomic limit (superscript *at*) are

$$A^{at}_{d\downarrow}(\omega, T) = \left\langle n_{d\uparrow} \right\rangle 2\pi\delta(\omega - \epsilon - 2U) + \left\langle 1 - n_{d\uparrow} \right\rangle 2\pi\delta(\omega - \epsilon + 2U), \tag{4.44}$$

$$A^{at}_{d\uparrow}(\omega, T) = \left\langle n_{d\downarrow} \right\rangle 2\pi\delta(\omega - 2U) + \left\langle 1 - n_{d\downarrow} \right\rangle 2\pi\delta(\omega + 2U), \tag{4.45}$$

where $\langle n_{d\sigma} \rangle$ is the mean occupation of impurity spin $\sigma \in \{\uparrow, \downarrow\}$. The two infinitely sharp peaks in $A_{d\downarrow}$ at the energies $\omega_{\pm} = \epsilon \pm 2U$ correspond to localised charge excitations ($|\uparrow\rangle \to |\uparrow\downarrow\rangle$ and $|0\rangle \to |\downarrow\rangle$ respectively) that can occur from injecting a $d_\downarrow$-fermion on the quantum dot. The spectral weight (probability) for ω_+ ($|\uparrow\rangle \to |\uparrow\downarrow\rangle$) is greater as it is proportional to the $d_\uparrow$-fermion occupancy $\left\langle n_\uparrow \right\rangle$, which is favoured over $d_\downarrow$-fermion occupancy for $\epsilon > 0$ since the latter has a chemical potential of $\epsilon - 2U$ while the former has one of $-2U$. Flipping the sign of ϵ reverses this asymmetry, for $d_\downarrow$-fermion occupancy is then favoured (see Figure 4.4) — the spectral weight of $\omega_- < 0$

[3] This is just the spectral function in the basis specified by the exact eigenstates of the Hamiltonian, and is given by [108]

$$A_{d\sigma}(\omega, T) = \frac{2\pi}{Z} \sum_{mn} \left| \langle m | d^\dagger_\sigma | n \rangle \right|^2 \left(e^{-\beta E_m} + e^{-\beta E_n} \right) \delta(\omega - E_m + E_n),$$

where $\beta = T^{-1}$ and the states summed over are the exact many-body eigenstates of the Hamiltonian under consideration. There are sharp peaks (delta functions) at the exact excitation energies of the system.

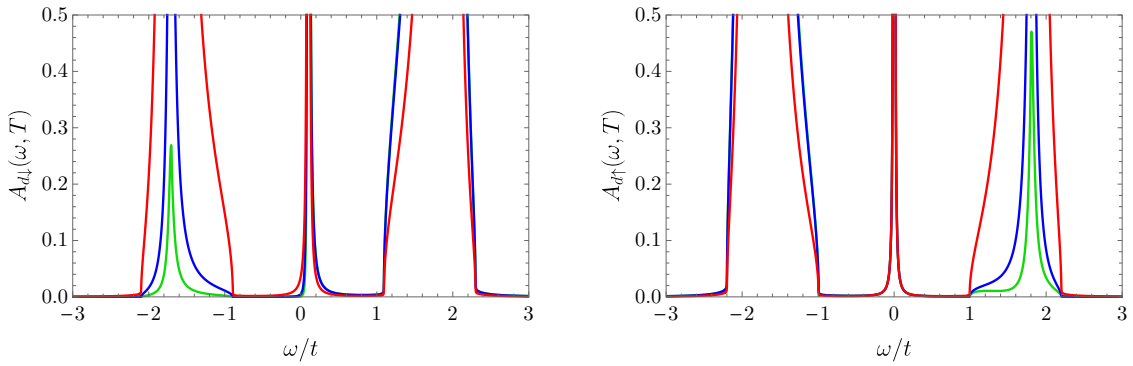

FIGURE 4.5 – Spectral functions of (a) localised $d_\downarrow$ and (b) hybridising $d_\uparrow$-fermions for various interaction strengths U, shown in the topological phase. In all plots, $\mu = 0.2t$, $\Delta = 0.5t$, $V = 0.4t$, $\epsilon = 0.1t$, $T = 0.05t$ are fixed. $U = 0.05t$ (green), $U = 0.8t$ (blue), $U = 1.2t$ (red).

is then greater than that of ω_+. The temperature dependence of $A_{d\uparrow}$ can be similarly explained. This behaviour with temperature carries over when the hybridisation V is finite, which is the case in Figures 4.3-4.4. Of course, then the eigenstates of H_A are not the true stationary states of the system, and the charge excitations with energies $\omega_\pm$ acquire a finite lifetime, which is reflected as a broadening of the sharp spectral peaks at those energies that were present in the atomic limit.

In the topological phase of the KMAI model, when the hybridisation (V) and interaction (U) are both non-zero, both impurity GFs have three poles which manifest as quasiparticle peaks in their spectral functions (Figure 4.5). The two side peaks correspond to impurity charge excitations, present also in the atomic limit ($V = 0$), with a gap that increases monotonically with both U and V. For small U and V, these excitations feature as sharp peaks inside the energy gap of the Kitaev SC. As U or V is increased, they fall into the SC energy bands and broaden, and then eventually again become sharp peaks when they move out of the bandwidth of the SC. The fact that the gap increases monotonically with U is not so surprising, as these excited states differ in charge/occupancy, and the same behaviour is seen in the atomic limit. The reason for the monotonicity of the gap with hybridisation V is unclear.[4]

The third quasiparticle peak, at $\omega = \epsilon$ in $A_{d\downarrow}$ and $\omega = 0$ in $A_{d\uparrow}$ is never broadened

[4]The monotonicity of the gap with V is also present only in the topological phase.

and persists for any non-zero U, V. Let us first consider the peak at $\omega = \epsilon$ in $A_{d\downarrow}$. This is where a sharp peak would occur were the $d_\downarrow$-fermion free ($U = 0$), but it is not and the peak persists for large U. This is actually a signature of the presence of a MZM, as can be understood from the small U/V limit. A semi-infinite Kitaev chain in the topological phase implies that there must be an exact zero energy Majorana mode at the boundary.[5] But the original MZM $(c_1 + c_1^\dagger)$ of the Kitaev chain is now fused/paired with $(d_\uparrow + d_\uparrow^\dagger)$ to form a local complex fermion at some non-zero energy (proportional to V) due to the hybridisation term H_{hyb} in the Hamiltonian. Neither of the two Majorana modes that make up the $d_\downarrow$-fermion can be the new MZM as $n_{d\downarrow}$ is conserved. The only choice left is $-i(d_\uparrow - d_\uparrow^\dagger)$, and therefore this must be the new MZM in the small U/V limit. Note that this is permitted as $n_{d\uparrow}$ is not conserved in the KMAI model. As it has to be an exact zero energy mode, interactions cannot change its energy. In this limit then, the $d_\downarrow$-fermion becomes free, and this features as a sharp 'free fermion' peak in $A_{d\downarrow}$ at $\omega = \epsilon$. That $-i(d_\uparrow - d_\uparrow^\dagger)$ is the preferred MZM in this limit features as a sharp peak at zero energy $\omega = 0$ in $A_{d\uparrow}$.

This picture is further corroborated by spectral functions of the Majorana modes $(d_\uparrow + d_\uparrow^\dagger)$ and $-i(d_\uparrow - d_\uparrow^\dagger)$, shown in Figures 4.6a-b. As expected, the zero energy ($\omega = 0$) peak is only present in the spectral function of $-i(d_\uparrow - d_\uparrow^\dagger)$. In the large U/V limit, energetics suggest that the original mode $(c_1 + c_1^\dagger)$ will be the preferred MZM. This is because $-i(d_\uparrow - d_\uparrow^\dagger)$ participates in the interaction, which tends to split the zero energy level. Therefore, the hybridisation and interaction terms in the KMAI model compete over the preferred MZM, with the former selecting $-i(d_\uparrow - d_\uparrow^\dagger)$ and the latter $(c_1 + c_1^\dagger)$. Another check of this picture is provided by the local density of states of the host c_j-fermions, and will be discussed below in section 4.6.

[5] Recall from section 2.1.1 that the non-local zero energy level due to the MZMs splits away from zero energy only if the Kitaev chain is of finite length (or gapless in the bulk), with a splitting that is exponentially suppressed in the length.

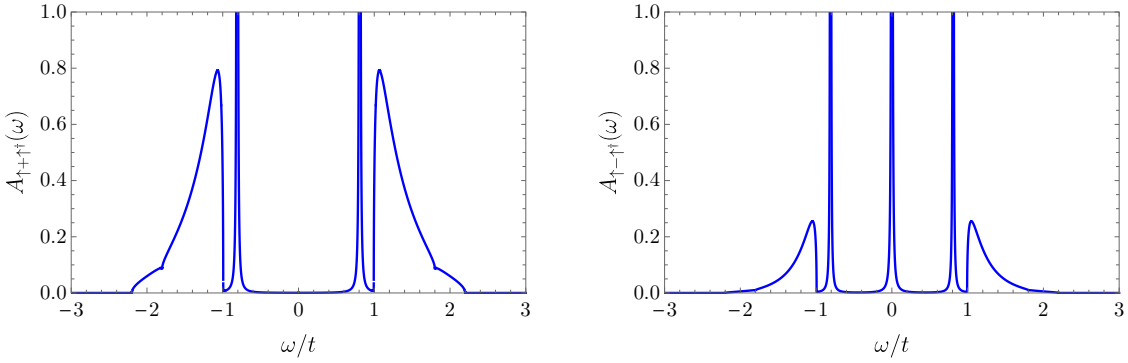

FIGURE 4.6 – Spectral functions of the Majorana modes (a) $(d_\uparrow + d_\uparrow^\dagger)$ and (b) $-i(d_\uparrow - d_\uparrow^\dagger)$, shown in the topological phase. In both plots, $\mu = 0.2t$, $\Delta = 0.5t$, $V = 0.3t$, $U = 0.3t$. The spectral peak at $\omega = 0$ in (b) has weight that increases with hybridisation V, implying that $-i(d_\uparrow - d_\uparrow^\dagger)$ is a Majorana zero mode in the small U/V limit. The absence of a similar zero energy excitation in (a) is consistent with the fact that $(d_\uparrow + d_\uparrow^\dagger)$ pairs up with the original MZM $(c_1 + c_1^\dagger)$ to form a complex fermion at non-zero energy.

4.3 LOCAL FERMI LIQUID

A Fermi liquid is an interacting fermionic phase of matter with a ground state that is adiabatically connected to a free fermion ground state [24, 108, 111]. The momentum (k) spectral function in a Fermi liquid is given by $A(k,\omega) = Z_k \delta(\omega - \epsilon_k) + g(k,\omega)$, where $g(k,\omega)$ is a smooth function that contributes a diffuse, featureless background, and ϵ_k is the dispersion of excitations. Z_k, called the *quasiparticle weight*, captures the essence of Fermi liquid theory and indicates that there still exists a Fermi surface where a discontinuity in the fermion occupation number occurs.

Since the free-fermion peak at $\omega = \epsilon$ in $A_{d\downarrow}(\omega)$ remains sharp even in the presence of interactions, a natural quantity to study is the associated quasiparticle weight $\mathcal{Z}$. This can be calculated from Eqs. (4.41)-(4.42). For $\omega \approx \epsilon$ in Eq. (4.41), $A_{d\downarrow}^{ph}$ is evaluated at zero energy. Inside the SC gap, the retarded GF of the MZM γ_1 of a semi-infinite Kitaev chain takes the form

$$g_{\gamma_1}(\omega) = \frac{\lambda(\mu,\Delta)}{\omega + i\eta}, \qquad \omega \in \text{SC gap} \tag{4.46}$$

where η is a positive infinitesimal and $\lambda(\mu,\Delta)$ is the spectral weight (characterising the localisation) of the MZM peak in the boundary LDOS of the Kitaev chain. For

example, at the Kitaev point $\lambda(\mu=0,\Delta=t)=2$, and thus $g_{\gamma_1}(\omega)$ is a free Majorana GF, which reflects the fact that the MZM is exactly localised at the boundary and decoupled from the bulk. Thus, $\max(\lambda)=2$ and $\lambda\to 0$ at the topological phase transition $\left|\mu\right|=2t$. Given the complicated form of $g_{\gamma_1}(\omega)$ [see Appendix A], it is difficult to derive a general closed-form expression for the function $\lambda(\mu,\Delta)$. However, the allowed values of λ can be derived by numerically integrating the Majorana LDOS $-2\,\mathrm{Im}\,g_{\gamma_1}(\omega)$ over an infinitesimal neighbourhood of $\omega=0$. In the expression (4.41) for the spectral function away from particle-hole symmetry, since $n_F(\omega-\epsilon)\to 1/2$ for $\omega\approx\epsilon$, the temperature dependent pre-factor of $A^{ph}_{d\downarrow}$ becomes $[1+2n_B(\epsilon)][1+2n_F(\epsilon)]=1$. Therefore, near $\omega=\epsilon$, the spectral function is temperature independent and given by

$$A_{d\downarrow}(\omega)\approx 2\pi\mathcal{Z}(U/V)\delta(\omega-\epsilon),\qquad \omega\in\{\epsilon-\eta,\epsilon+\eta\},\tag{4.47}$$

where η is a positive infinitesimal and the quasiparticle weight $\mathcal{Z}$ is found to be

$$\mathcal{Z}(U/V)=\frac{1}{1+(2/\lambda)(U/V)^2}.\tag{4.48}$$

In the non-interacting limit $U=0$, the $d_\downarrow$-fermion is free and so $\mathcal{Z}=1$. The interaction renormalises $\mathcal{Z}$ to a value less than one (Figure 4.7), and transfers some spectral weight to other excitations, thus giving credence to a *local Fermi liquid* picture [107] for the $d_\downarrow$-fermion. It should be noted that this picture holds only in the topological phase, as the free-fermion peak for finite U and V has its origins in $-i(d_\uparrow-d_\uparrow^\dagger)$ being an MZM candidate, which is not true in the trivial phase. This can be seen from the fact that $\lambda\to 0$ at the transition ($\left|\mu\right|=2t$) into the trivial phase ($\lambda=0$), which also implies $\mathcal{Z}\to 0$ at the transition (and equal to zero in the trivial phase).

The local Fermi liquid picture is also not valid for the hybridising $d_\uparrow$-fermion, in spite of the presence of a seemingly free-fermion peak at $\omega=0$ in its spectral function (Figure 4.5b). The spectral weight of this peak is trivially less than one due to proximity coupling with the Kitaev chain, even in the absence of interactions. For $U=0$, it is easy to see from Eq. (4.43) that $A_{d\uparrow}(\omega)\to -2\,\mathrm{Im}(2\omega+i\eta)^{-1}=\pi\delta(\omega)$ for $\omega\approx 0$ and so the peak there has spectral weight 0.5. It is as if half the $d_\uparrow$-fermion is localised on the quantum dot with zero energy – this is the new MZM $-i(d_\uparrow-d_\uparrow^\dagger)$, as can also be

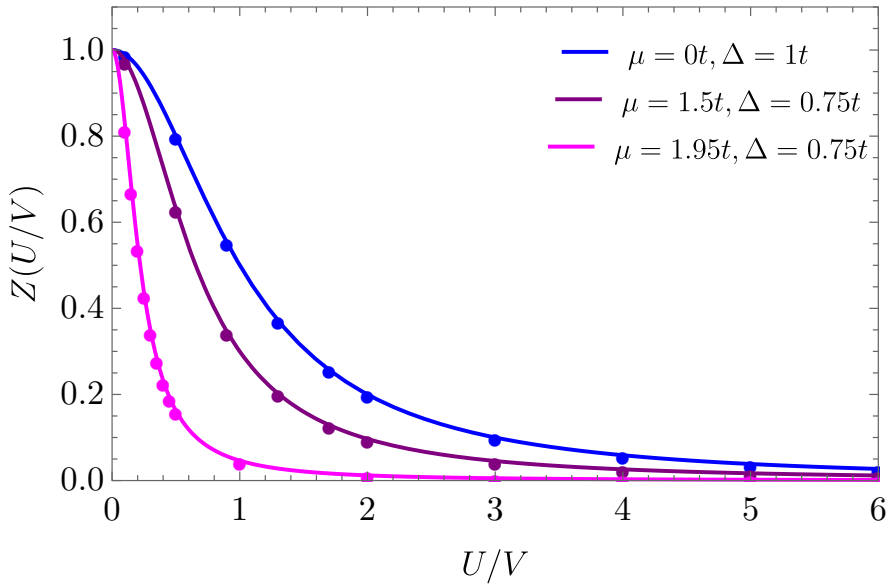

FIGURE 4.7 – Interaction dependence of the $d_\downarrow$-fermion quasiparticle weight $\mathcal{Z}$, for several values of μ and Δ, which control the localisation length of the original end MZM $(c_1 + c_1^\dagger)$ of the Kitaev chain. Continuous curves correspond to Eq. 4.48, while dots are the result of numerically integrating $A_{d\downarrow}(\omega, T)$ over a small neighbourhood of $\omega = \epsilon$.

seen from Figures 4.6a-b. Conforming with this picture discussed in detail in section 4.2, $\mathcal{Z}$ is suppressed at large U, the regime in which $(c_1 + c_1^\dagger)$ is the preferred MZM.

4.4 DENSITY FLUCTUATIONS ON THE QUANTUM DOT

Another measure of inter-particle correlations on the quantum dot is provided by the mean-squared density fluctuation

$$D = \frac{1}{2}\left\langle [n_d - \langle n_d \rangle]^2 \right\rangle = \frac{1}{2}\left[\left\langle n_d^2 \right\rangle - \langle n_d \rangle^2 \right], \tag{4.49}$$

where $n_d = n_{d\uparrow} + n_{d\downarrow}$ is the total number of impurity fermions. Consider the particle-hole symmetric model with $\epsilon = 0$. Since the physical Hamiltonian H [see Eq. (4.2)] enjoys full particle-hole symmetry, $\mathcal{D} H \mathcal{D}^{-1} = H$ where $\mathcal{D} d_\sigma \mathcal{D}^{-1} = d_\sigma^\dagger$ for $\sigma \in \{\uparrow, \downarrow\}$, and

therefore

$$\begin{aligned}\langle n_d\rangle &= \frac{1}{Z}\operatorname{tr}\mathcal{D}e^{-\beta H}\mathcal{D}^{-1}n_d,\\ &= \frac{1}{Z}\operatorname{tr}e^{-\beta H}\mathcal{D}n_d\mathcal{D}^{-1},\\ &= \frac{1}{Z}\operatorname{tr}e^{-\beta H}(2-n_d),\\ &= 2-\langle n_d\rangle,\end{aligned} \tag{4.50}$$

where the cyclicity of the trace has been used in the second line, and the fact that $\mathcal{D}(n_{d\uparrow}+n_{d\downarrow})\mathcal{D}^{-1}=1-n_{d\uparrow}+1-n_{d\downarrow}$ has been used in the third line. This immediately implies $\langle n_d\rangle=1$ in the particle-hole symmetric ($\epsilon=0$) model. In this case then, the mean-squared density fluctuation D in Eq. (4.49) reduces to the double occupancy $D=\left\langle n_{d\uparrow}n_{d\downarrow}\right\rangle$. Since $n_{d\uparrow}n_{d\downarrow}$ is not invariant under $\mathcal{D}_\uparrow$, the partial particle-hole transformation that acts only on $d_\uparrow$, the double occupancy cannot be calculated in the SS representation without constraint (see the discussion in section 3.4). Even though the constraint can be explicitly implemented, there is a simpler way to calculate D directly from the partition function. Recall from section 3.4 that the physical partition function can be calculated without constraint in the SS representation and is given by $Z=Z_{SS}/2$. In the particle-hole symmetric model, as

$$Z=\operatorname{tr}\exp-\beta\Big[H_K+H_{\text{hyb}}+U(2n_{d\uparrow}-1)(2n_{d\downarrow}-1)\Big], \tag{4.51}$$

it is easy to see that

$$-\frac{\partial\ln Z}{\partial(\beta U)}=4D-1, \tag{4.52}$$

with D the double occupancy defined previously. Therefore, D can be calculated directly from a derivative of the slave-spin partition function Z_{SS}, which can be exactly calculated as it is defined by a quadratic action. However, this is true only for the particle-hole symmetric model with $\epsilon=0$.

The coherent state functional integral for the SS representation of the KMAI model, in the form given in Eq. (4.13), is[6]

$$Z_{SS}=\int D[\bar{c},c]D[\bar{f}_\downarrow,f_\downarrow]D[\bar{\eta},\eta]D[\Gamma^z_\uparrow]D[\gamma'_{f\uparrow}]e^{-S[\bar{c},c,\bar{f}_\downarrow,f_\downarrow,\bar{\eta},\eta,\Gamma^z_\uparrow,\gamma'_{f\uparrow}]}, \tag{4.53}$$

[6]Since coherent states are not definable for Majorana operators, a coherent state functional integral

where the (slave-spin) action is defined as

$$S\left[\bar{c},c,\bar{f}_\downarrow,f_\downarrow,\bar{\eta},\eta,\Gamma^z_\uparrow,\gamma'_{f\uparrow}\right]=\int_0^\beta \mathrm{d}\tau\,[\sum_{j=1}^{\infty}\bar{c}_j\partial_\tau c_j+\bar{f}_\downarrow\partial_\tau f_\downarrow+\bar{\eta}\partial_\tau\eta+\frac{1}{4}\Gamma^z_\uparrow\partial_\tau\Gamma^z_\uparrow+\frac{1}{4}\gamma'_{f\uparrow}\partial_\tau\gamma'_{f\uparrow}$$
$$+H_{SS}(\bar{c},c,\bar{f}_\downarrow,f_\downarrow,\bar{\eta},\eta)]. \quad (4.54)$$

The dependence on imaginary time (τ) of all fermion fields integrated over has been suppressed for notational clarity. Note that, although $\Gamma^z_\uparrow$ and $\gamma'_{f\uparrow}$ are zero modes that do not appear in H_{SS}, their inclusion via Berry phase terms in the path integral is necessary to obtain a faithful representation of the physical problem – the dimension of the SS impurity Hilbert space must equal eight.[7] The exact Nambu GF of the η fermions was calculated in section 4.1.1. Therefore, if the Kitaev chain is integrated out (c_j-fermions), the effective action must be

$$S_{\text{eff}}\left[\bar{f}_\downarrow,f_\downarrow,\bar{\eta},\eta,\Gamma^z_\uparrow,\gamma'_{f\uparrow}\right]=\int_0^\beta \mathrm{d}\tau\left[\bar{f}_\downarrow(\partial_\tau+\epsilon)f_\downarrow+\frac{1}{4}\Gamma^z_\uparrow\partial_\tau\Gamma^z_\uparrow+\frac{1}{4}\gamma'_{f\uparrow}\partial_\tau\gamma'_{f\uparrow}\right]$$
$$+\frac{1}{2}\sum_{ik_n}\begin{bmatrix}\bar{\eta}(ik_n) & \eta(-ik_n)\end{bmatrix}\left[-\mathbf{G}^{-1}_\eta(ik_n)\right]\begin{bmatrix}\eta(ik_n)\\ \bar{\eta}(-ik_n)\end{bmatrix}. \quad (4.55)$$

As the Nambu spinor $\Psi_\eta=(\eta \quad \bar{\eta})^\intercal$ satisfies the Majorana condition $\Psi^\dagger=\Psi^\intercal\sigma^x$, $\Psi^\dagger$ is not linearly independent from Ψ and it suffices to integrate over the latter field in the functional integral [113–115] (also see Appendix B). Setting $\epsilon=0$ and performing the functional integral, we obtain

$$Z_{SS}\propto \mathrm{Pf}[-\beta\mathbf{G}^{-1}_\eta(ik_n)]\propto\sqrt{\mathrm{Det}[-\beta\mathbf{G}^{-1}_\eta(ik_n)]}, \quad (4.56)$$

where Pf is the Pfaffian and is, up to an irrelevant sign, the square root of the determinant. Constants that result from the functional integral over $f_\downarrow$, $\Gamma^z_\uparrow$, $\gamma'_{f\uparrow}$ have been ignored and buried in the proportionality sign, as only factors which depend on

of Majorana fields, strictly speaking, does not exist. This is not a problem here as we have an even number of Majorana fermions that can be paired up as complex fermions. See Appendix B for a discussion on how this problem can be circumvented in general and more details on Majorana path integrals.

[7] See the discussion of this point in section 3.2. A Majorana fermion can be thought of as nominally spanning a Hilbert space dimension of $\sqrt{2}$.

the interaction strength U are relevant for the double occupancy D. Det indicates a determinant over both, the Nambu matrix structure of $\mathbf{G}_\eta^{-1}$ and over Matsubara frequencies. Using the operator identity $\mathrm{Det}\, M = \exp(\mathrm{Tr}\ln M)$, it is easy to show that $Z_{SS} = \exp\frac{1}{2}\mathrm{Tr}\ln[-\beta\mathbf{G}_\eta^{-1}]$. Using the result for $\mathbf{G}_\eta^{-1}$ from section 4.1.1, we thus obtain

$$\ln Z_{SS} = \frac{1}{2}\sum_{ik_n} \ln\beta^2\left[-(ik_n)^2 + 2V^2 ik_n g_{\gamma_1}(ik_n) + 4U^2\right] + \text{const.} \tag{4.57}$$

Therefore, using Eq. (4.52), the double occupancy is given by

$$\begin{aligned} D &= 1 + \frac{2U}{\beta}\sum_{ik_n} \frac{2}{(ik_n)^2 - 4U^2 - 2V^2 ik_n g_{\gamma_1}(ik_n)}, \\ &= 1 + \frac{2U}{\beta}\sum_{ik_n} \frac{\mathcal{G}^{xx}_\uparrow(ik_n)}{ik_n}, \end{aligned} \tag{4.58}$$

where the slave-fermion GF $\mathcal{G}^{xx}_\uparrow(\tau) = -\left\langle T_\tau \Gamma^x_\uparrow(\tau)\Gamma^x_\uparrow(0)\right\rangle_{SS}$ has been introduced using the result in section 4.1.1. Introducing the spectral representation of this GF with spectral function $A^{xx}_\uparrow(\omega) = -2\,\mathrm{Im}\,\mathcal{G}^{xx}_\uparrow(ik_n \to \omega + i\eta)$ and performing the resulting Matsubara sum, we obtain the result

$$D = \frac{1}{4} + \frac{U}{2}\int_{-\infty}^{\infty}\frac{\mathrm{d}\omega}{2\pi} A^{xx}_\uparrow(\omega)\frac{n_F(\omega)}{\omega} - \cancel{U\int_{-\infty}^{\infty}\frac{\mathrm{d}\omega}{2\pi\omega} A^{xx}_\uparrow(\omega).} \tag{4.59}$$

The last term vanishes as $A^{xx}_\uparrow$ is even in ω, making the integrand odd in ω.[8] Plots of D (Figure 4.8) reveal that density fluctuations (or double occupancy for $\epsilon = 0$) are suppressed at large U and low T, but encouraged by hybridisation V. Therefore, at low temperatures in the interaction dominated regime, we expect a local (Ising) moment to develop on the quantum dot.

[8] This property of $A^{xx}_\uparrow(\omega)$ can be seen in the spectral representation,

$$\mathcal{G}^{xx}_\uparrow(ip_n) = \int_{-\infty}^{\infty}\frac{\mathrm{d}\omega}{2\pi}\frac{A^{xx}_\uparrow(\omega)}{ip_n - \omega}.$$

By virtue of being a Majorana GF, $\mathcal{G}^{xx}_\uparrow(-ip_n) = -\mathcal{G}^{xx}_\uparrow(ip_n)$. Using this property and changing integration variables $\omega \to -\omega$, it is easy to show that $A^{xx}_\uparrow(\omega) = A^{xx}_\uparrow(-\omega)$.

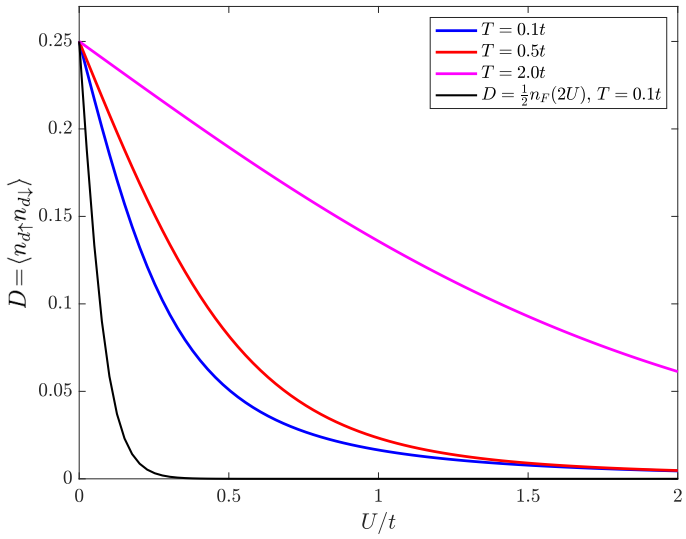

FIGURE 4.8 – Interaction dependence of impurity double occupancy for various temperatures T in the particle-hole symmetric KMAI model ($\epsilon = 0$). Black: atomic limit ($V = 0$), all other curves: $\mu = 0.2t$, $\Delta = 0.5t$, $V = 0.4t$, $\epsilon = 0$. .

4.5 ODD-FREQUENCY SUPERCONDUCTIVITY

The essence of superconductivity is captured by a non-zero anomalous Green function, called the Gor'kov function, $\Delta_{\sigma_1\sigma_2}(r_1 - r_2, t_1 - t_2) = -\left\langle T_\tau c_{\sigma_1}(r_1, t_1) c_{\sigma_2}(r_2, t_2) \right\rangle$, where σ_i is a spin index, r_i and τ_i are space and (real) time coordinates respectively. Berezinskii [116] noticed that Fermi statistics imposes specific symmetry constraints on the Gor'kov function under permutations of its spin, spatial, and temporal arguments ($1 \leftrightarrow 2$). Let us denote the respective permutation operators as P_σ, P_r, and P_t. For example, $P_\sigma \Delta_{\sigma_1\sigma_2}(r_1 - r_2, t_1 - t_2) \equiv \Delta_{\sigma_2\sigma_1}(r_1 - r_2, t_1 - t_2)$. Specifically, Berezinskii showed that $P_\sigma P_r P_t \Delta_{\sigma_1\sigma_2}(r_1 - r_2, t_1 - t_2) = -\Delta_{\sigma_1\sigma_2}(r_1 - r_2, t_1 - t_2)$, which is denoted symbolically as $P_\sigma P_r P_t = -1$. A Gor'kov function that changes sign under P_t is said to denote *odd-frequency* pairing of electrons [117].

Unlike the $d_\downarrow$-fermion, the number $n_{d\uparrow}$ of the hybridising $d_\uparrow$-fermion is not conserved. In fact, Majorana hybridisation with the Kitaev chain results in proximity-induced superconductivity for the $d_\uparrow$-fermions on the quantum dot. The only possibility in this case is pure odd-frequency pairing [118], characterised by the real (imaginary) part of the retarded Gor'kov function being odd (even) in frequency

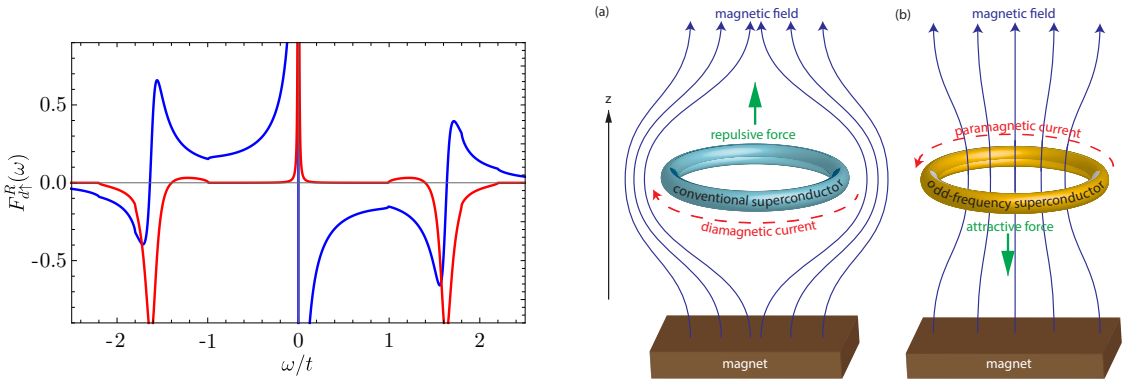

FIGURE 4.9 – **Left panel** – Real (blue) and imaginary (red) parts of the impurity retarded Gor'kov function $F^R_{d\uparrow}(\omega)$ in the topological phase of the KMAI model, showing odd-frequency pairing correlations on the quantum dot. Parameters are chosen as $\mu = 0.2t$, $\Delta = 0.5t$, $V = 0.4t$, $U = 0.7t$. **Right panel** – Meissner effect of (a) a conventional superconducting ring and (b) an odd-frequency superconducting ring. An external magnetic field induces a paramagnetic supercurrent in the odd-frequency superconductor, which leads to an attractive force between the ring and the magnet. Figure and caption adapted from Lee *et al.* [118].

[116, 117, 119, 120] (Figure 4.9). The latter is obtained by analytic continuation of the Matsubara Gor'kov function $F(\tau) = -\left\langle T_\tau d_\uparrow(\tau) d_\uparrow(0)\right\rangle$, which can be calculated in the SS representation by implementing the gauge constraint exactly, following a similar calculation as that of the $d_\uparrow$-fermion Matsubara GF in section 4.1.1. The frequency representation of $F(\tau)$ is given by

$$F(ik_n) = \frac{V^2 g_{\gamma_1}(ik_n)}{(ik_n)^2 - 4U^2 - 2V^2 ik_n g_{\gamma_1}(ik_n)}, \tag{4.60}$$

where $g_{\gamma_1}(ik_n)$ is odd in ik_n by virtue of being a Majorana GF [121, 122]. The explicit form of the pairing terms on the quantum dot can be seen by integrating out the Kitaev chain in the physical action for the KMAI model. Introducing the Nambu (Majorana) spinors $\Psi_j = (c_j \quad \bar{c}_j)^\intercal$ and $\chi_\sigma = (d_\sigma \quad \bar{d}_\sigma)^\intercal$, the physical partition function of the KMAI model can be written as a functional integral,

$$Z = \int D[\chi_\sigma] D[\Psi_j] e^{-\tilde{S}[\chi_\sigma, \Psi_j]}, \tag{4.61}$$

where the physical action[9] is defined as

$$\tilde{S}[\chi_\sigma, \Psi_j] = \int_0^\beta \mathrm{d}\tau \left[\frac{1}{2} \sum_j \Psi_j^\dagger \partial_\tau \Psi_j + \frac{1}{2} \sum_\sigma \chi_\sigma^\dagger \partial_\tau \chi_\sigma - iV \chi_\uparrow^\dagger (1+\sigma^x) \Psi_1 + H_K + H_A \right], \tag{4.62}$$

where H_K is the Kitaev chain and H_A is the physical Hamiltonian of the Anderson impurity, given by Eqs. (4.1) and (3.2) respectively. The third term in the action is the hybridisation H_{hyb} written in terms of Nambu spinors. Now, if the fields Ψ_j for $j>1$ (the Kitaev chain minus its boundary site) are integrated out, we must obtain

$$\begin{aligned} \tilde{S}_{\text{eff}}[\chi_\sigma, \Psi_1] = \int_0^\beta \mathrm{d}\tau \left[\frac{1}{2} \sum_\sigma \chi_\sigma^\dagger(\tau) \partial_\tau \chi_\sigma(\tau) + H_A - iV \chi_\uparrow^\dagger(\tau) (1+\sigma^x) \Psi_1(\tau) \right] \\ + \int_0^\beta \mathrm{d}\tau \, \mathrm{d}\tau' \, \frac{1}{2} \Psi_1(\tau) \left[-\mathbf{g}_S^{-1}(\tau - \tau') \right] \Psi_1(\tau'), \end{aligned} \tag{4.63}$$

where $\mathbf{g}_S(\tau-\tau')$ is the boundary Nambu GF of the Kitaev chain calculated in Appendix A. The Gaussian functional integral over Ψ_1 can now be performed (see Appendix B to see how) to obtain an effective action for the quantum dot,

$$\begin{aligned} \tilde{S}_{\text{eff}}[\chi_\sigma] = \int_0^\beta \mathrm{d}\tau \left[\frac{1}{2} \sum_\sigma \chi_\sigma^\dagger(\tau) \partial_\tau \chi_\sigma(\tau) + H_A \right] \\ + \frac{V^2}{2} \int_0^\beta \mathrm{d}\tau \, \mathrm{d}\tau' \, \chi_\uparrow^\dagger(\tau) g_{\gamma_1}(\tau - \tau') (1+\sigma^x) \chi_\uparrow(\tau'), \end{aligned} \tag{4.64}$$

where $g_{\gamma_1} = \sum_{\mu,\nu=1}^2 \mathbf{g}_S^{\mu\nu}$ is the Majorana GF of the MZM $(c_1 + c_1^\dagger)$ in the Kitaev chain. Rewriting $\tilde{S}_{\text{eff}}$ in terms of $(d_\sigma, \bar{d}_\sigma)$, we have

$$\begin{aligned} \tilde{S}_{\text{eff}}[\bar{d}_\sigma, d_\sigma] = \int_0^\beta \mathrm{d}\tau \left[\frac{1}{2} \sum_\sigma \chi_\sigma^\dagger(\tau) \partial_\tau \chi_\sigma(\tau) + H_A \right] \\ + \int_0^\beta \mathrm{d}\tau \, \mathrm{d}\tau' \, \frac{V^2}{2} g_{\gamma_1}(\tau - \tau') \left[\bar{d}_\uparrow(\tau) d_\uparrow(\tau') + d_\uparrow(\tau) \bar{d}_\uparrow(\tau') + d_\uparrow(\tau) d_\uparrow(\tau') + \bar{d}_\uparrow(\tau) \bar{d}_\uparrow(\tau') \right]. \end{aligned} \tag{4.65}$$

The last two terms in the second integral are effective pairing terms that emerge due to coupling with the superconducting Kitaev chain. Since the frequency-dependent,

[9] This is not the slave-spin action introduced in Eq. 4.54.

effective pairing potential is proportional to $V^2 g_{\gamma_1}(\tau - \tau')$, which is odd in $(\tau - \tau')$ by virtue of being a Majorana GF, we see that the inherited superconductivity is purely odd-frequency. Note also that odd-frequency pairing on the quantum dot is a consequence of the Majorana hybridisation (H_{hyb}) and in fact obtains regardless of the specific host c-fermion Hamiltonian. It is a consequence of the fact that it is a Majorana mode of the host that couples to the impurity, and Majorana GFs are always odd in frequency.

Since the quantum dot considered here is essentially a 'zero dimensional' local system, some elaboration is needed as regards the statement that it is superconducting. If one considers a host Hamiltonian that supports an array of MZMs, and if each MZM is coupled to a quantum dot similar to the hybridisation in our MAI models, then this array of quantum dots would be a bonafide pure odd-frequency superconductor. For example, a ring of such odd-frequency superconducing dots would exhibit a paramagnetic Meissner response to an external magnetic field [118]. In practice however, the Kitaev chains that host the MZMs are realised as semiconducting Rashba nanowires proximitized by bulk s-wave superconductors. This means that the net Meissner response, dominated by the bulk s-wave superconductors, would be diamagnetic.

4.6 LOCAL DENSITY OF STATES OF THE HOST

The local Nambu GFs $\mathbf{G}_c(j;\omega)$ of the host c_j-fermions were calculated in section 4.1.1. The LDOS on site i is then simply obtained as $\rho(i;\omega) = -\operatorname{Im}\operatorname{tr}\mathbf{G}_c(i;\omega)$. At the boundary ($i = 1$), the LDOS displays three quasiparticle peaks in the topological phase for non-zero hybridisation and interaction (Figure 4.10a), similar to the impurity spectral functions in section 4.2. The two subgap states at non-zero energy in Figure 4.10a are non-topological Andreev bound states induced by the quantum dot, reminiscent of Yu-Shiba-Rusinov states [66–68, 123]. By tuning (increasing) the interaction and hybridisation strengths, it is possible to push these states out of the SC gap.

The third quasiparticle peak is at zero energy and appears at any finite interaction

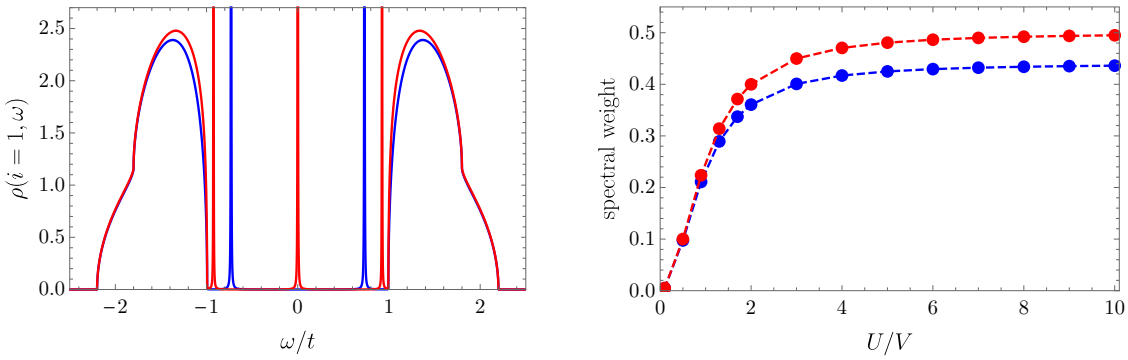

FIGURE 4.10 – (a) Interaction dependence of the boundary local density of states $\rho(i=1;\omega)$ of the host c-fermions, for $\mu=0.2t$, $\Delta=0.5t$, $V=0.4t$, and $U=0$ (blue), $U=0.3t$ (red). (b) Spectral weight of the MZM peak ($\omega=0$) in the c-fermion boundary LDOS shown in (a) as a function of U/V. For $\mu=0, \Delta=t$ (red) and $\mu=0.2t$, $\Delta=0.5t$ (blue).

strength U and hybridisation V, but disappears for $U=0$ (V still non-zero). This is consistent with the analysis of the impurity spectral functions in the small and large U/V limits in section 4.2, as we now explain. If the hybridisation with the impurity is switched off ($V=0$), then the LDOS is just that of the Kitaev chain. There are no side peaks, and the lone subgap zero energy quasiparticle peak corresponds to the MZM of the Kitaev chain. In the presence of hybridisation, but still in the non-interacting limit, the MZM peak immediately disappears for any finite V, which is consistent with $-i(d_\uparrow - d_\uparrow^\dagger)$ becoming the new MZM as discussed in section 4.2. Now, as soon as interactions are switched on, the MZM peak at $\omega=0$ immediately reappears, along with two other subgap quasiparticle states. The reappearance of the MZM peak at any finite U is an omen of what happens in the large U/V limit - the interaction-favoured $(c_1+c_1^\dagger)$ regains its status as the MZM of the model. If this is correct, then the spectral weight of the zero-energy peak must *increase* monotonically with U. This is confirmed numerically, with the result shown in Figure 4.10b. This is to be compared with the *suppression* of the quasiparticle weight $\mathcal{Z}$ of the $d_\downarrow$-fermion with increasing interaction strength U (Figure 4.7).

Since all local GFs in the KMAI model can be calculated (see section 4.1.1), it is also possible to study the effect the quantum dot has on the localisation of the MZM.

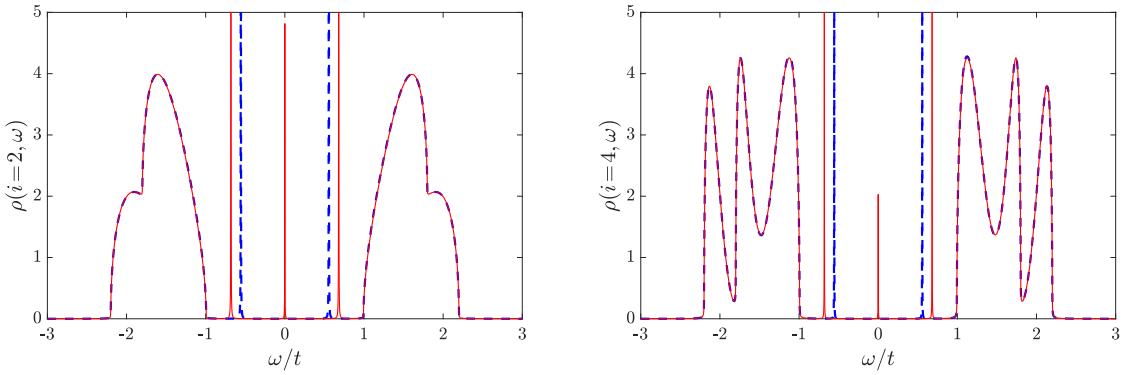

FIGURE 4.11 – LDOS $\rho(i;\omega)$ of the host c-fermions on (a) site $i=2$ and (b) site $i=4$. Parameters chosen as $\mu=0.2t$, $\Delta=0.5t$, $V=0.3t$, and $U=0$ (blue, dashed), $U=0.2t$ (red, solid).

Away from the special point $(\mu=0,\Delta=t)$ on the phase diagram of the Kitaev chain, we know that the MZM $(c_1+c_1^\dagger)$ has a finite localisation length with a wavefunction that exponentially decays into the bulk. However, in the presence of hybridisation with the impurity, particularly for weak interactions (small U/V), we have found previously that $-i(d_\uparrow-d_\uparrow^\dagger)$ is the preferred MZM, and this mode is exactly localised on the quantum dot. As seen in Figures 4.11a-b, the LDOS on interior sites do not support zero-energy peaks in the non-interacting limit, even when $(\mu,\Delta)\neq(0,t)$. When $U\neq 0$, the zero-energy peaks reappear, and thus interactions allow a finite penetration depth of the MZM wavefunction. Generically then, we expect the characteristic localisation length of the MZM in the KMAI model to differ from that in the Kitaev chain (without an impurity). This can be quantified by studying the decay of spectral weight of the zero-energy peak with distance away from the boundary, but we do not pursue this here.

A curious feature of the LDOS of the interior sites shown in Figures 4.11a-b is a seemingly oscillatory behaviour inside the SC bands. These oscillations are greatly enhanced as one proceeds into the bulk of the chain, with the oscillations tracing on average, but not converging to the bulk LDOS of the Kitaev chain (Figures 4.12a-b). The oscillations are due to interference effects from scattering off the boundary of the chain, and the lack of convergence to the bulk LDOS is a generic feature of

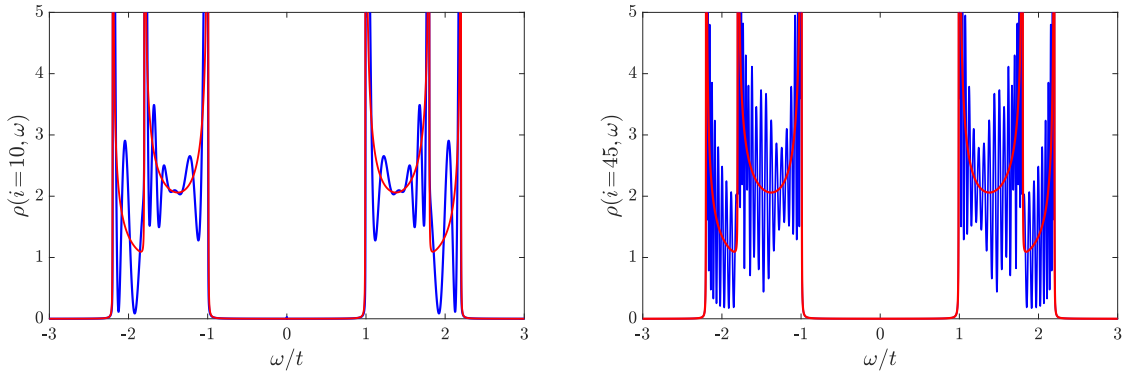

FIGURE 4.12 – LDOS $\rho(i;\omega)$ of the host c-fermions in blue on (a) site $i=10$ and (b) site $i=45$. Parameters chosen as $\mu=0.2t$, $\Delta=0.5t$, $V=0.4t$, $U=0.7t$. Shown in red in both plots is the bulk LDOS of the Kitaev chain.

one-dimensional systems [124–126].

4.7 DEPARTURES FROM EXACT SOLVABILITY

We now consider deviations from the exactly solvable point $\epsilon=h$ of the KMAI model. Defining $\delta=(\epsilon-h)/2$, the new physical Hamiltonian H' [see Eq. (4.2)] can be written as

$$H' = H(\mu,\Delta,V,U,\epsilon) + \delta(n_{d\uparrow} - n_{d\downarrow}), \tag{4.66}$$

where H is the exactly solvable part with $\epsilon=h$. In the SS representation, using Eq. (3.15) specialised to the KMAI model, this becomes

$$H'_{SS} = H_{SS}(\epsilon=h) - \delta(n_{f\downarrow} - 1/2) - i\delta\Gamma^x_\uparrow\Gamma^y_\uparrow(n_{f\downarrow} - 1/2), \tag{4.67}$$

where $H_{SS}(\epsilon=h)$ is the bilinear exactly solvable part. For sufficiently small δ, corrections to physical observables away from the exactly solvable limit can be computed by treating the last term in Eq. 4.67 in perturbation theory, in analogy to the perturbative analysis of small departures from the Toulouse point in the Kondo problem [127]. We emphasise that this is distinct from ordinary perturbation theory in the physical interaction strength U; here U can be arbitrarily large, and the perturbation corresponds to a change in the Zeeman field, as evident from Eq. (4.66).

As an example, let us calculate the correction to the free energy away from the exactly solvable point, to linear order in δ. The functional integral for the KMAI model [see Eq. (4.53)] away from the exactly solvable point is now defined with respect to an action

$$S' = S - \delta(n_{f\downarrow} - 1/2) - i\delta\Gamma^x_\uparrow\Gamma^y_\uparrow(n_{f\downarrow} - 1/2) \equiv S + S_\delta$$

where S is the quadratic action that appears in Eqs. (4.53)-(4.54). The physical free energy corresponding to H' is given in the SS representation by[10]

$$F' = -\frac{1}{\beta}\ln Z'_{SS} = F - \frac{1}{\beta}\ln\frac{Z'_{SS}}{Z_{SS}},$$

where unprimed quantities are defined with respect to the exactly solvable limit $\epsilon = h$ of the KMAI model and are thus independent of δ. Using the linked cluster theorem [24, 115],

$$\ln\frac{Z'_{SS}}{Z_{SS}} = \left\langle e^{-S_\delta}\right\rangle_c - 1 = \sum_{m=1}^{\infty}\frac{(-1)^m}{m!}\langle S_\delta\rangle_c,$$

where the *connected* (subscript c) average is with respect to the functional integral defined by the unprimed action S, that is Eq. (4.53)-(4.54). It is easy to see that the corrections to the free energy are thus connected, closed-loop Feynman diagrams. For example, the first order correction to the free energy is

$$\frac{1}{\beta}\langle S_\delta\rangle_c = -\frac{\delta}{\beta}\int_0^\beta d\tau\left\langle f^\dagger_\downarrow(\tau)f_\downarrow(\tau) - 1/2\right\rangle_c - \frac{i\delta}{\beta}\int_0^\beta d\tau\left\langle\Gamma^x_\uparrow(\tau)\Gamma^y_\uparrow(\tau)\right\rangle_c\left\langle f^\dagger_\downarrow(\tau)f_\downarrow(\tau) - 1/2\right\rangle_c. \quad (4.68)$$

Fourier transforming to the Matsubara frequency domain,

$$\frac{1}{\beta}\langle S_\delta\rangle_c = \frac{i\delta}{\beta^2}\sum_{ik_n, ip_n}\mathcal{G}^{xy}_\uparrow(ik_n)\mathcal{G}_{f\downarrow}(ip_n) - \frac{\delta}{\beta}\sum_{ik_n}\mathcal{G}_{f\downarrow}(ik_n) - \frac{i\delta}{2\beta}\sum_{ik_n}\mathcal{G}^{xy}_\uparrow(ik_n). \quad (4.69)$$

Substituting in the relevant slave-fermion GFs from section (4.1.1) and performing the Matsubara sums over $\mathcal{G}_{f\downarrow}$, we get

$$\frac{1}{\beta}\langle S_\delta\rangle_c = -\delta\left[n_F(\epsilon) - 1/2\right]\left[\frac{2U}{\beta}\sum_{ik_n}\frac{2}{(ik_n)^2 - 4U^2 - 2V^2 ik_n g_{\gamma_1}(ik_n)}\right] - \delta n_F(\epsilon). \quad (4.70)$$

[10] Recall from section 3.4 that the proofs presented there for disposal of constraints in the partition and correlation functions did not depend on the exact solvability of the KMAI model, only on its transformation properties under a partial particle-hole transformation $\mathcal{D}_\uparrow$.

Recognising the Matsubara sum above as the same that appears in the calculation of the double occupancy [see Eqs. (4.58)-(4.59)], the correction to the free energy to linear order in δ can be written as

$$F'_{(1)} = 2[1 - 2n_F(\epsilon)][1/4 - D] - n_F(\epsilon),$$

where $F'_{(1)}$ is defined through the perturbative expansion $F' = F + F'_{(1)}\delta + F'_{(2)}\delta^2 + \mathcal{O}(\delta^3)$, and D is the temperature-dependent double occupancy in the particle-hole symmetric, exactly solvable model, given in Eq. (4.59).

CHAPTER 5

Read-Green Majorana-Anderson impurity model

We now consider the two-dimensional spinless p_x+ip_y superconductor, or the Read-Green superconductor [32], on a semi-infinite square lattice coupled to an Anderson impurity on its edge. The geometry of the setup is depicted schematically in Figure 5.1. The Read-Green superconductor is described by a Hamiltonian,

$$H_R = \sum_{x=-\infty}^{\infty}\sum_{y=1}^{\infty}\Big[-t\left(c^\dagger_{x+1,y}c_{x,y} + c^\dagger_{x,y+1}c_{x,y} + \text{h.c.}\right) + \left(\Delta c^\dagger_{x+1,y}c^\dagger_{x,y} + i\Delta c^\dagger_{x,y+1}c^\dagger_{x,y} + \text{h.c.}\right) - \mu c^\dagger_{x,y}c_{x,y}\Big], \quad (5.1)$$

with hopping integral t, p-wave pairing potential Δ, and chemical potential μ. The Read-Green superconductor supports three distinct phases – two topological SC phases for $0<\mu<4t$ and $-4t<\mu<0$ that support gapless, chiral Majorana edge modes with opposite chiralities, and a topologically trivial SC phase for $|\mu|>4t$. Note that the system described by H_R has a single edge ($y=1$) and no corners.

The Anderson impurity is coupled locally to the edge modes on the $(x=0, y=1)$

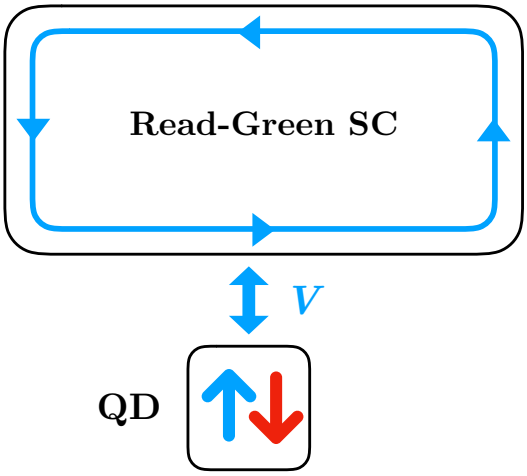

FIGURE 5.1 – Geometry of setup described by the RMAI model.

site, and the resulting system is described by a Hamiltonian,

$$H = H_R - iV(c_{0,1} + c_{0,1}^\dagger)(d_\uparrow + d_\uparrow^\dagger) + H_A, \tag{5.2}$$

where V is the hybridisation strength and H_A is the Anderson impurity Hamiltonian given by Eq. (3.2). This model is hereafter referred to as the RMAI model, for brevity and to distinguish it from the KMAI model. The slave-spin representation of the RMAI model is simply obtained by substituting $H_C = H_R$ and $V_j = V_{x,y} = V\delta_{x,0}\delta_{y,1}$ in Eq. (3.15) to get

$$H_{SS} = H_R - iV(c_{0,1} + c_{0,1}^\dagger)\Gamma_\uparrow^x - iU\Gamma_\uparrow^x\Gamma_\uparrow^y + \epsilon(n_{f\downarrow} - 1/2), \tag{5.3}$$

where we have assumed the exactly solvable limit $\epsilon = h$ of the MAI class of models, discussed in Chapter 3.1.

5.1 CALCULATION OF CORRELATION FUNCTIONS

We now discuss the calculation of correlation functions in the RMAI model. Since the calculations in the KMAI and RMAI cases are similar, this section is less complete than section 4.1, and we refer the reader there for further details regarding calculational methods.

5.1.1 *Slave-fermion Green functions*

As in the case of the KMAI model, all physical Green functions can be expressed in terms of the one-particle Green functions of slave-fermions $\{\Gamma^x_\uparrow, \Gamma^y_\uparrow, \Gamma^z_\uparrow, f_\downarrow, \gamma'_{f\uparrow}\}$. The one-particle Green functions of $\Gamma^z_\uparrow, \gamma'_{f\uparrow}$, and $f_\downarrow$ in the RMAI model are the same as those in the KMAI model, and given by Eqs. (4.9)-(4.11). Those of $\Gamma^x_\uparrow$ and $\Gamma^y_\uparrow$ require boundary Green function methods. Defining

$$\eta = \frac{1}{2}(\Gamma^y_\uparrow + i\Gamma^x_\uparrow), \qquad \eta^\dagger = \frac{1}{2}(\Gamma^y_\uparrow - i\Gamma^x_\uparrow), \tag{5.4}$$

the slave-spin representation of the RMAI model in Eq. (5.3) can be expressed as

$$H_{SS} = H_R - V(c^\dagger_{0,1} + c_{0,1}\eta + \text{h.c.}) + U(2\eta^\dagger\eta - 1) + \epsilon(n_{f\downarrow} - 1/2). \tag{5.5}$$

Defining a Nambu spinor $\Psi_c(x,y) = (c_{x,y} \quad c^\dagger_{x,y})^\intercal$, we may write H_R as

$$H_R = \frac{1}{2}\sum_{x=-\infty}^{\infty}[\Psi^\dagger_c(x,y)T_x\Psi_c(x+1,y) + \Psi^\dagger_c(x,y)T_y\Psi_c(x,y+1) + \text{h.c.}] - \Psi^\dagger_c(x,y)\mu\sigma^z\Psi_c(x,y), \tag{5.6}$$

where σ^z is a Pauli matrix defined in Nambu space, and the matrices T_x, T_y are defined as

$$T_x = \begin{pmatrix} -t & -\Delta \\ \Delta & t \end{pmatrix}, \qquad T_y = \begin{pmatrix} -t & -i\Delta \\ -i\Delta & t \end{pmatrix}. \tag{5.7}$$

While H_R itself breaks translation invariance in $\hat{y}$, coupling to the impurity breaks translation invariance in both $\hat{x}$ and $\hat{y}$ directions. However, we choose to work in a mixed (k_x, y) representation, in which the Nambu spinors are defined as $\Psi_c(k_x,y) = [c_y(k_x) \quad c^\dagger_y(-k_x)]^\intercal$ and the SS representation of the RMAI model is

$$\begin{aligned} H_{SS} = \frac{1}{2}\sum_{k_x}\sum_{y=1}^{\infty}\Big\{\Big[\Psi^\dagger_c(k_x,y)T_y\Psi_c(k_x,y+1) + \text{h.c.}\Big] + \Psi^\dagger_c(k_x,y)\Xi(k_x)\Psi_c(k_x,y)\Big\} \\ - V\sum_{k_x}\Big[c^\dagger_1(-k_x)\eta + c_1(k_x)\eta + \text{h.c.}\Big] + 2U(\eta^\dagger\eta - 1) + \epsilon(n_{f\downarrow} - 1/2), \end{aligned} \tag{5.8}$$

where the matrix $\Xi(k_x)$ has been defined as

$$\Xi(k_x) = \begin{pmatrix} -2t\cos k_x - \mu & -2i\Delta\sin k_x \\ 2i\Delta\sin k_x & 2t\cos k_x + \mu \end{pmatrix}. \tag{5.9}$$

We use periodic boundary conditions in $\hat{x}$, that is the system is wrapped onto a semi-infinite (along $\hat{y}$) cylinder of infinite cross-sectional radius, such that k_x assumes values in the first Brillouin zone. In this mixed representation, H_{SS} can be written in Bogoliubov-de Gennes (BdG) form with a semi-infinite BdG matrix h_{SS}, Defining the matrices

$$\begin{aligned} Y_k &= \mathrm{diag}[\Xi(-\pi),\ldots,\Xi(\pi)], \\ \mathbf{T}_Y &= \mathrm{diag}(T_y,\ldots,T_y), \\ H_A &= \mathrm{diag}(\epsilon\sigma^z, 2U\sigma^z), \\ J &= \begin{pmatrix} 0 & \ldots & 0 \\ C & \ldots & C \end{pmatrix}, \quad C = \begin{pmatrix} -V & -V \\ V & V \end{pmatrix} \end{aligned} \tag{5.10}$$

the BdG matrix h_{SS} can be written in block tridiagonal form as

$$h_{SS} = \left(\begin{array}{c|c|c|c} H_A & J & 0 & \ldots \\ \hline J^\dagger & Y_k & \mathbf{T}_Y & 0 \\ \hline 0 & \mathbf{T}_Y^\dagger & Y_k & \mathbf{T}_Y \\ \hline \vdots & 0 & \mathbf{T}_Y^\dagger & \ddots \end{array}\right). \tag{5.11}$$

Each Y_k block is itself block diagonal, with the diagonal blocks being the 2x2 matrix function $\Xi(k_x)$ evaluated at every point in the first Brillouin zone. In the limit of infinite length along $\hat{x}$, Y_k has elements parametrised by a continuous momentum $k_x \in (-\pi, \pi)$, taking values in the first Brillouin zone. Each Y_k block of h_{SS} represents a single layer of the two-dimensional superconductor along the $\hat{y}$ direction, with the first Y_k block corresponding to terms in H_{SS} that describe the edge ($y = 1$) in momentum space (k_x). $\mathbf{T}_Y = \mathrm{diag}(T_y, ..., T_y)$ has the same dimensions as Y_k and describes hopping and pairing between neighbouring layers along $\hat{y}$. J couples the impurity (H_A) equally to every k_x mode of $\Psi_c(k_x, y = 1)$ on the edge, and so to the site ($x = 0, y = 1$) in real space.

Partitioning the resolvent matrix $\mathbf{G} = (z - h_{SS})^{-1}$ as in Eq. (4.17), in correspondence with the partitions of h_{SS} in Eq. (5.11), and solving for $\mathbf{G}_A$ from the simultaneous

equations obtained as $(z-h_{SS})\mathbf{G}=1$, we get

$$\mathbf{G}_A^{-1}=b\begin{pmatrix} z-\epsilon\sigma^z & 0 \\ 0 & z-2U\sigma^z-V^2\sum_{k_x} g_\gamma(k_x;y=1;z)\end{pmatrix}, \tag{5.12}$$

where $g_\gamma(k_x;y=1;z)$ is the frequency representation of the boundary Matsubara GF

$$g_\gamma(k_x;y=1;\tau)=-\left\langle T_\tau \gamma(k_x;y=1;\tau)\gamma(-k_x;y=1;0)\right\rangle, \tag{5.13}$$

ad with $\gamma(k_x;y=1)=[c_1(k_x)+c_1^\dagger(-k_x)]$. This is the sum of all matrix elements of the Nambu GF of $[c_1(k_x)+c_1^\dagger(-k_x)]^\intercal$, which has been calculated explicitly in Appendix A. The sum over k_x of $g_\gamma(k_x;y=1;\tau)$, in the limit of infinite $\hat{x}$, is an integral over the first Brillouin zone, and defines

$$g_\gamma(x=0;y=1;z)=\int_{-\pi}^{\pi}\frac{\mathrm{d}k_x}{2\pi}g_\gamma(k_x;y=1;z), \tag{5.14}$$

which is the local GF of the Majorana mode $(c_{0,1}+c_{0,1}^\dagger)$ that the impurity hybridises with. The integral must be computed numerically. Inverting the second diagonal block of $\mathbf{G}_A^{-1}$, we find the Nambu GF of $(\eta \quad \eta^\dagger)^\intercal$ as

$$\begin{aligned}\mathbf{G}_\eta=&\frac{1}{z^2-4U^2-2V^2 z g_\gamma(x=0;y=1;z)}\\ &\times\begin{pmatrix} z+2U-V^2g_\gamma(x=0;y=1;z) & -V^2g_\gamma(x=0;y=1;z)\\ -V^2g_\gamma(x=0;y=1;z) & z-2U-V^2g_\gamma(x=0;y=1;z)\end{pmatrix}.\end{aligned} \tag{5.15}$$

As in section 4.1.1 for the case of the KMAI model, all GFs of the form $\mathcal{G}_\uparrow^{\alpha\beta}(\tau)=-\left\langle T_\tau\Gamma_\uparrow^x(\tau)\Gamma_\uparrow^y(0)\right\rangle$ with $\alpha,\beta\in\{x,y\}$ can be calculated from appropriate linear combinations of the matrix elements of $\mathbf{G}_\eta$. The results are

$$\mathcal{G}_\uparrow^{yy}(z)=\frac{2z-4V^2g_\gamma(x=0;y=1;z)}{z^2-4U^2-2V^2zg_\gamma(x=0;y=1;z)}, \tag{5.16}$$

$$\mathcal{G}_\uparrow^{xx}(z)=\frac{2z}{z^2-4U^2-2V^2zg_\gamma(x=0;y=1;z)}, \tag{5.17}$$

$$\mathcal{G}_\uparrow^{xy}(z)=-\frac{4iU}{z^2-4U^2-2V^2zg_\gamma(x=0;y=1;z)}. \tag{5.18}$$

5.1.2 *Impurity Green functions*

One can now do the same computations for the physical impurity GFs as done in the KMAI model in section 4.1.2, with the slave-fermion GFs there appropriately replaced with the results for the RMAI model obtained in the previous subsection. We simply list the relevant results here, referring to section 4.1.2 for more details on specific calculations. Although the one-particle GF for the $d_\downarrow$-fermion does not admit a closed form expression, its spectral function is given by

$$A_{d\downarrow}(\omega,T) = 2\left[1-2n_F(\epsilon)\right]\{n_B(\epsilon)n_F(\omega-\epsilon)+\left[1+n_B(\epsilon)\right]\left[1-n_F(\omega-\epsilon)\right]\}A^{ph}_{d\downarrow}(\omega-\epsilon), \tag{5.19}$$

where

$$A^{ph}_{d\downarrow}(\omega) = -\operatorname{Im}\mathcal{G}^{yy}_{\uparrow}(\omega) = -2\operatorname{Im}\frac{\omega+i\eta-2V^2g_\gamma(x=0;y=1;\omega)}{(\omega+i\eta)^2-4U^2-2V^2(\omega+i\eta)g_\gamma(x=0;y=1;\omega)}, \tag{5.20}$$

with $\eta>0$ is a positive infinitesimal, is the temperature independent spectral function in the particle-hole symmetric model with $\epsilon=0$.

The Matsubara GF for the hybridising $d_\uparrow$-fermion can be calculated by explicitly implementing the gauge constraint, with the result being

$$\mathcal{G}_{d\uparrow}(ik_n) = \frac{ik_n - V^2g_{\gamma_1}(ik_n)+2U\left[2n_F(\epsilon)-1\right]}{(ik_n)^2-4U^2-2ik_nV^2g_{\gamma_1}(ik_n)}, \tag{5.21}$$

from which the spectral function is obtained as $A_{d\uparrow}(\omega,T)=-2\operatorname{Im}\mathcal{G}_{d\uparrow}(ik_n\to\omega+i\eta)$.

5.1.3 *Local Green functions of the host fermions*

The local GFs of the $c_{x,y}$ fermions that form the Read-Green superconductor can be calculated in the boundary GF framework described earlier in this section, by repartitioning and considering appropriate blocks of the BdG and resulting resolvent matrices. However, the BdG matrix in Eqs. (5.11) is expressed in a mixed (k_x,y) representation. To calculate local GFs, it is better to work with a real space (x,y) representation of the BdG matrix. Recall that each block Y_k in the BdG matrix of Eq. (5.11) describes an infinite one-dimensional layer of the system (infinite number of x

sites), but in the momentum k_x representation. Working in the momentum representation allows us to work with a bounded 'matrix' Y_k that has elements parametrised by the continuous variable $k_x \in (-\pi, \pi)$. However, Y_k is infinite dimensional when expressed in the real space (x) representation. To circumvent this problem, we work with a large but finite system and numerically calculate blocks of the resolvent matrix. The BdG matrix in the (x, y) representation of a finite $N_x \times N_y$ RMAI model can be written similar to Eq. (5.11) as a block tridiagonal matrix,

$$h_{BdG}^{(N_x,N_y)} = \begin{pmatrix} H_A & \tilde{J} & 0 & \dots & 0 \\ \tilde{J}^\dagger & Y & \tilde{\mathbf{T}}_Y & \dots & \vdots \\ 0 & \tilde{\mathbf{T}}_Y^\dagger & \ddots & \ddots & 0 \\ \vdots & \vdots & \ddots & Y & \tilde{\mathbf{T}}_Y \\ 0 & 0 & 0 & \tilde{\mathbf{T}}_Y^\dagger & Y \end{pmatrix}, \tag{5.22}$$

where there are N_y blocks of Y. The various matrix blocks are defined as follows; Y is simply Y_k written in the (x, y) representation i.e. an inverse Fourier transform of Y_k and describes hopping and pairing in $\hat{x}$ between sites on a single layer. Nearest neighbour hopping and pairing implies Y is also a block tridiagonal matrix of dimensions $2N_x \times 2N_x$. $\tilde{\mathbf{T}}_Y = \mathrm{diag}(T_y, \dots, T_y)$ similar to $\mathbf{T}_Y$ in Eq. (5.11), but now of dimensions $2N_x \times 2N_x$ like Y. Since Y is written in the (x, y) basis, and the impurity couples only to a single site on the bulk edge[1], J has to be modified accordingly to $\tilde{J}$. We choose N_x odd and couple the impurity to the median site. Therefore, we have

$$Y = \begin{pmatrix} -\mu\sigma^z & T_x & \dots & 0 \\ T_x^\dagger & \ddots & \ddots & \vdots \\ \vdots & \ddots & -\mu\sigma^z & T_x \\ 0 & \dots & T_x^\dagger & -\mu\sigma^z \end{pmatrix}, \qquad \tilde{J} = \begin{pmatrix} 0 & \dots & 0 & \dots & 0 \\ 0 & \dots & C & \dots & 0 \end{pmatrix}, \tag{5.23}$$

where T_x has been defined in Eq. (5.7). The matrix $\tilde{J}$ couples the η-fermion block of H_A to the median diagonal block of Y with coupling matrix C (assuming N_x is odd). The $2N_x \times 2N_x$ diagonal blocks of the resolvent matrix $(z - h_{BdG})^{-1}$ corresponding to the

[1] The bulk edge is simply the bulk of the edge layer $y = 1$, far away from the corners.

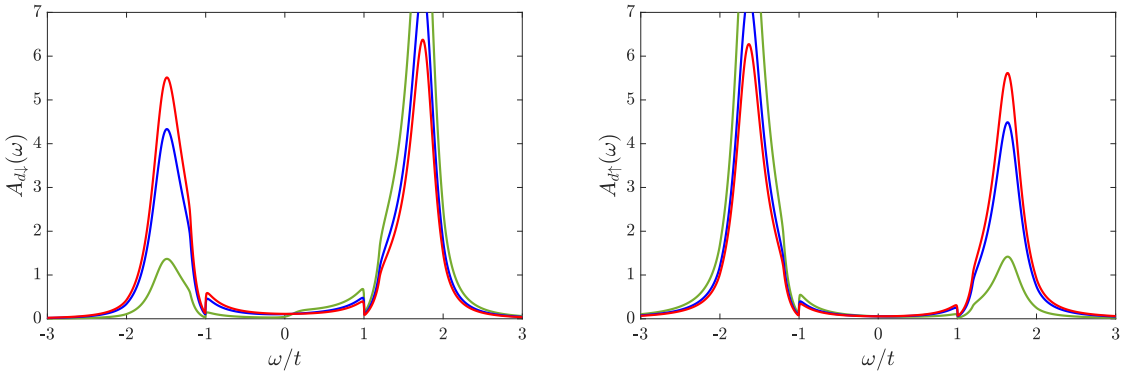

FIGURE 5.2 – Spectral functions of (a) localised $d_\downarrow$ and (b) hybridising $d_\uparrow$-fermions for various temperatures T, shown in the topological phase. In all plots, $\mu = 2.0t$, $\Delta = 0.5t$, $V = 0.4t$, $U = 0.8t$, $\epsilon = 0.1t$ are fixed. $T = 0.05t$ (green), $T = 0.2t$ (blue), $T = 0.9t$ (red).

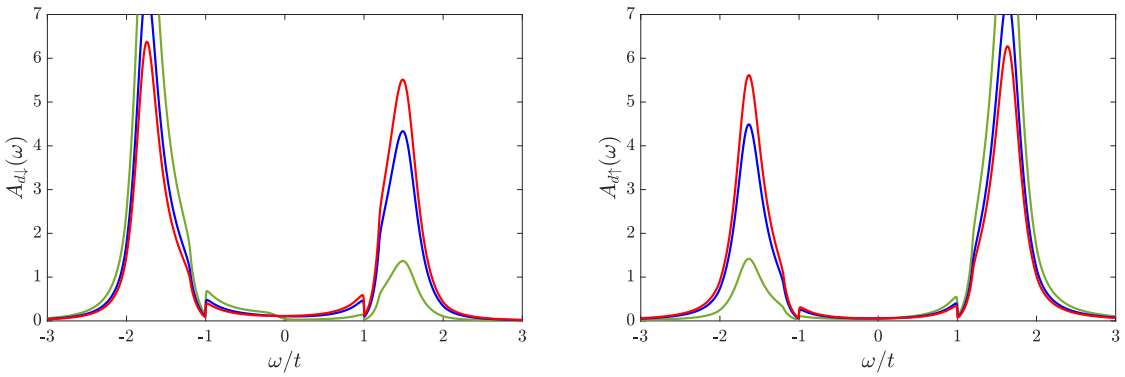

FIGURE 5.3 – Spectral functions of (a) localised $d_\downarrow$ and (b) hybridising $d_\uparrow$-fermions for various temperatures T, shown in the topological phase. In all plots, $\mu = 2.0t$, $\Delta = 0.5t$, $V = 0.4t$, $U = 0.8t$, $\epsilon = -0.1t$ are fixed. $T = 0.05t$ (green), $T = 0.2t$ (blue), $T = 0.9t$ (red). Note that $\epsilon < 0$ and the spectral asymmetry is reversed here in comparison to the plots in Figure 5.2.

matrices Y are then computed numerically, using efficient algorithms for computing blocks of the inverse of a block tridiagonal matrix [128]. These blocks contain the c-fermion local (Nambu) Green functions $\mathbf{G}_c(xx';yy;z)$, from which we may compute the LDOS of the host fermions on various sites. One can also calculate the spatial distribution of the LDOS at a given energy around the impurity.

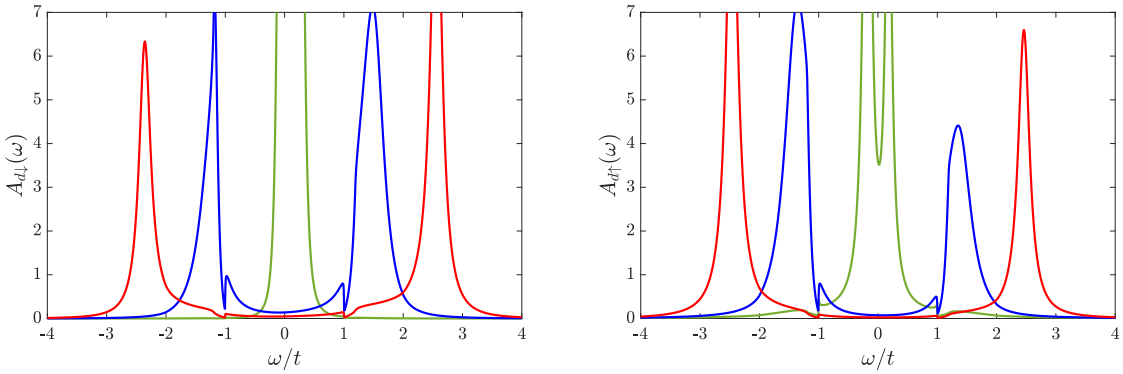

FIGURE 5.4 – Spectral functions of (a) localised $d_\downarrow$ and (b) hybridising $d_\uparrow$ fermions for various interaction strengths U, shown in the topological phase. In all plots, $\mu = 2.0t$, $\Delta = 0.5t$, $V = 0.4t$, $T = 0.2t$, $\epsilon = 0.1t$ are fixed. $U = 0.1t$ (green), $U = 0.7t$ (blue), $U = 1.2t$ (red).

5.2 IMPURITY FERMION PROPERTIES

We now discuss various features of the impurity spectral functions $A_{d\sigma}(\omega, T)$ in the RMAI model, given by Eqs. (5.19)-(5.21). The behaviour with temperature of the spectral functions is the same as that found in the case of the KMAI model, where the impurity hybridises with the end mode of a Kitaev chain. The deviation ϵ from particle-hole symmetry sets the scale for the interaction-induced temperature dependence of both spectral functions $A_{d\sigma}$. For $\epsilon > 0$ and $T \lesssim \epsilon$, there is pronounced spectral asymmetry about $\omega = \epsilon$ ($\omega = 0$) in $A_{d\downarrow}$ ($A_{d\uparrow}$), with larger weight for excitations with $\omega > 0$ ($\omega < 0$) (see Figure 5.2). Flipping the sign of ϵ reverses this asymmetry (Figure 5.3), and $T \gg \epsilon$ removes it. As in section 4.2, this behaviour can be intuitively understood from the impurity spectral functions in the atomic limit ($V = 0$), which are independent of the host material and are given in Eqs. (4.44)-(4.45). The reader is referred to the discussion there for more detail on the temperature dependence of impurity spectral functions, which seems to be largely independent of the specific host material.

Let us now consider the interaction dependence of the impurity spectral functions in the topological phase of the RMAI model, as shown in Figures 5.4a-b. The line shape of the spectral functions here is very different to that of the impurities in the

KMAI model, discussed in detail in section 4.2 The two key features not present in the KMAI spectral functions are as follows; (i) both impurity spectral functions do not exhibit a gap in the excitation spectrum, and (ii) there are only two (broadened) quasiparticle peaks that manifest in the spectral function, which can be traced back to the charge excitations present in the atomic limit ($V = 0$). These differences are due to the differences between the Majorana edge states in the Kitaev chain and the Read-Green superconductor, which the $d_\uparrow$-fermion tunnels into. In the former, the Majorana end mode manifests as a localised zero-energy state protected from other excitations by an energy gap. Half the $d_\uparrow$-fermion [specifically $-i(d_\uparrow - d_\uparrow^\dagger)$] could tunnel into this state, which resulted in a subgap quasiparticle peak in its spectral function in the KMAI model, in addition to the charge excitation peaks at non-zero energy. The absence of such a localised, gap-protected excitation in the Read-Green superconductor explains why the impurity spectral functions have only the two charge excitation peaks in the RMAI model. Recall that the Read-Green superconductor supports chiral Majorana edge modes that have a gapless, linear dispersion. This is why the impurity spectral functions are also not gapped; there is a continuum of edge states the $d_\uparrow$-fermion can tunnel into.

Recall also the Fermi liquid picture that existed for the localised $d_\downarrow$-fermions in the KMAI model. This was due to the presence of a gap-protected zero-energy state that (half) the $d_\uparrow$-fermion could tunnel into. Since the energy of this state was pinned to zero due to the bulk gap and the topology of the Kitaev chain, local interactions with the $d_\downarrow$-fermion could not affect this state. This manifested as a free-fermion peak in the $d_\downarrow$-fermion spectral function at $\omega = \epsilon$ with a reduced quasiparticle weight, which gave credence to a local Fermi liquid picture. The absence of this gap-protected zero-energy state on the edge of the Read-Green superconductor implies no such picture exists for the $d_\downarrow$-fermions in the RMAI model. However, as discussed in section 2.1.2, a vortex in the Read-Green superconductor traps a MZM that is protected by an energy gap from other local excitations. We then expect a local Fermi liquid picture to hold in the case of an Anderson impurity hybridising with these vortex modes in

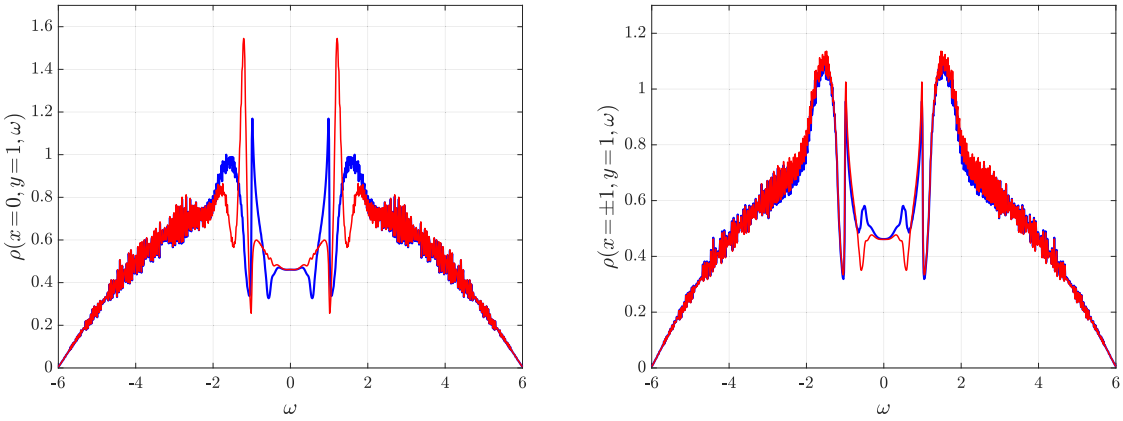

FIGURE 5.5 – LDOS of the c-fermions at (a) impurity site $(x,y)=(0,1)$ for various interaction strengths $U=0.3t$ (blue), $U=0.7t$ (red) (b) sites $(x,y)=(\pm1,1)$ (red/blue) for interaction strength $U=0.3t$. In all plots, $\mu=2.0t$, $\Delta=0.5t$, $V=0.4t$ are fixed..

the manner considered above.

5.3 HOST FERMION PROPERTIES

A prescription for calculating all Nambu GFs $\mathbf{G}_c(xx';yy;z)$ was described in section 5.1.3, for the case of a finite RMAI model of size $N_x \times N_y$ sites. The local density of states on a specific site is then simply $-\mathrm{Im}\,\mathrm{tr}\,\mathbf{G}_c(xx';yy;z)$. In contrast to the semi-infinite plane geometry considered in Appendix A, the chiral edge modes in the finite size system are not gapless, but quantised with a level spacing that goes as $(N_x N_y)^{-1}$. A qualitatively new feature in a finite size Read-Green superconductor is the emergence of localised zero energy states at the corners [129, 130]. In the case of odd N_x and N_y, Komnik and Heinze [129] have shown that a non-local zero-energy fermionic state is fractionalised between the four corners. While the corner modes are not Majorana fermions like the end modes of a Kitaev chain, these can still be used to construct a protected qubit for the purposes of quantum information and computation. In the present discussion, we only focus on the 'bulk edge' states that the impurity hybridises with.

The impurity induces localised bound states (inside the bulk gap), reminiscent of Yu-Shiba-Rusinov states [66–68, 123], that the c-fermions can tunnel into. These

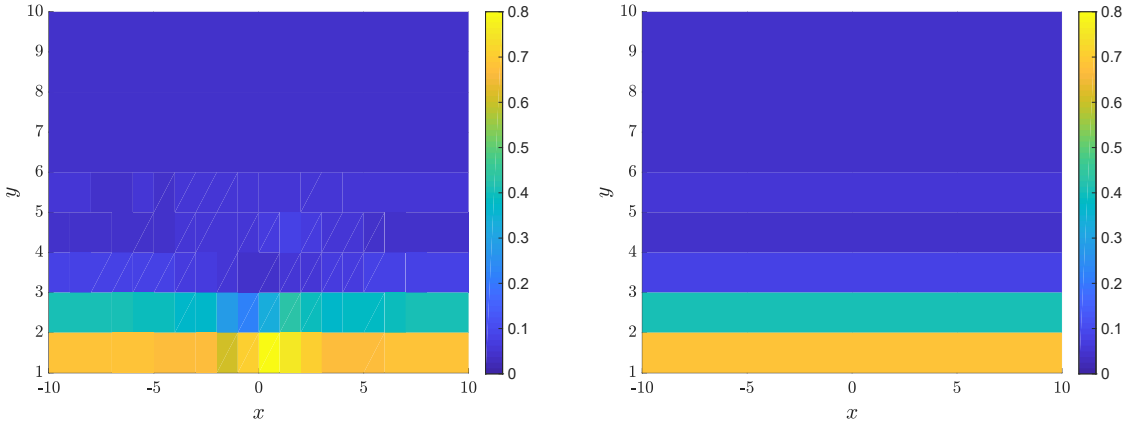

FIGURE 5.6 – Spatial profile of the c-fermion LDOS (intensity plot) near the edge at an energy $\omega = 0.9t$ (inside the bulk energy gap) for (a) non-zero hybridisation $V = 0.4t$, $U = 0.3t$, $\mu = 2.0t$, $\Delta = 0.5t$ (b) zero hybridisation $V = 0$ and $\mu = 2.0t$, $\Delta = 0.5t$. The ticks on the x-axis correspond to the boxes on the immediate right, while ticks on the y-axis correspond to the boxes immediately above..

states feature as two quasiparticle peaks in the c-fermion LDOS on sites near the impurity site $(x = 0, y = 1)$ [see Figures 5.5a-b]. In the case of the KMAI model, impurity induced bound states with energies inside the bulk gap featured as sharp peaks (infinite limetime) in the c-fermion LDOS. However, such states acquire a finite lifetime in the RMAI model due to the absence of an energy gap at the edge of the Read-Green superconductor.

A curious feature in Figure 5.5b is the inequality between the LDOS on sites $(x = 1, y = 1)$ and $(x = -1, y = 1)$. This is seen more prominently in a map of the spatial profile of the LDOS at a certain energy, as shown in Figure 5.6a. Such a map, at energies of the impurity induced bound states, also shows the spatial decay of these local excitations away from the impurity site. We now show that the mirror asymmetry present in the c-fermion LDOS near the edge (Figure 5.6a) is actually due to the symmetry properties of the bulk Hamiltonian. To this end, consider a 'mirror transformation' M_x such that

$$M_x c_{x,y} M_x^{-1} = c_{-x,y}, \qquad M_x c_{x,y}^\dagger M_x^{-1} = c_{-x,y}^\dagger. \tag{5.24}$$

Let us consider the transformation of the bulk Hamiltonian of the Read-Green

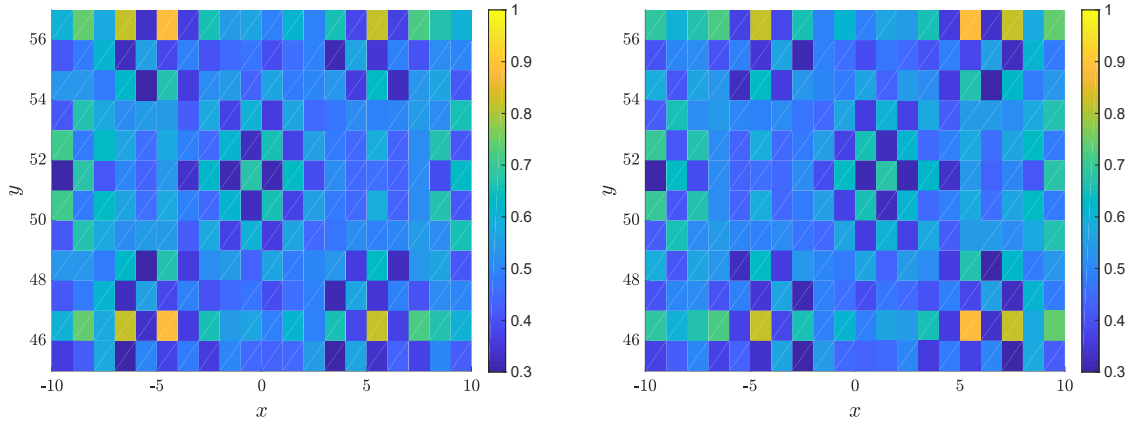

FIGURE 5.7 – Spatial profile of the c-fermion LDOS (intensity plot) in the bulk at an energy $\omega = 3.0t$ (inside SC energy bands) for (a) $\Delta_x = 0.5t$ (b) $\Delta_x = -0.5t$. In all plots, $\mu = 2.0t$, $\Delta_y = 0.5t$ are fixed. The ticks on the x-axis correspond to the boxes on the immediate right, while ticks on the y-axis correspond to the boxes immediately above..

superconductor under M_x. The bulk Hamiltonian is given by

$$H_R = \sum_{x,y=-\infty}^{\infty} \Big[-t\left(c^\dagger_{x+1,y}c_{x,y} + c^\dagger_{x,y+1}c_{x,y} + \text{h.c.}\right) + \left(\Delta c^\dagger_{x+1,y}c^\dagger_{x,y} + i\Delta c^\dagger_{x,y+1}c^\dagger_{x,y} + \text{h.c.}\right) - \mu c^\dagger_{x,y}c_{x,y}\Big]. \quad (5.25)$$

Clearly, the terms that are diagonal in x are invariant under M_x; a simple relabelling $x \to -x$ restores them to their original form. Therefore, let us consider the transformation of terms off-diagonal in x. To this end, it is convenient to work with anisotropic coupling constants t_x, t_y and Δ_x, Δ_y that describe hopping and pairing along $\hat{x}, \hat{y}$ respectively. The terms in H_R that describe hopping along x (which we collectively denote as $\hat{T}_x$) transform as

$$\begin{aligned} M_x \hat{T}_x M_x^{-1} &= -t_x \sum_{x,y} \left(c^\dagger_{-x-1,y}c_{-x,y} + c^\dagger_{-x,y}c_{-x-1,y}\right), \\ &= -t_x \sum_{x',y} \left(c^\dagger_{x'-1,y}c_{x',y} + c^\dagger_{x',y}c_{x'-1,y}\right), \quad x' = -x, \\ &= -t_x \sum_{x'',y} \left(c^\dagger_{x'',y}c_{x''+1,y} + c^\dagger_{x''+1,y}c_{x'',y}\right), \quad x'' = x'-1, \\ &= \hat{T}_x, \end{aligned} \quad (5.26)$$

and therefore are invariant under M_x. The pairing terms off-diagonal in x, collectively denoted as $\hat{\Delta}_x$, transform as

$$\begin{aligned} M_x \hat{\Delta}_x M_x^{-1} &= \Delta_x \sum_{x,y} \left(c^\dagger_{-x-1,y} c^\dagger_{-x,y} + c_{-x,y} c_{-x-1,y} \right), \\ &= \Delta_x \sum_{x',y} \left(c^\dagger_{x'-1,y} c^\dagger_{x',y} + c_{x',y} c_{x'-1,y} \right), \quad x' = -x, \\ &= \Delta_x \sum_{x'',y} \left(c^\dagger_{x'',y} c^\dagger_{x''+1,y} + c_{x''+1,y} c_{x'',y} \right), \quad x'' = x' - 1, \\ &= -\hat{\Delta}_x. \end{aligned} \tag{5.27}$$

Therefore, one has the result $M_x H_R(\Delta_x) M_x^{-1} = H_R(-\Delta_x)$, where the dependence of H_R on other coupling constants has been suppressed as they are unaffected by M_x. Since the bulk Hamiltonian itself transforms non-trivially under M_x, we expect the mirror asymmetry in the LDOS near the edge (Figure 5.6a) to also be present in the bulk. Specifically, the result above indicates that $\rho(x, y, \omega; \Delta_x) = \rho(-x, y, \omega; -\Delta_x)$. This is clearly verified by inspection of separate plots of the left and right hand sides of this equation, for a given energy ω and in the bulk of the system, shown in Figures 5.7a-b.

CHAPTER 6

Conclusion

In summary, we have introduced a general class of exactly solvable quantum impurity models describing the local hybridisation of a Majorana mode in an arbitrary host material with an interacting quantum dot, with broad relevance to current experiments on 1d topological superconductor-quantum dot hybrid structures. A general model in this class is exactly solved by mapping it via the $\mathbb{Z}_2$ slave-spin representation to a non-interacting resonant level model for auxiliary Majorana degrees of freedom. The resulting gauge constraint is then eliminated by exploiting the transformation properties of the Hamiltonian under a special local particle-hole transformation. We then showed that correlation functions in this many-body problem can be computed exactly at both zero and finite temperature when the deviation in impurity chemical potential from the particle-hole symmetric point precisely equals the impurity Zeeman energy.

To highlight the utility and specific features of our exact solution, we studied a hybrid system of an interacting quantum dot coupled to the end MZM of a Kitaev chain (KMAI model), motivated by recent experimental progress in realising such a setup. Since this model falls within the MAI class, exact expressions for the dot

spectral functions and host LDOS can be calculated using the model's free-fermion slave-spin representation. We found a non-trivial temperature dependence in the dot spectral functions, indicative of the fact that the physical dot fermions are interacting, even though the slave-fermions are not. It was shown that the interaction and hybridisation with the quantum dot favoured different MZMs, and affected its localisation length. We then found that the non-hybridising fermion on the quantum dot could be described by a local Fermi liquid picture, and calculated the associated interaction-dependent quasiparticle weight. It was then established that hybridisation with the end MZM of the Kitaev chain induced purely odd-frequency pairing correlations for the hybridising fermions on the quantum dot. In addition, we also studied the interaction-dependence of the double occupancy on the quantum dot for various temperatures, finding a general suppression with increasing interactions strengths. Finally, departures from the exactly solvable limit were considered, and we demonstrated how corrections to the free energy could be calculated perturbatively, with the perturbation corresponding to a shift in the chemical potential or Zeeman field on the quantum dot.

As another distinct example, a hybrid system of a quantum dot coupled to the chiral Majorana edge modes of a spinless p_x+ip_y superconductor was then considered (RMAI model). The dot spectral functions and host LDOS were then studied, and the key differences from those functions in the KMAI model were traced to the chiral nature of the gapless edge modes in a $p_x + ip_y$ superconductor.

Several extensions of our work are possible. For example, one can consider a class of periodic Anderson models, describing a lattice of interacting impurities hybridising with Majorana modes. Such models could potentially be realised in an Abrikosov vortex lattice of a topological $p_x + ip_y$ superconductor, with each vortex hosting a localised and unpaired Majorana mode. It was shown in 3.5 that this class of models also admits an exact solution by the $\mathbb{Z}_2$ slave-spin method. It would be interesting to study both zero and finite temperature phase transitions in models of this class.

Another direct application of the MAI class of models is to transport in junctions of topological superconductors and quantum dots. Specifically, one would like to study the various fractional a.c. and d.c. Josephson effects found in such junctions [131–134] in an exactly solvable model. In Appendix C, we set up one representative transport problem in a topological superconductor-quantum dot-topological superconductor (TSC-QD-TSC) junction, and prove that the average non-equilibrium current can be calculated exactly without constraint in the quadratic slave-spin representation of the model.

Bibliography

[1] G. Shankar and J. Maciejko, "*Exactly Solvable Majorana-Anderson Impurity Models*," arXiv:1905.06983 [cond-mat] (2019).

[2] E. Majorana, "*Teoria Simmetrica Dell'elettrone e Del Positrone*," Nuovo Cim **14**, 171 (1937).

[3] J. Alicea, "*New Directions in the Pursuit of Majorana Fermions in Solid State Systems*," Rep. Prog. Phys. **75**, 076501 (2012).

[4] M. Sato and S. Fujimoto, "*Majorana Fermions and Topology in Superconductors*," J. Phys. Soc. Jpn. **85**, 072001 (2016).

[5] C. Nayak, S. H. Simon, A. Stern, M. Freedman, and S. Das Sarma, "*Non-Abelian Anyons and Topological Quantum Computation*," Rev. Mod. Phys. **80**, 1083 (2008).

[6] R. Aguado, "*Majorana Quasiparticles in Condensed Matter*," Riv. Nuovo Cimento **40**, 523 (2017).

[7] S. D. Sarma, M. Freedman, and C. Nayak, "*Majorana Zero Modes and Topological Quantum Computation*," npj Quantum Information **1**, 15001 (2015).

[8] A. Rahmani and M. Franz, "*Interacting Majorana Fermions*," Rep. Prog. Phys. **82**, 084501 (2019).

[9] B. Béri and N. R. Cooper, "*Topological Kondo Effect with Majorana Fermions*," Phys. Rev. Lett. **109**, 156803 (2012).

[10] L. Herviou, K. Le Hur, and C. Mora, "*Many-Terminal Majorana Island: From Topological to Multichannel Kondo Model*," Phys. Rev. B **94**, 235102 (2016).

[11] A. Altland and R. Egger, "*Multiterminal Coulomb-Majorana Junction*," Phys. Rev. Lett. **110**, 196401 (2013).

[12] F. Hassler and D. Schuricht, "*Strongly Interacting Majorana Modes in an Array of Josephson Junctions*," New J. Phys. **14**, 125018 (2012).

[13] M. T. Deng, S. Vaitiekėnas, E. B. Hansen, J. Danon, M. Leijnse, K. Flensberg, J. Nygård, P. Krogstrup, and C. M. Marcus, "*Majorana Bound State in a Coupled Quantum-Dot Hybrid-Nanowire System*," Science **354**, 1557 (2016).

[14] M. A. Nielsen and I. L. Chuang, *Quantum Computation and Quantum Information* (Cambridge University Press, Cambridge, 2010).

[15] A. Y. Kitaev, "*Unpaired Majorana Fermions in Quantum Wires*," Phys.-Usp. **44**, 131 (2001).

[16] A. Y. Kitaev, "*Fault-Tolerant Quantum Computation by Anyons*," Annals of Physics **303**, 2 (2003).

[17] F. Konschelle and F. Hassler, "*Effects of Nonequilibrium Noise on a Quantum Memory Encoded in Majorana Zero Modes*," Phys. Rev. B **88**, 075431 (2013).

[18] C. Zeng, C. Moore, A. M. Rao, T. D. Stanescu, and S. Tewari, "*Analytical Solution of the Finite-Length Kitaev Chain Coupled to a Quantum Dot*," Phys. Rev. B **99**, 094523 (2019).

[19] J. Alicea, Y. Oreg, G. Refael, F. von Oppen, and M. P. A. Fisher, "*Non-Abelian Statistics and Topological Quantum Information Processing in 1D Wire Networks*," Nature Physics **7**, 412 (2011).

[20] M. Sato and Y. Ando, "*Topological Superconductors: A Review*," Rep. Prog. Phys. **80**, 076501 (2017).

[21] X.-L. Qi and S.-C. Zhang, "*Topological Insulators and Superconductors*," Rev. Mod. Phys. **83**, 1057 (2011).

[22] B. A. Bernevig and T. L. Hughes, *Topological Insulators and Topological Superconductors* (Princeton University Press, Princeton, 2013).

[23] P. W. Anderson, "*Random-Phase Approximation in the Theory of Superconductivity*," Phys. Rev. **112**, 1900 (1958).

[24] P. Coleman, *Introduction to Many Body Physics* (Cambridge University Press, Cambridge, 2015).

[25] F. von Oppen, Y. Peng, and F. Pientka, "*Topological Superconducting Phases in One-Dimension*," in *Topological Aspects of Condensed Matter Physics (Les Houches 2014, Session CIII)*, edited by C. Chamon, M. Goerbig, R. Moessner, and L. Cugliandolo (Oxford University Press, Oxford, 2017).

[26] A. Hatcher, *Algebraic Topology* (Cambridge University Press, Cambridge, 2002).

[27] A. Kitaev, "*Periodic Table for Topological Insulators and Superconductors*," AIP Conf. Proc. **1134**, 22 (2009).

[28] C.-K. Chiu, J. C. Y. Teo, A. P. Schnyder, and S. Ryu, "*Classification of Topological Quantum Matter with Symmetries*," Rev. Mod. Phys. **88**, 035005 (2016).

[29] S. Ryu, A. P. Schnyder, A. Furusaki, and A. W. W. Ludwig, "*Topological Insulators and Superconductors: Tenfold Way and Dimensional Hierarchy*," New J. Phys. **12**, 065010 (2010).

[30] L. Fidkowski and A. Kitaev, "*Effects of Interactions on the Topological Classification of Free Fermion Systems*," Phys. Rev. B **81**, 134509 (2010).

[31] L. Fidkowski and A. Kitaev, "*Topological Phases of Fermions in One Dimension*," Phys. Rev. B **83**, 075103 (2011).

[32] N. Read and D. Green, "*Paired States of Fermions in Two Dimensions with Breaking of Parity and Time-Reversal Symmetries and the Fractional Quantum Hall Effect*," Phys. Rev. B **61**, 10267 (2000).

[33] J. Milnor, *Topology from the Differentiable Viewpoint*, (rev. ed.) ed. (Princeton University Press, Princeton, N.J., 1997).

[34] M. Stone and R. Roy, "*Edge modes, edge currents, and gauge invariance in $p_x + ip_y$ superfluids and superconductors*," Phys. Rev. B **69**, 184511 (2004).

[35] R. Jackiw and P. Rossi, "*Zero Modes of the Vortex-Fermion System*," Nucl. Phys. B **190**, 681 (1981).

[36] R. R. Biswas, "*Majorana Fermions in Vortex Lattices*," Phys. Rev. Lett. **111**, 136401 (2013).

[37] M. Cheng, R. M. Lutchyn, V. Galitski, and S. Das Sarma, "*Splitting of Majorana-Fermion Modes due to Intervortex Tunneling in a $p_x + ip_y$ Superconductor*," Phys. Rev. Lett. **103**, 107001 (2009).

[38] M. Cheng, R. M. Lutchyn, V. Galitski, and S. Das Sarma, "*Tunneling of Anyonic Majorana Excitations in Topological Superconductors*," Phys. Rev. B **82**, 094504 (2010).

[39] N. D. Mermin and H. Wagner, "*Absence of Ferromagnetism or Antiferromagnetism in One- or Two-Dimensional Isotropic Heisenberg Models*," Phys. Rev. Lett. **17**, 1133 (1966).

[40] P. C. Hohenberg, "*Existence of Long-Range Order in One and Two Dimensions*," Phys. Rev. **158**, 383 (1967).

[41] S. Coleman, "*There Are No Goldstone Bosons in Two Dimensions*," Commun.Math. Phys. **31**, 259 (1973).

[42] A. Akhmerov, J. Sau, and B. van Heck, "*Topology in Condensed Matter*," https://topocondmat.org (2019).

[43] G. Bihlmayer, O. Rader, and R. Winkler, "*Focus on the Rashba Effect*," New J. Phys. **17**, 050202 (2015).

[44] Y. A. Bychkov and E. I. Rashba, "*Properties of a 2D Electron Gas with Lifted Spectral Degeneracy*," JETP Lett. **39**, 78 (1984).

[45] R. M. Lutchyn, J. D. Sau, and S. Das Sarma, "*Majorana Fermions and a Topological Phase Transition in Semiconductor-Superconductor Heterostructures*," Phys. Rev. Lett. **105**, 077001 (2010).

[46] Y. Oreg, G. Refael, and F. von Oppen, "*Helical Liquids and Majorana Bound States in Quantum Wires*," Phys. Rev. Lett. **105**, 177002 (2010).

[47] J. Alicea, "*Majorana Fermions in a Tunable Semiconductor Device*," Phys. Rev. B **81**, 125318 (2010).

[48] J. D. Sau, R. M. Lutchyn, S. Tewari, and S. Das Sarma, "*Generic New Platform for Topological Quantum Computation Using Semiconductor Heterostructures*," Phys. Rev. Lett. **104**, 040502 (2010).

[49] L. Fu and C. L. Kane, "*Superconducting Proximity Effect and Majorana Fermions at the Surface of a Topological Insulator*," Phys. Rev. Lett. **100**, 096407 (2008).

[50] L. Fu and C. L. Kane, "*Josephson Current and Noise at a Superconductor/Quantum-Spin-Hall-Insulator/Superconductor Junction*," Phys. Rev. B **79**, 161408 (2009).

[51] M. Z. Hasan and C. L. Kane, "*Colloquium: Topological Insulators*," Rev. Mod. Phys. **82**, 3045 (2010).

[52] J. Maciejko, T. L. Hughes, and S.-C. Zhang, "*The Quantum Spin Hall Effect*," Annu. Rev. Condens. Matter Phys. **2**, 31 (2011).

[53] S. Nadj-Perge, I. K. Drozdov, B. A. Bernevig, and A. Yazdani, "*Proposal for Realizing Majorana Fermions in Chains of Magnetic Atoms on a Superconductor*," Phys. Rev. B **88**, 020407 (2013).

[54] A. P. Mackenzie and Y. Maeno, "*The superconductivity of* Sr_2RuO_4 *and the physics of spin-triplet pairing*," Rev. Mod. Phys. **75**, 657 (2003).

[55] G. Xu, B. Lian, P. Tang, X.-L. Qi, and S.-C. Zhang, "*Topological Superconductivity on the Surface of Fe-Based Superconductors*," Phys. Rev. Lett. **117**, 047001 (2016).

[56] Z. Wang, P. Zhang, G. Xu, L. K. Zeng, H. Miao, X. Xu, T. Qian, H. Weng, P. Richard, A. V. Fedorov, H. Ding, X. Dai, and Z. Fang, "*Topological nature of the* $FeSe_{0.5}Te_{0.5}$ *superconductor*," Phys. Rev. B **92**, 115119 (2015).

[57] N. Hao and J. Hu, "*Topological Phases in the Single-Layer FeSe*," Phys. Rev. X **4**, 031053 (2014).

[58] T. Mizushima, Y. Tsutsumi, T. Kawakami, M. Sato, M. Ichioka, and K. Machida, "*Symmetry-Protected Topological Superfluids and Superconductors —From the Basics to 3He—*," J. Phys. Soc. Jpn. **85**, 022001 (2016).

[59] R. M. Lutchyn, E. P. a. M. Bakkers, L. P. Kouwenhoven, P. Krogstrup, C. M. Marcus, and Y. Oreg, "*Majorana Zero Modes in Superconductor–Semiconductor Heterostructures*," Nat Rev Mater **3**, 52 (2018).

[60] K. T. Law, P. A. Lee, and T. K. Ng, "*Majorana Fermion Induced Resonant Andreev Reflection*," Phys. Rev. Lett. **103**, 237001 (2009).

[61] K. Flensberg, "*Tunneling Characteristics of a Chain of Majorana Bound States*," Phys. Rev. B **82**, 180516 (2010).

[62] V. Mourik, K. Zuo, S. M. Frolov, S. R. Plissard, E. P. a. M. Bakkers, and L. P. Kouwenhoven, "*Signatures of Majorana Fermions in Hybrid Superconductor-Semiconductor Nanowire Devices*," Science **336**, 1003 (2012).

[63] J. Liu, A. C. Potter, K. T. Law, and P. A. Lee, "*Zero-Bias Peaks in the Tunneling Conductance of Spin-Orbit-Coupled Superconducting Wires with and without Majorana End-States*," Phys. Rev. Lett. **109**, 267002 (2012).

[64] C.-X. Liu, J. D. Sau, T. D. Stanescu, and S. Das Sarma, "*Andreev Bound States versus Majorana Bound States in Quantum Dot-Nanowire-Superconductor Hybrid Structures: Trivial versus Topological Zero-Bias Conductance Peaks*," Phys. Rev. B **96**, 075161 (2017).

[65] S. Nadj-Perge, I. K. Drozdov, J. Li, H. Chen, S. Jeon, J. Seo, A. H. MacDonald, B. A. Bernevig, and A. Yazdani, "*Observation of Majorana Fermions in Ferromagnetic Atomic Chains on a Superconductor*," Science **346**, 602 (2014).

[66] L. Yu, "*Bound State in Superconductors with Paramagnetic Impurities*," Acta Phys. Sin. **21**, 75 (1965).

[67] H. Shiba, "*Classical Spins in Superconductors*," Prog. Theor. Phys. **40**, 435 (1968).

[68] A. I. Rusinov, "*On the Theory of Gapless Superconductivity in Alloys Containing Paramagnetic Impurities*," Sov. Phys. JETP **56**, 2047 (1969).

[69] R. Pawlak, M. Kisiel, J. Klinovaja, T. Meier, S. Kawai, T. Glatzel, D. Loss, and E. Meyer, "*Probing Atomic Structure and Majorana Wavefunctions in Mono-Atomic Fe Chains on Superconducting Pb Surface*," npj Quantum Information **2**, 16035 (2016).

[70] M. Ruby, F. Pientka, Y. Peng, F. von Oppen, B. W. Heinrich, and K. J. Franke, "*End States and Subgap Structure in Proximity-Coupled Chains of Magnetic Adatoms*," Phys. Rev. Lett. **115**, 197204 (2015).

[71] S. Jeon, Y. Xie, J. Li, Z. Wang, B. A. Bernevig, and A. Yazdani, "*Distinguishing a Majorana Zero Mode Using Spin-Resolved Measurements*," Science **358**, 772 (2017).

[72] B. E. Feldman, M. T. Randeria, J. Li, S. Jeon, Y. Xie, Z. Wang, I. K. Drozdov, B. Andrei Bernevig, and A. Yazdani, "*High-Resolution Studies of the Majorana Atomic Chain Platform*," Nature Physics **13**, 286 (2017).

[73] T. Machida, Y. Sun, S. Pyon, S. Takeda, Y. Kohsaka, T. Hanaguri, T. Sasagawa, and T. Tamegai, "*Zero-Energy Vortex Bound State in the Superconducting Topological Surface State of Fe(Se,Te)*," Nat. Mater. **18**, 811 (2019).

[74] H.-H. Sun and J.-F. Jia, "*Detection of Majorana Zero Mode in the Vortex*," npj Quant Mater **2**, 1 (2017).

[75] D. Wang, L. Kong, P. Fan, H. Chen, S. Zhu, W. Liu, L. Cao, Y. Sun, S. Du, J. Schneeloch, R. Zhong, G. Gu, L. Fu, H. Ding, and H.-J. Gao, "*Evidence for Majorana Bound States in an Iron-Based Superconductor*," Science **362**, 333 (2018).

[76] P. Zhang, K. Yaji, T. Hashimoto, Y. Ota, T. Kondo, K. Okazaki, Z. Wang, J. Wen, G. D. Gu, H. Ding, and S. Shin, "*Observation of Topological Superconductivity on the Surface of an Iron-Based Superconductor*," Science **360**, 182 (2018).

[77] C.-K. Chiu, T. Machida, Y. Huang, T. Hanaguri, and F.-C. Zhang, "*Scalable Majorana Vortex Modes in Iron-Based Superconductors*," arXiv:1904.13374 [cond-mat] (2019).

[78] C.-K. Chiu, D. I. Pikulin, and M. Franz, "*Strongly Interacting Majorana Fermions*," Phys. Rev. B **91**, 165402 (2015).

[79] G. C. Menard, S. Guissart, C. Brun, R. T. Leriche, M. Trif, F. Debontridder, D. Demaille, D. Roditchev, P. Simon, and T. Cren, "*Two-Dimensional Topological Superconductivity in Pb/Co/Si(111)*," Nat Commun **8**, 1 (2017).

[80] S. B. Chung, X.-L. Qi, J. Maciejko, and S.-C. Zhang, "*Conductance and Noise Signatures of Majorana Backscattering*," Phys. Rev. B **83**, 100512 (2011).

[81] S. B. Chung and S.-C. Zhang, "*Detecting the Majorana Fermion Surface State of* ^{3}He–*B through Spin Relaxation*," Phys. Rev. Lett. **103**, 235301 (2009).

[82] R. Shindou, A. Furusaki, and N. Nagaosa, "*Quantum Impurity Spin in Majorana Edge Fermions*," Phys. Rev. B **82**, 180505 (2010).

[83] A. Rahmani and M. Franz, "*Interacting Majorana Fermions*," Rep. Prog. Phys. **82**, 084501 (2019).

[84] T. Hayata and A. Yamamoto, "*Quantum Monte Carlo Simulation of a Two-Dimensional Majorana Lattice Model*," Phys. Rev. B **96**, 035129 (2017).

[85] A. Rahmani, D. Pikulin, and I. Affleck, "*Phase Diagrams of Majorana-Hubbard Ladders*," Phys. Rev. B **99**, 085110 (2019).

[86] K. Wamer and I. Affleck, "*Renormalization Group Analysis of Phase Transitions in the Two-Dimensional Majorana-Hubbard Model*," Phys. Rev. B **98**, 245120 (2018).

[87] C. Li and M. Franz, "*Majorana-Hubbard Model on the Honeycomb Lattice*," Phys. Rev. B **98**, 115123 (2018).

[88] I. Affleck, A. Rahmani, and D. Pikulin, "*Majorana-Hubbard Model on the Square Lattice*," Phys. Rev. B **96**, 125121 (2017).

[89] A. Rahmani, X. Zhu, M. Franz, and I. Affleck, "*Emergent Supersymmetry from Strongly Interacting Majorana Zero Modes*," Phys. Rev. Lett. **115**, 166401 (2015).

[90] X.-H. Li, Z. Chen, and T.-K. Ng, "*Majorana Falicov-Kimball Models*," arXiv:1903.05013 [cond-mat] (2019).

[91] Z. Chen, X. Li, and T. K. Ng, "*Exactly Solvable BCS-Hubbard Model in Arbitrary Dimensions*," Phys. Rev. Lett. **120**, 046401 (2018).

[92] C. Prosko, S.-P. Lee, and J. Maciejko, "*Simple $\mathbb{Z}_2$ lattice gauge theories at finite fermion density*," Phys. Rev. B **96**, 205104 (2017).

[93] A. Rüegg, S. D. Huber, and M. Sigrist, "$\mathbb{Z}_2$ *Slave-Spin Theory for Strongly Correlated Fermions*," Phys. Rev. B **81**, 155118 (2010).

[94] Y. Hu and C. L. Kane, "*Fibonacci Topological Superconductor*," Phys. Rev. Lett. **120**, 066801 (2018).

[95] M. Cheng, M. Becker, B. Bauer, and R. M. Lutchyn, "*Interplay between Kondo and Majorana Interactions in Quantum Dots*," Phys. Rev. X **4**, 031051 (2014).

[96] S. Hoffman, D. Chevallier, D. Loss, and J. Klinovaja, "*Spin-Dependent Coupling between Quantum Dots and Topological Quantum Wires*," Phys. Rev. B **96**, 045440 (2017).

[97] M. Lee, J. S. Lim, and R. López, "*Kondo Effect in a Quantum Dot Side-Coupled to a Topological Superconductor*," Phys. Rev. B **87**, 241402 (2013).

[98] D. E. Liu, M. Cheng, and R. M. Lutchyn, "*Probing Majorana Physics in Quantum-Dot Shot-Noise Experiments*," Phys. Rev. B **91**, 081405 (2015).

[99] G. D. Mahan, "*Excitons in Degenerate Semiconductors*," Phys. Rev. **153**, 882 (1967).

[100] P. Nozieres and C. T. De Dominicis, "*Singularities in the X-Ray Absorption and Emission of Metals. III. One-Body Theory Exact Solution*," Phys. Rev. **178**, 1097 (1969).

[101] L. de'Medici, A. Georges, and S. Biermann, "*Orbital-Selective Mott Transition in Multiband Systems: Slave-Spin Representation and Dynamical Mean-Field Theory*," Phys. Rev. B **72**, 205124 (2005).

[102] S. D. Huber and A. Rüegg, "*Dynamically Generated Double Occupancy as a Probe of Cold Atom Systems*," Phys. Rev. Lett. **102**, 065301 (2009).

[103] D. Guerci, "*Transport through a Magnetic Impurity: A Slave-Spin Approach*," Phys. Rev. B **99**, 195409 (2019).

[104] J. Fu, J. Knolle, and N. B. Perkins, "*Three Types of Representation of Spin in Terms of Majorana Fermions and an Alternative Solution of the Kitaev Honeycomb Model*," Phys. Rev. B **97**, 115142 (2018).

[105] D. Guerci and M. Fabrizio, "*Unbinding Slave Spins in the Anderson Impurity Model*," Phys. Rev. B **96**, 201106 (2017).

[106] R. Zitko and M. Fabrizio, "$\mathbb{Z}_2$ *Gauge Theory Description of the Mott Transition in Infinite Dimensions*," Phys. Rev. B **91**, 245130 (2015).

[107] A. C. Hewson, *The Kondo Problem to Heavy Fermions* (Cambridge University Press, Cambridge, 1997).

[108] H. Bruus and K. Flensberg, *Many-Body Quantum Theory in Condensed Matter Physics* (Oxford University Press, Oxford, 2004).

[109] A. Umerski, "*Closed-Form Solutions to Surface Green's Functions*," Phys. Rev. B **55**, 5266 (1997).

[110] S. Datta, *Electronic Transport in Mesoscopic Systems* (Cambridge University Press, Cambridge, 2009).

[111] A. Altland and B. D. Simons, *Condensed Matter Field Theory*, 2nd ed. (Cambridge University Press, Cambridge, 2010).

[112] T. Jonckheere, J. Rech, A. Zazunov, R. Egger, and T. Martin, "*Hanbury Brown and Twiss Noise Correlations in a Topological Superconductor Beam Splitter*," Phys. Rev. B **95**, 054514 (2017).

[113] R. Shankar and A. Vishwanath, "*Equality of Bulk Wave Functions and Edge Correlations in Some Topological Superconductors: A Spacetime Derivation*," Phys. Rev. Lett. **107**, 106803 (2011).

[114] R. Shankar, *Quantum Field Theory and Condensed Matter* (Cambridge University Press, Cambridge, 2017).

[115] M. A. Srednicki, *Quantum Field Theory* (Cambridge University Press, Cambridge, 2007).

[116] V. L. Berezinskii, "*New Model of the Anisotropic Phase of Superfluid Helium-3*," JETP Lett. **20**, 287 (1974).

[117] J. Linder and A. V. Balatsky, "*Odd-Frequency Superconductivity*," arXiv:1709.03986 [cond-mat] (2017).

[118] S.-P. Lee, R. M. Lutchyn, and J. Maciejko, "*Odd-Frequency Superconductivity in a Nanowire Coupled to Majorana Zero Modes*," Phys. Rev. B **95**, 184506 (2017).

[119] A. Balatsky and E. Abrahams, "*New Class of Singlet Superconductors Which Break the Time Reversal and Parity*," Phys. Rev. B **45**, 13125 (1992).

[120] T. R. Kirkpatrick and D. Belitz, "*Disorder-Induced Triplet Superconductivity*," Phys. Rev. Lett. **66**, 1533 (1991).

[121] Y. Asano and Y. Tanaka, "*Majorana Fermions and Odd-Frequency Cooper Pairs in a Normal-Metal Nanowire Proximity-Coupled to a Topological Superconductor*," Phys. Rev. B **87**, 104513 (2013).

[122] Z. Huang, P. Wölfle, and A. V. Balatsky, "*Odd-Frequency Pairing of Interacting Majorana Fermions*," Phys. Rev. B **92**, 121404 (2015).

[123] A. V. Balatsky, I. Vekhter, and J.-X. Zhu, "*Impurity-Induced States in Conventional and Unconventional Superconductors*," Rev. Mod. Phys. **78**, 373 (2006).

[124] M. G. Reuter, "*Closed-Form Green Functions, Surface Effects, and the Importance of Dimensionality in Tight-Binding Metals*," J. Chem. Phys. **133**, 034703 (2010).

[125] M. G. Reuter, T. Seideman, and M. A. Ratner, "*Probing the Surface-to-Bulk Transition: A Closed-Form Constant-Scaling Algorithm for Computing Subsurface Green Functions*," Phys. Rev. B **83**, 085412 (2011).

[126] M. G. Reuter, N. M. Boffi, M. A. Ratner, and T. Seideman, "*The Role of Dimensionality in the Decay of Surface Effects*," J. Chem. Phys. **138**, 084707 (2013).

[127] P. B. Wiegmann and A. M. Finkelstein, "*Resonant-Level Model in the Kondo Problem*," Sov. Phys. JETP **48**, 102 (1978).

[128] M. G. Reuter and J. C. Hill, "*An Efficient, Block-by-Block Algorithm for Inverting a Block Tridiagonal, Nearly Block Toeplitz Matrix*," Comput. Sci. Disc. **5**, 014009 (2012).

[129] A. Komnik and S. Heinze, "*Analytical Results for the Green's Functions of Lattice Fermions*," Phys. Rev. B **96**, 155103 (2017).

[130] Y. Peng, Y. Bao, and F. von Oppen, "*Boundary Green Functions of Topological Insulators and Superconductors*," Phys. Rev. B **95**, 235143 (2017).

[131] L. P. Rokhinson, X. Liu, and J. K. Furdyna, "*The Fractional a.c. Josephson Effect in a Semiconductor–Superconductor Nanowire as a Signature of Majorana Particles*," Nature Physics **8**, 795 (2012).

[132] P. Stefanski, "*Properties of the Majorana-State Tunneling Josephson Junction Mediated by an Interacting Quantum Dot*," J. Phys.: Condens. Matter **31**, 185301 (2019).

[133] C. Laflamme, J. C. Budich, P. Zoller, and M. Dalmonte, "*Non-equilibrium 8π Josephson effect in atomic Kitaev wires*," Nature Communications **7**, 12280 (2016).

[134] E. Grosfeld and A. Stern, "*Observing Majorana Bound States of Josephson Vortices in Topological Superconductors*," PNAS **108**, 11810 (2011).

[135] F. Bastianelli and P. Van Nieuwenhuizen, *Path Integrals and Anomalies in Curved Space* (Cambridge University Press, Cambridge, 2006).

[136] J. Zinn-Justin, *Quantum Field Theory and Critical Phenomena*, 4th ed. (Oxford University Press, Oxford, 2002).

[137] J. Maciejko, *An Introduction to Nonequilibrium Many-Body Theory* (2007).

APPENDIX A

Boundary Green functions of topological superconductors

A.1 Kitaev chain

In this section, we provide a derivation of the left boundary Green function (GF) of a semi-infinite Kitaev chain [15], following the method outlined in Appendix A of Ref. [112]. The strategy is as follows - we first calculate the bulk GF of an infinite Kitaev chain and then obtain the boundary GF from the Dyson equation one gets when the chain is cut in half by an infinite local potential. The Hamiltonian for an infinite Kitaev chain is

$$H_K = \sum_i \left[-t c_i^\dagger c_{i+1} + \Delta c_i c_{i+1} + \text{h.c.} \right] - \mu \sum_{i=1}^{\infty} c_i^\dagger c_i. \tag{A.1}$$

Imposing periodic boundary conditions and exploiting translational invariance to Fourier transform to momentum space, the Hamiltonian can be written as a Bogoliubov-de-Gennes (BdG) equation,

$$H_K = \frac{1}{2} \sum_k \Psi_k^\dagger \begin{pmatrix} -2t\cos k - \mu & -2i\Delta \sin k \\ 2i\Delta \sin k & 2t\cos k + \mu \end{pmatrix} \Psi_k \equiv \frac{1}{2} \sum_k \Psi_k^\dagger h_k \Psi_k, \tag{A.2}$$

where $\Psi_k = (c_k \quad c_{-k}^\dagger)^\intercal$ is a Nambu spinor. The real space bulk (Nambu) GF is then obtained as an inverse Fourier transform of the momentum space GF,

$$\begin{aligned}\mathbf{g}_B(i-j;z) &= \int_{-\pi}^{\pi} \frac{dk}{2\pi} e^{ik(x_j-x_i)} (z-h_k)^{-1}, \\ &= \int_{-\pi}^{\pi} \frac{dk}{2\pi} e^{ik(x_j-x_i)} \frac{z-(2t\cos k+\mu)\sigma^z + 2\Delta \sin k \sigma^y}{z^2-(\mu-2t\cos k)^2 - 4\Delta^2 \sin^2 k},\end{aligned} \tag{A.3}$$

where $\{\sigma^x, \sigma^y, \sigma^z\}$ is a set of Pauli matrices in Nambu space. z is a general complex-valued frequency such that $z = ik_n$ (fermionic Matsubara frequencies) on the imaginary axis and $z = \omega$ (real frequencies) on the real axis. For example. evaluating $\mathbf{g}_B(i-j;z)$ on the imaginary axis or for $z = \omega + i0^+$ yields the Matsubara or retarded GFs respectively. Placing a local scattering potential of strength ϕ at the site $i = 0$, the Hamiltonian is modified to $H_K' = H_K + \phi c_0^\dagger c_0$. The Dyson equation for the new real space GF is then

$$\mathbf{g}'(ij;z) = \mathbf{g}_B(i-j;z) + \mathbf{g}_B(i-0;z)\phi\sigma^z\mathbf{g}'(ij;z). \tag{A.4}$$

Taking the limit $\phi \to \infty$ to cut the chain, we obtain the left boundary GF of the semi-infinite chain as

$$\begin{aligned}\mathbf{g}'(11;z) &= \mathbf{g}_B(0;z) - \mathbf{g}_B(1-0;z)\mathbf{g}_B^{-1}(0;z)\mathbf{g}_B(0-1;z), \\ &\equiv \mathbf{g}_S(z)\end{aligned} \tag{A.5}$$

To calculate $\mathbf{g}_B(0;z)$, $\mathbf{g}_B(1-0;z)$, and $\mathbf{g}_B(0-1;z)$, one needs to compute the integral in Eq. (A.3). To do so, we make the substitution $w = -\cos k$ to get

$$\begin{aligned}\mathbf{g}_B(i-j;z) = \int_{-\pi}^{\pi} \frac{dw}{2\pi\sqrt{1-w^2}} \sum_{s=\pm1} &\frac{\left(-w+is\sqrt{1-w^2}\right)^{x_j-x_i}}{z^2-(2tw-\mu)^2-4\Delta^2(1-w^2)} \\ &\times \left[z+(2tw-\mu)\sigma^z + 2s\Delta\sqrt{1-w^2}\right].\end{aligned} \tag{A.6}$$

Factorising the denominator in the summand, we find

$$\begin{aligned}\mathbf{g}_B(i-j;z) = \frac{1}{8\pi(\Delta^2-t^2)} &\int_{-\pi}^{\pi} dw \frac{1}{\sqrt{1-w^2}(w-Q_+)(w-Q_-)} \\ &\times \sum_{s=\pm1} \left(-w+is\sqrt{1-w^2}\right)^{x_j-x_i} \left[z+(2tw-\mu)\sigma^z + 2s\Delta\sqrt{1-w^2}\right], \quad \Delta \neq t\end{aligned} \tag{A.7}$$

where the roots are

$$Q_{\pm}(z) = \frac{1}{2(\Delta^2 - t^2)}\left[-t\mu \pm \sqrt{\Delta^2\mu^2 - (\Delta^2 - t^2)(z^2 - 4\Delta^2)}\right]. \tag{A.8}$$

The equation above only holds when $\Delta \neq t$ as it is easy to see that the denominator inside the summand in Eq. (A.6) is quadratic in w only if this condition holds. Using the following integrals,

$$\frac{1}{\pi}\int_{-1}^{1} dx \frac{1}{\sqrt{1-x^2}(x-a)} = \frac{-1/a}{\sqrt{1-1/a^2}}, \quad \mathrm{Im}\, a \neq 0 \tag{A.9}$$

$$\frac{1}{\pi}\int_{-1}^{1} dx \frac{x^n}{\sqrt{1-x^2}(x-a)} = a^{n-1}\left(1 - \frac{1}{\sqrt{1-1/a^2}}\right), \quad n \in \{1,2\}, \mathrm{Im}\, a \neq 0 \tag{A.10}$$

we obtain

$$\mathbf{g}_B(0;z) = (z - \mu\sigma^z)\mathcal{F}_{-1}(z) + 2t\sigma^z\mathcal{F}_0(z), \tag{A.11}$$

$$\mathbf{g}_B(1-0;z) = 2i\Delta\mathcal{F}_{-1}(z)\sigma^y - (z-\mu\sigma^z)\mathcal{F}_0(z) + (2t\sigma^z + 2i\Delta\sigma^y)\left[\frac{1}{4(t^2-\Delta^2)} - \mathcal{F}_1(z)\right], \tag{A.12}$$

$$\mathbf{g}_B(0-1;z) = -2i\Delta\mathcal{F}_{-1}(z)\sigma^y - (z-\mu\sigma^z)\mathcal{F}_0(z) + (2t\sigma^z - 2i\Delta\sigma^y)\left[\frac{1}{4(t^2-\Delta^2)} - \mathcal{F}_1(z)\right], \tag{A.13}$$

where for $m \in \{0, \pm 1\}$

$$\mathcal{F}_m(z) = \frac{1}{4(t^2-\Delta^2)} \cdot \frac{1}{Q_+(z) - Q_-(z)} \sum_{s=\pm 1} \frac{sQ_s^m(z)}{\sqrt{1 - 1/Q_s^2(z)}}. \tag{A.14}$$

The left boundary GF of a semi-infinite Kitaev chain is then obtained by inserting Eqs. (A.11)-(A.13) into the expression for $\mathbf{g}_S(z)$ in Eq. (A.5). The local density of states (LDOS) at the boundary (normalised to 2π) is obtained from the left boundary (retarded) GF as $-\mathrm{Im}\,\mathrm{tr}\,\mathbf{g}_S(\omega + i\eta)$ and is shown in the topological phase in Figure A.1 and in the trivial phase in Figure A.1. The bulk LDOS is also shown in both plots for comparison. That the topological phase hosts localised zero energy end modes manifests as a subgap spectral peak at $\omega = 0$ in the LDOS.

A.2 READ-GREEN SUPERCONDUCTOR

Using the same method as in the previous section, one can calculate the boundary GF of a semi-infinite two-dimensional spinless $p_x + ip_y$ or Read-Green supercon-

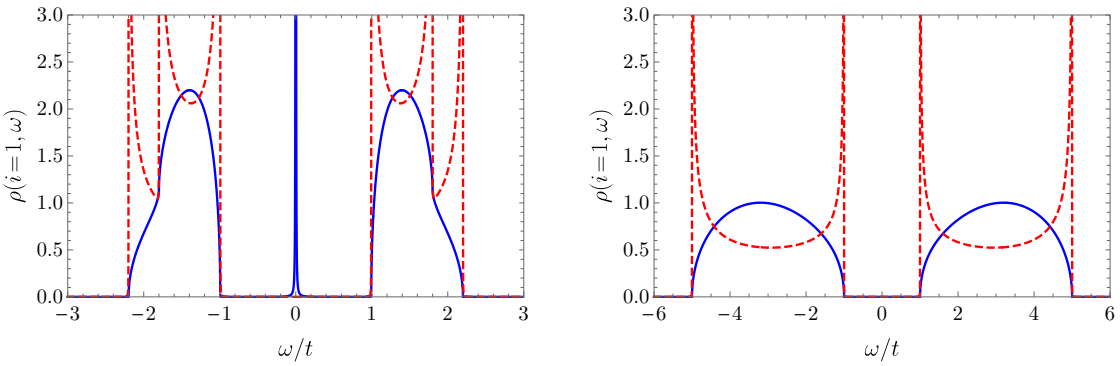

FIGURE A.1 – Local density of states (blue) at the left boundary of a semi-infinite Kitaev chain in (a) the topological phase: $\mu = 0.5t, \Delta = 0.5t$ and (b) the trivial phase: $\mu = 3.0t, \Delta = 0.5t$. That the topological phase hosts localised zero energy end modes (Majorana zero modes) manifests as a subgap spectral peak at $\omega = 0$ in the LDOS shown in (a). The bulk LDOS is shown in dashed red for comparison.

ductor [32]. The bulk superconductor is described by a fully translation invariant Hamiltonian,

$$H_R = \sum_{x,y}\Big[-t\left(c^\dagger_{x+1,y}c_{x,y} + c^\dagger_{x,y+1}c_{x,y} + \text{h.c.}\right) + \left(\Delta c^\dagger_{x+1,y}c^\dagger_{x,y} + i\Delta c^\dagger_{x,y+1}c^\dagger_{x,y} + \text{h.c.}\right) - \mu c^\dagger_{x,y}c_{x,y}\Big], \quad \text{(A.15)}$$

where t is the hopping integral, μ is the chemical potential, and Δ is the p-wave pairing potential that can be made real by a suitable gauge transformation in the phase of the Cooper pair wavefunction. Imposing periodic boundary conditions and Fourier transforming to momentum space $\mathbf{k} = (k_x, k_y)$, H_R can be written in BdG form with Nambu spinor $\Psi_\mathbf{k} = (c_\mathbf{k} \quad c^\dagger_{-\mathbf{k}})^\intercal$ as

$$H_R = \frac{1}{2}\sum_\mathbf{k} \Psi^\dagger_\mathbf{k}\begin{pmatrix} \xi_\mathbf{k} & 2i\Delta_\mathbf{k} \\ -2i\Delta^*_\mathbf{k} & -\xi_\mathbf{k} \end{pmatrix}\Psi_\mathbf{k} \equiv \frac{1}{2}\sum_k \Psi^\dagger_\mathbf{k} h_R(\mathbf{k})\Psi_\mathbf{k}, \quad \text{(A.16)}$$

where $\xi_\mathbf{k} = -2t(\cos k_x + \cos k_y) - \mu$ and $\Delta_\mathbf{k} = 2\Delta(\sin k_x + i \sin k_y)$. The bulk GF in momentum-frequency space is then $[z - h_R(\mathbf{k})]^{-1}$, which when evaluated gives

$$\mathbf{g}_B(k_x, k_y; z) = \frac{1}{z^2 - E^2(\mathbf{k})}\left[z + h_R(\mathbf{k})\right], \quad \text{(A.17)}$$

where $E(\mathbf{k}) = \sqrt{\xi^2_\mathbf{k} + |\Delta_\mathbf{k}|^2}$. We now cut the system to obtain an edge by adding a term $J\sum_x c^\dagger_{x,0}c_{x,0}$ to H_R and sending $J \to \infty$. Note that translation invariance is lost

only along y in this procedure. The Dyson equation for Nambu GFs in the new semi-infinite system can be written as

$$\mathbf{g}'(k_x; y, y'; z) = \mathbf{g}_B(k_x; y - y'; z) + \mathbf{g}_B(k_x; y - 0; z) J\sigma^z \mathbf{g}'(k_x; 0 - y'; z), \tag{A.18}$$

where we work in a mixed (k_x, y) representation with Nambu spinors defined as $(c_{k_x,y} \quad c^\dagger_{-k_x,y})^\intercal$. The edge GF $\mathbf{g}_E(k_x; z) = \mathbf{g}'(k_x; 1, 1; z)$ is then obtained in the limit $J \to \infty$ as

$$\mathbf{g}_E(k_x; z) = \mathbf{g}_B(k_x; 0; z) - \mathbf{g}_B(k_x; 1 - 0; z)\mathbf{g}_B^{-1}(k_x; 0; z)\mathbf{g}_B(k_x; 0 - 1; z). \tag{A.19}$$

The GFs appearing on the RHS can be computed from a partial inverse Fourier transform of the momentum-space bulk GF $\mathbf{g}_B(k_x, k_y; z)$, given by

$$\mathbf{g}_B(k_x; y - y'; z) = \int_{-\pi}^{\pi} \frac{\mathrm{d}k_y}{2\pi} \frac{e^{ik_y(y-y')}}{z^2 - E^2(\mathbf{k})} [z + h_R(\mathbf{k})]. \tag{A.20}$$

This integrals for $y - y' = 0, \pm 1$ can be computed following the same steps as in the previous section – using the substitution $w = -\cos k_y$ and the standard integrals in Eqs. (A.9)-(A.10). The results are

$$\mathbf{g}_B(k_x; 0; z) = [z - (\mu + 2t\cos k_x)\sigma^z - 2\Delta \sin k_x \sigma^y]\, \mathcal{F}_{-1}(k_x; z) + 2t\sigma^z \mathcal{F}_0(k_x; z), \tag{A.21}$$

$$\begin{aligned}\mathbf{g}_B(k_x; 1 - 0; z) = {} & 2i\Delta \mathcal{F}_{-1}(k_x; z)\sigma^x - [z - (\mu + 2t\cos k_x)\sigma^z - 2\Delta \sin k_x \sigma^y]\, \mathcal{F}_0(k_x; z) \\ & + (2t\sigma^z + 2i\Delta\sigma^x)\left[\frac{1}{4(t^2 - \Delta^2)} - \mathcal{F}_1(k_x; z)\right],\end{aligned} \tag{A.22}$$

$$\begin{aligned}\mathbf{g}_B(k_x; 0 - 1; z) = {} & -2i\Delta \mathcal{F}_{-1}(k_x; z)\sigma^x - [z - (\mu + 2t\cos k_x)\sigma^z - 2\Delta \sin k_x \sigma^y]\, \mathcal{F}_0(k_x; z) \\ & + (2t\sigma^z - 2i\Delta\sigma^x)\left[\frac{1}{4(t^2 - \Delta^2)} - \mathcal{F}_1(k_x; z)\right],\end{aligned} \tag{A.23}$$

where for $m \in \{0, \pm 1\}$

$$\mathcal{F}_m(k_x; z) = \frac{1}{4(t^2 - \Delta^2)} \cdot \frac{1}{Q_+(k_x; z) - Q_-(k_x; z)} \sum_{s=\pm 1} \frac{s Q_s^m(k_x; z)}{\sqrt{1 - 1/Q_s^2(k_x; z)}}, \tag{A.24}$$

$$\begin{aligned}Q_\pm(k_x; z) = \frac{1}{2(\Delta^2 - t^2)} \Bigg\{ & -t(\mu + 2t\cos k_x) \\ & \pm \sqrt{\Delta^2(\mu + 2t\cos k_x)^2 - (\Delta^2 - t^2)\left[z^2 - 4\Delta^2(1 + \sin^2 k_x)\right]} \Bigg\}.\end{aligned} \tag{A.25}$$

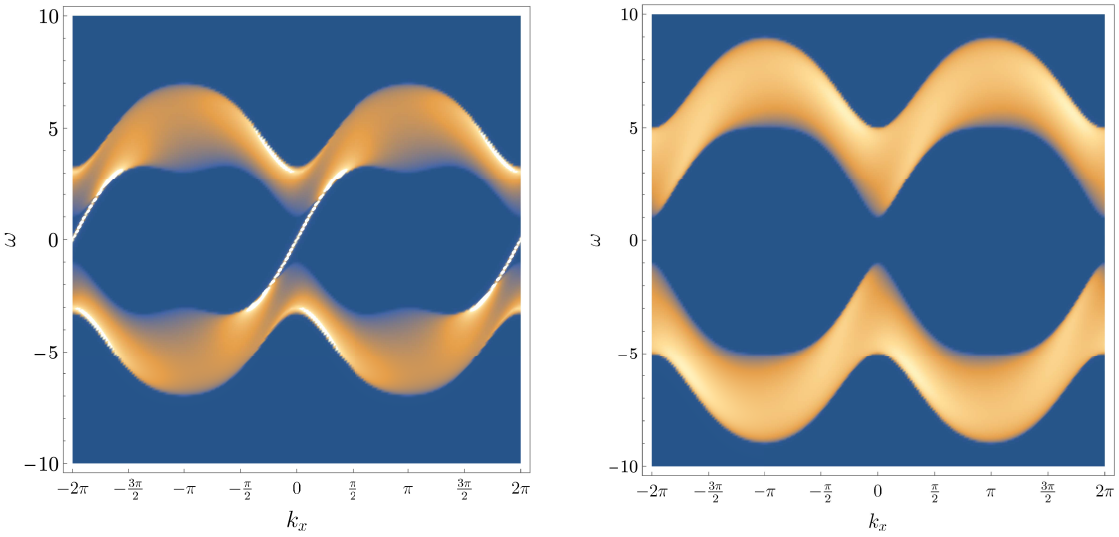

FIGURE A.2 – Intensity plot of the spectral function $A_E(k_x;\omega)$ on the edge of a semi-infinite Read-Green superconductor in the (a) topological phase: $\mu = -3.0t, \Delta = 1.5t$ and (b) trivial phase: $\mu = -5.0t, \Delta = 0.5t$. The topological phase hosts chiral Majorana fermions as edge modes, featuring as linearly dispersing subgap states in the surface spectral function.

The spectral function $A_E(k_x;\omega)$ at the edge is obtained from the retarded edge GF as $-\mathrm{Im}\,\mathrm{tr}\,\mathbf{g}_E(k_x;\omega+i\eta)$, and is shown in Figures A.2a-b in both, topological and trivial phases. The linearly dispersing subgap edge states present in the topological phase are chiral Majorana fermions. Reversing the sign of μ reverses the chirality of the Majorana edge modes.

APPENDIX B

Path integrals for Majorana fermions

Partition functions of Fermi and Bose systems admit representations as *coherent state functional integrals.* This involves working in the (overcomplete) basis of fermion or boson coherent states, which are eigenstates of fermion or boson annihilation operators.[1] Since Hamiltonians of condensed matter systems are usually expressed in second quantised form, the coherent state basis is a natural basis to work in. However, Majorana operators do not admit coherent states that form a complete or over-complete basis. In this section, we outline the construction of coherent state functional integrals for Majorana fermions following Refs. [113, 114], although our conventions differ from those references.

Consider a Hamiltonian that is bilinear in Majorana fermions,

$$H = i \sum_{ij} \gamma_i h_{ij} \gamma_j, \tag{B.1}$$

where the Majorana operators are Hermitian $\gamma_j^\dagger = \gamma_j$ and satisfy the Clifford algebra $\{\gamma_i, \gamma_j\} = 2\delta_{ij}$. The factor of i is required in order for H to be Hermitian. The problem of non-existent coherent states for Majorana fermions can be circumvented by

[1] For details of the construction of such functional integrals, see Ref. [114]. This is necessary background that is assumed in the rest of this section.

expressing all the Majorana fermions in terms of complex fermions. There are two ways in which this can be done: (i) fermion halving – all the Majorana fermions in the problem are paired up as complex fermions, and (ii) fermion doubling – introducing an extra, unphysical Majorana fermion for each physical one and then pairing up the two to create complex fermions. The latter approach is discussed here. For more details on both constructions, see Ref. [135]. To this end, we introduce a spurious species of Majorana fermions η_i that exist alongside γ_i on every site. Combining η and γ to create complex fermions as

$$\psi_j = \frac{1}{2}\left(\gamma_j + i\eta_j\right), \qquad \psi_j^\dagger = \frac{1}{2}\left(\gamma_j - i\eta_j\right), \tag{B.2}$$

the Hamiltonian in Eq. (B.1) can be expressed as

$$H = i\sum_{ij}(\psi_i + \psi_i^\dagger)h_{ij}(\psi_j + \psi_j^\dagger). \tag{B.3}$$

The partition function $Z = \mathrm{tr}\exp(-\beta H)$ with inverse temperature β can now be expressed as a path integral using coherent states for complex fermions in the standard way. Note that H must be normal ordered in this procedure in order to make the replacements $\hat{\psi} \to \psi$ and $\hat{\psi}^\dagger \to \bar{\psi}$, from fermion operators to Grassmann numbers. Since

$$:H: = i\sum_{ij} h_{ij}\left(\psi_i^\dagger\psi_j - \psi_j^\dagger\psi_i + \psi_i\psi_j + \psi_i^\dagger\psi_j^\dagger\right), \tag{B.4}$$

the path integral representation of Z is

$$Z = \int D[\bar{\psi},\psi]e^{-S[\bar{\psi},\psi]}, \tag{B.5}$$

where the action is defined in the usual way as

$$\begin{aligned} S[\bar{\psi},\psi] &= \int_0^\beta \mathrm{d}\tau\left[\sum_j \bar{\psi}_j\partial_\tau\psi_j + i\sum_{ij} h_{ij}\left(\bar{\psi}_i\psi_j - \bar{\psi}_j\psi_i + \psi_i\psi_j + \bar{\psi}_i\bar{\psi}_j\right)\right], \\ &= \int_0^\beta \mathrm{d}\tau\left[\sum_j \bar{\psi}_j\partial_\tau\psi_j + i\sum_{ij}(\psi_i + \bar{\psi}_i)h_{ij}(\psi_j + \bar{\psi}_j)\right], \end{aligned}$$

where we have made the replacement $-\bar{\psi}_j\psi_i = \psi_i\bar{\psi}_j$ in the second line (since Grassmann numbers anti-commute) to get back the original form of H. In summary, we do

not have to worry about normal ordering of the Hamiltonian when writing down the action for the path integral. $\tau \in [0, \beta]$ is a compactified imaginary time variable.

Since the Majorana fermions η introduced earlier are spurious, one must ensure that they do not contribute to the thermodynamics. Going back to the original Majorana representation in terms of γ and η, we find

$$S[\gamma, \eta] = \int_0^\beta \mathrm{d}\tau \left[\frac{1}{4} \sum_j \left(\gamma_j \partial_\tau \gamma_j + \eta_j \partial_\tau \eta_j + i \gamma_j \partial_\tau \eta_j - i \eta_j \partial_\tau \gamma_j \right) + i \sum_{ij} \gamma_i h_{ij} \gamma_j \right]. \quad \text{(B.6)}$$

The cross terms in the Berry phase part of the action can be written as a total derivative $i\partial_\tau(\gamma_j \eta_j)$. Performing the τ integral, this gives rise to boundary terms that evaluate to zero, of the form

$$\begin{aligned} i\gamma_j(\tau)\eta_j(\tau)\big|_0^\beta &= \left[\psi_j(\tau) + \bar{\psi}_j(\tau) \right] \left[\psi_j(\tau) - \bar{\psi}_j(\tau) \right] \Big|_0^\beta, \\ &= 2 \left[\bar{\psi}_j(\beta)\psi_j(\beta) - \bar{\psi}_j(0)\psi_j(0) \right], \\ &= 0, \end{aligned} \quad \text{(B.7)}$$

where the last line follows because the complex fermions (Grassmann fields) obey anti-periodic boundary conditions in imaginary time, $\psi(\beta) = -\psi(0)$ and similarly for $\bar{\psi}$ [114]. The action therefore simplifies to

$$S = \int_0^\beta \mathrm{d}\tau \left[\frac{1}{4} \sum_j \gamma_j \partial_\tau \gamma_j + i \sum_{ij} \gamma_i h_{ij} \gamma_j + \frac{1}{4} \sum_j \eta_j \partial_\tau \eta_j \right] \equiv S[\gamma] + S[\eta]. \quad \text{(B.8)}$$

The action therefore separates into terms that only involve either γ or η with no cross-terms. The measure of the path integral can also be expressed in terms of the Majorana fermions γ and η. To see this, note that the path integral measure in Eq. (B.5) is [114], using a discretised imaginary time variable m,

$$\begin{aligned} D[\bar{\psi}, \psi] &= \lim_{N \to \infty} \prod_{m=1}^{N} \prod_j \mathrm{d}\bar{\psi}_j(m) \mathrm{d}\psi_j(m), \\ &= \lim_{N \to \infty} \prod_{m=1}^{N} \prod_j \frac{i}{2} \mathrm{d}\gamma_j(m) \mathrm{d}\eta_j(m), \\ &= D[\gamma] D[\eta]. \end{aligned} \quad \text{(B.9)}$$

The pre-factor $\lim_{N\to\infty}(i/2)^{N\times N_{\text{sites}}}$ is a constant multiplier to the partition function that can be ignored. The path integral in Eq. (B.5) can thus be written as

$$Z = \int D[\gamma]e^{-S[\gamma]} \int D[\eta]e^{-S[\eta]}. \tag{B.10}$$

The η fermions are just spectators in calculating properties of the physical γ fermions and can thus be ignored. In this case, the path integral over the η fermions can be carried out explicitly, resulting in a constant multiplicative factor to Z that can be dropped. Therefore, given a Majorana fermion (γ) Hamiltonian such as Eq. (B.1), one can write down a coherent state functional integral similar to the complex fermion case with two caveats:

- The path integral measure $D[\gamma]$ only involves γ as there is no 'conjugate' Grassmann field, in contrast to $D[\bar{\psi},\psi]$ for a theory of complex fermions ψ;
- The Berry phase term $(\gamma_j\partial_\tau\gamma_j)/4$ in the action carries a pre-factor of 1/4, which arises because γ_j operators satisfy a Clifford algebra. It is convenient at times to think of this as $\frac{1}{2}\gamma_j(\frac{1}{2}\partial_\tau)\gamma_j \to \frac{1}{2}\gamma_j(\frac{-ik_n}{2})\gamma_j$, where the latter is obtained upon Fourier transforming to the Matsubara frequency representation. One can then interpret $ik_n/2$ as a 'Majorana Matsubara frequency', which is half the complex fermion Matsubara frequency $ik_n = (2n+1)\pi T$.

Consider now a general Gaussian functional integral for Majorana fermions γ, with a real Grassmann source J, given by

$$Z[J] = \int D[\gamma]e^{-\frac{1}{2}\int \mathrm{d}x\mathrm{d}x'\gamma(x)A(x-x')\gamma(x')+\int \mathrm{d}xJ(x)\gamma(x)}. \tag{B.11}$$

This continuum functional integral is obtained from a limiting procedure $N\to\infty$ on the discretised version,

$$Z[J] = \int \mathrm{d}\gamma_1 \ldots \mathrm{d}\gamma_{2N}\, e^{-\frac{1}{2}\gamma_i A_{ij}\gamma_j + J_i\gamma_i}, \tag{B.12}$$

where the Einstein summation convention has been used. Since the $\{\gamma_i\}$ anti-commute, $A_{ij} = -A_{ji}$ can be taken to be anti-symmetric without loss of generality. Let us first calculate the source-free integral,

$$Z[0] = \int \mathrm{d}\gamma_1 \ldots \mathrm{d}\gamma_{2N} \sum_{m=0}^{\infty} \frac{(-1)^m}{m!2^m}(\gamma_i A_{ij}\gamma_j)^m, \tag{B.13}$$

where the exponential has been expanded into a power series. Since $\int \mathrm{d}\gamma = 0$ by definition, only terms with all $\gamma_1, ..., \gamma_{2N}$ will give a non-zero contribution to the integral, that is only the $m = N$ term in the power series contributes. Therefore,

$$\begin{aligned} Z[0] &= \frac{(-1)^N}{N!2^N} \int \mathrm{d}\gamma_1 ... \mathrm{d}\gamma_{2N} \, (\gamma_i A_{ij} \gamma_j)^N, \\ &= \frac{1}{N!2^N} \sum_{P \in S_{2N}} \mathrm{sgn}(P) A_{P(1)P(2)} A_{P(3)} A_{P(4)} ... A_{P(2N-1)} A_{P(2N)} \\ &\equiv \mathrm{Pf}\, A, \end{aligned}$$

where in the second line, the sum is over all permutations P of $\{1, 2, ..., 2N\}$, and the third line defines the *Pfaffian* of the matrix A [136]. It can be shown that $\mathrm{Pf}^2 A = \det A$; to see this, consider $Z[0]^2$ with an action of the form $-(\frac{1}{2}\gamma_i A_{ij} \gamma_j + \frac{1}{2}\gamma'_i A_{ij} \gamma'_j)$. The γ and γ' Majorana fermions can be paired up to form complex fermions ψ with the action $-\bar{\psi}_i A_{ij} \psi$ – the path integral defined by this action then gives the regular $\det A$, which immediately proves that $\det A = \mathrm{Pf}^2 A$.

To compute a general $Z[J]$ with non-zero source, we invoke a change of variables, defining

$$\chi_i = \gamma_i - A^{-1}_{ij} J_j. \tag{B.14}$$

Using the antisymmetry of A_{ij}, it is easy to show that the path integral in Eq. (B.12) transforms in the continuum limit to

$$\begin{aligned} Z[J] &= \lim_{N \to \infty} \int \mathrm{d}\chi_1 ... \mathrm{d}\chi_{2N} \, e^{-\frac{1}{2}\chi_i A_{ij} \chi_j} e^{-\frac{1}{2} J_i A^{-1}_{ij} J_j}, \\ &= \mathrm{Pf}(A) \exp\left[-\frac{1}{2} \int \mathrm{d}x \, \mathrm{d}x' \, J(x) A^{-1}(x - x') J(x') \right]. \end{aligned} \tag{B.15}$$

APPENDIX C

Transport in a TSC-QD-TSC junction

In the MAI class of models [1], consider a TSC-QD-TSC junction (see Figure C.1) with Hamiltonian

$$H = H_L + H_R + H_{QD} + H_{\text{hyb}}, \tag{C.1}$$

where H_L and H_R are Kitaev chains that form the left and right leads (LL and RL) respectively:

$$H_L = \frac{i}{2}\sum_{j=1}^{N-1}(\Delta_L + t_L)\gamma'_{-j-1}\gamma_{-j} + (\Delta_L - t_L)\gamma_{-j-1}\gamma'_{-j} - \mu_L\gamma_{-j}\gamma'_{-j}, \tag{C.2}$$

$$H_R = \frac{i}{2}\sum_{j=1}^{N-1}(\Delta_R + t_R)\gamma'_{j}\gamma_{j+1} + (\Delta_R - t_R)\gamma_{j}\gamma'_{j+1} - \mu_L\gamma_{j}\gamma'_{j}, \tag{C.3}$$

where the Majorana operators are defined in terms of complex fermions as $\gamma_j = (c_j + c_j^\dagger)$ and $\gamma'_j = -i(c_j - c_j^\dagger)$, and satisfy the Clifford algebra $\left\{\gamma_i, \gamma_j\right\} = 2\delta_{ij}$ and $\left\{\gamma_i, \gamma'_j\right\} = 0$. $\Delta_{L,R}$ are the p-wave pairing potentials, $t_{L,R}$ are hopping integrals, and $\mu_{L,R}$ are chemical potentials. In the topological phases of LL and RL, i.e. for $\left|\mu_L\right| < 2t_L$ and $\left|\mu_R\right| < 2t_R$, the LL hosts Majorana zero modes (MZMs) γ'_{-1} and γ_{-N} while the RL has γ_1 and γ'_N as its MZMs. Henceforth, we will assume semi-infinite leads given by the limit $N \to \infty$.

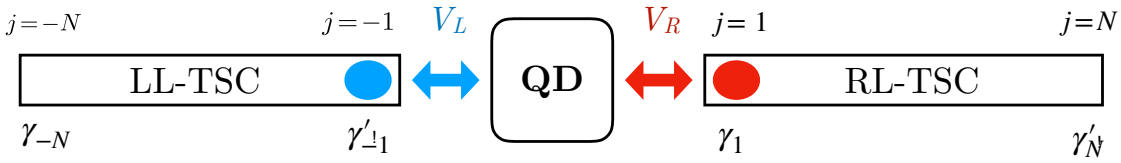

FIGURE C.1 – Setup of the TSC-QD-TSC junction.

The QD is modelled as an Anderson impurity described by

$$H_{QD} = U(t)\left(2n_{d\uparrow}-1\right)\left(2n_{d\downarrow}-1\right)+\frac{\epsilon}{2}\left(n_{d\uparrow}+n_{d\downarrow}-1\right)-\frac{h}{2}\left(n_{d\uparrow}-n_{d\downarrow}\right), \tag{C.4}$$

where $n_{d\sigma} = d_\sigma^\dagger d_\sigma$ is the number operator for impurity spin σ. $U(t)$ describes a time-dependent on-site Coulomb repulsion (quench on the charging energy of the QD), h is a Zeeman field, and ϵ is a shift in the chemical potentials of the impurity fermions. The hybridisation between the leads and QD is

$$H_{\text{hyb}} = iV_L\gamma'_{-1}d_\uparrow + iV_R\gamma_1 d_\uparrow + \text{h.c.} = i\left(V_L\gamma'_{-1}+V_R\gamma_1\right)\left(d_\uparrow + d_\uparrow^\dagger\right) \tag{C.5}$$

where $V_{L,R}$ are the hybridisation strengths. We have coupled spin-up electrons on the QD to nearby MZMs in the leads. The fact that experimental realisations of the Kitaev chain involve proximitised spin-orbit coupled nanowires subjected to magnetic fields justifies a spin-selective choice of hybridisation, and the inclusion of a Zeeman term in the QD Hamiltonian (C.4).

Although we have considered here a quench on the QD charging energy U, one may also quench the hybridisation as in Ref. [103]. The proofs to be presented in the next section will hold in this case as well. However, note that exact solvability requires $\epsilon = h$ at all times. Departures from this limit have to be considered perturbatively as in Ref. [1].

The $\mathbb{Z}_2$ slave-spin representation [93] of H, obtained by fractionalising $d_\sigma \to \mu^x f_\sigma$ and using the resulting gauge constraint

$$\mu^z = 2(n_f - 1)^2 - 1, \tag{C.6}$$

is given by

$$H_{SS} = H_L + H_R + i\,(V_L\gamma'_{-1} + V_R\gamma_1)\left(f_\uparrow + f_\uparrow^\dagger\right)\mu^x + U(t)\mu^z + \frac{1}{2}\left[\epsilon + h + (\epsilon - h)\mu^z\right]\left(n_{f\downarrow} - \frac{1}{2}\right). \tag{C.7}$$

For $\epsilon = h$, this is bilinear in Majorana operators defined as $\Gamma^a_\uparrow = \mu^a(f_\uparrow + f_\uparrow^\dagger)$ for $a \in \{x, y, z\}$ [1]:

$$H_{SS} = H_L + H_R + i\,(V_L\gamma'_{-1} + V_R\gamma_1)\,\Gamma^x_\uparrow - iU(t)\Gamma^x_\uparrow\Gamma^y_\uparrow + \frac{1}{2}\left[\epsilon + h - i(\epsilon - h)\Gamma^x_\uparrow\Gamma^y_\uparrow\right]\left(n_{f\downarrow} - \frac{1}{2}\right). \tag{C.8}$$

Henceforth, we will assume the exactly solvable limit $\epsilon = h$ of Eq. (C.8) unless otherwise mentioned. We show now that the projector

$$\mathbb{P} = \frac{1}{2}\left[1 + (-1)^{n_f}\mu^z\right] \tag{C.9}$$

constructed from the gauge constraint [Eq. (C.6)] can be disposed of in calculating the non-equilibrium current in the slave-spin representation, similar to Ref. [103].

Say at time $t = 0$, the charging energy of the QD is $U(t = 0) = U_0$ and the system is in thermal equilibrium at an inverse temperature β with a density matrix

$$\rho(t = 0; V, U_0, \epsilon, h) = \frac{1}{Z(V, U_0, \epsilon, h)}\exp\left(-\beta H(V, U_0, \epsilon, h)\right), \tag{C.10}$$

where Z is the physical partition function $\mathrm{tr}\exp(-\beta H)$. In the Heisenberg picture, the current operators for the leads in equilibrium (at $t = 0$) are given by

$$\begin{aligned} j_L(t = 0) = \frac{\mathrm{d}N_L}{\mathrm{d}t} &= -i[N_L, H] \\ &= -i\sum_{j=1}^{\infty}\left[c^\dagger_{-j}c_{-j}, H_L\right] - \sum_{j=1}^{\infty} iV_L\left[c^\dagger_{-j}c_{-j}, c_{-1} - c^\dagger_{-1}\right]\left(d_\uparrow + d^\dagger_\uparrow\right) \\ &= \Omega_L + iV_L\left(c_{-1} + c^\dagger_{-1}\right)\left(d_\uparrow + d^\dagger_\uparrow\right), \end{aligned} \tag{C.11}$$

and similarly, $$j_R(t = 0) = \Omega_R + iV_R\left(c_1 - c^\dagger_1\right)\left(d_\uparrow + d^\dagger_\uparrow\right). \tag{C.12}$$

In the case of normal metallic leads that conserve total particle number, $\Omega_{L,R} = 0$, but as a superconductor spontaneously breaks this symmetry, these terms will contribute to the current. Therefore, the total current through the QD in equilibrium is

$$j(t = 0) = \frac{1}{2}(j_L - j_R) = \frac{\Omega_L - \Omega_R}{2} + \frac{i}{2}\left[V_L\left(c_{-1} + c^\dagger_{-1}\right) - V_R\left(c_1 - c^\dagger_1\right)\right]\left(d_\uparrow + d^\dagger_\uparrow\right) \tag{C.13}$$

Defining a particle-hole transformation $\mathcal{D}_\uparrow d_\uparrow \mathcal{D}_\uparrow^{-1} = d_\uparrow^\dagger$, observe that

$$\mathcal{D}_\uparrow j(t=0)\mathcal{D}_\uparrow^{-1} = j(t=0) \tag{C.14}$$

$$\mathcal{D}_\uparrow \rho(t=0;V_\alpha,U_0,\epsilon,h)\mathcal{D}_\uparrow^{-1} = \rho(t=0;V_\alpha,-U,h,\epsilon) \tag{C.15}$$

where the second equality comes from the fact that $\mathcal{D}_\uparrow H(V_\alpha,U,\epsilon,h)\mathcal{D}_\uparrow^{-1} = H(V_\alpha,-U,h,\epsilon)$ and $Z(V_\alpha,U,\epsilon,h) = Z(V_\alpha,-U,h,\epsilon)$.

After a quench on the QD charging energy, the average current at any $t>0$ is given by [137]

$$\langle j\rangle(t;V_\alpha,U,\epsilon,h) = \mathrm{tr}\,\rho(t=0;V_\alpha,U_0,\epsilon,h)K^\dagger(t;V_\alpha,U,\epsilon,h)j(t=0)K(t;V_\alpha,U,\epsilon,h), \tag{C.16}$$

where $K(t,0)$ is the evolution operator,

$$K(t;V_\alpha,U,\epsilon,h) = \hat{T}\exp\left(-i\int_0^t dt' H(t')\right) \tag{C.17}$$

Inserting identities $\mathcal{D}_\uparrow^{-1}\mathcal{D}_\uparrow$ thrice inside the trace in Eq. (C.16), using cyclicity, and the relations Eqs. (C.14)-(C.15), it is easy to see that

$$\langle j\rangle(t;V_\alpha,U,\epsilon,h) = \langle j\rangle(t;V_\alpha,-U,h,\epsilon). \tag{C.18}$$

In the slave-spin representation, the current operator at $t=0$ is

$$j_{SS}(t=0) = \frac{1}{2}(j_L^{(SS)} - j_R^{(SS)}) = \frac{\Omega_L-\Omega_R}{2} + \frac{i}{2}\left[V_L\left(c_{-1}+c_{-1}^\dagger\right) - V_R\left(c_1 - c_1^\dagger\right)\right]\Gamma_\uparrow^x. \tag{C.19}$$

Since the action of $\mathcal{D}_\uparrow^{-1}$ is represented on the slave-spin Hilbert space by μ^x, the physical average current at $t>0$ in Eq. (C.16) is expressed in the slave-spin representation as

$$\begin{aligned}\langle j\rangle_{SS}(t;V_\alpha,-U,h,\epsilon) = \mathrm{tr}\,\mu^x 2\rho_{SS}(t=0;V_\alpha,U_0,\epsilon,h)\mu^x\mu^x \\ \times K_{SS}^\dagger(t;V_\alpha,U,\epsilon,h)\mu^x j_{SS}(t=0)\mu^x K_{SS}(t;V_\alpha,U,\epsilon,h)\mu^x\mathbb{P},\end{aligned} \tag{C.20}$$

where we have used the relation $Z = Z_{SS}/2$ to obtain $\rho \to 2\rho_{SS}$, and

$$\rho_{SS}(t=0;V_\alpha,U_0,\epsilon,h) = \frac{1}{Z_{SS}(V_\alpha,U_0,\epsilon,h)}\exp\left(-\beta H_{SS}(t=0;V_\alpha,U_0,\epsilon,h)\right), \tag{C.21}$$

$$K_{SS}(t;V_\alpha,U,\epsilon,h) = \hat{T}\exp\left(-i\int_0^t dt' H_{SS}(t')\right). \tag{C.22}$$

Note that $H_{SS}(t)$ is quadratic in fermions, so Wick's theorem applies in calculation of averages. Again using the cyclicity of the trace, and the relations $\mu^x \mathbb{P} \mu^x = 1 - \mathbb{P}$ and $\mu^x j_{SS}(t=0)\mu^x = j_{SS}(t=0)$, Eq. (C.20) simplifies to

$$\langle j \rangle_{SS}(t; V_\alpha, U, \epsilon, h) = \operatorname{tr} \rho_{SS}(t=0, V_\alpha, U_0, \epsilon, h) K_{SS}^\dagger(t;U) \mu^x j_{SS}(t=0) K_{SS}(t;U) \quad \text{(C.23)}$$

with the projector disposed of.